LOSS OF CHAPERONE PROTEIN IN HUMAN CANCER

Omanma Adighibe

Submission for the degree of DPhil

Nuffield Department of Clinical Laboratory Sciences

St Cross College

University of Oxford

Michaelmas 2012

ABSTRACT

TRAP1 is a Heat Shock Protein (HSP) chaperone to retinoblastoma but also associated to the tumor necrosis factor receptor. HSPs are primarily up regulated in cancer. Work in our lab noted a down regulation of TRAP1 in some non-small cell lung cancers compared to normal lung. The first aim of this project was to evaluate the effect of the loss of TRAP1 on cell proliferation using a spheroid model. The presence of TRAP1 in spheroids promoted cell proliferation and a faster onset of hypoxia. This suggests an oncogenic role for TRAP1 since rapid hypoxia development equates to poor prognosis.

Micro array analysis showed that TRAP1's loss was associated with increased transcrpition of the Junctional Mediating and Regulatory protein (JMY). JMY possesses an oncogenic property due to its ability to facilitate cell motility. Additionally it has tumor suppressor activity in promoting p53 activation. The second aim of this project was to produce an anti-JMY antibody and use it to characterize JMY and additionally verify the association between TRAP1 and JMY.

JMY was found to be widely expressed in normal tissues and in many types of tumors. In neoplastic tissues, comparing primary versus metastatic tumors, JMY was found to have significantly higher expression in the metastatic compared with the primary tumors. A pilot study showed that nuclear co-expression of JMY and P53 was associated with shorter overall survival suggesting that a possible tumorigenesis mechanism could be via a deregulation/mutation of JMY/p53 or both.

Finally, using 3 dimensional constructions, I demonstrated the distinct morphological difference between an angiogenic tumor and a non-angiogenic tumor. Additionally, I showed a characteristic cytoplasmic p53 sequestration in the non-angiogenic phenotype that is absent in the angiogenic phenotype. This could be the mechanism that the non-angiogenic tumor uses to adapt to hypoxia. This would imply that there is a potential for cancers to escape therapy by switching between these 2 phenotypes.

To my brother Chibuzo Adighibe and my parents Simeon Adighibe and Mary Ihuaku

ACKNOWLEDGEMENTS

I would like to thank Professors Kevin Gatter and Francesco Pezzella for the opportunity to work in the CRUK Tumor Pathology Group and for all their help and support throughout this period. I also want to thank Professor Adrian Harris for his mentorship and support during my DPhil course and Ms Helen Turley who is the backbone for antibody production in the group and spear headed the anti-JMY antibody production project. I am very grateful to Dr Kingsley Micklem who played a crucial role in helping amalgamate different aspects of the projects of my thesis. His indispensable skills with images capturing, confocal microscope and assembling graphics facilitated the meticulous rendition of the graphics for my thesis. I also want to say thanks to the very kind Dr Andrew Graham for help with ordering my supplies, software application tutoring and prompt scanning of my blot and to Dr Russell Leek for helping with statistical analysis of data and mentoring me through the course of my DPhil. I must also thank Graham Steers the lab manager when I started my DPhil work, who acquainted me with the lab and taught me the Western blot technique that was crucial to my project. I am also grateful to Letica Campo and Margaret Jones for teaching me immunohistochemistry and helping with some of my studies. I also must thank Dr Jiangting Hu who helped with the set-up of the TRAP1 constructs; Drs Karim Bensaad, Alan McIntyre and members of Professor Alison Banham's group for their help and advice; and Dr Ioanna Ledaki for help with set-up of the spheroid production. Thanks also to Michaella Smart who never failed to ensure that I had no problems with paperwork and for her invaluable words of wisdom and encouragement.

I also extend my gratitude to the tissue bank team in providing specimens used for my Immunohistochemistry studies.

I would also want to thank Dr Debora Gill for facilitating the progress of my thesis and Louisa Chandler for helping to co-ordinate the submission of my thesis and arrangements for my viva.

Thanks also to Robin Roberts-Gant for helping with the printing of this thesis.

I am also grateful to my entire family (immediate and extended) and friends for all their supports and prayers.

Thanks very much to the Pathological Society of the UK and Ireland for providing some of the funding for this degree.

CONTENTS

Figures and Tables

ABBREVIATIONS

bp Base Pairs
BCL2 B cell Lymphoma 2
BNIP3 BCL2/adenovirus E1B 19 kDa protein-interacting protein 3
BrdU Bromodeoxyuridine
BSA Bovine serum albumin
CAIX Carbonic anhydrase IX
CDK Cyclin dependent kinase
Da Daltons
DEPC Diethyl pyrocarbonate
DMEM Dibecco's Modified Eagle's Medium
DMSO Dimethyl sulphoxide
DNA Deoxyribonucleic acid
CA9 Carbonic anhydrase 9
cDNA Complementary DNA
ECM Extracellular matrix
EDTA Ethylene diamine tetraacetic acid
EGFR Epidermal growth factor receptor
FCS Foetal calf serum
FGF Fibroblast growth factor
GAPDH glyceraldehyde-3-phosphate dehydrogenase
GLUT1 Glucose transporter 1
h hours
HA Haemagglutinin
HEK Human embryonic kidney
HIF Hypoxia-induced factor
HP1a Heterochromatin protein-1α
HSP90 Heat shock protein 90
HSP75 Heat shock protein 75
h hours
IGF1R Insulin-growth factor 1 receptor
JMY Junctional mediating and regulatory protein
kD Kilodaltons
MAPK Mitogen activated protein kinase
µg Microgram
µl Microliters
min minutes
ml Milliliters
mM Micromolar
MMP9 matrix metalloproteinase 9
mRNA Messenger ribonucleic acid
ng Nanograms
nM Nanomolar
TP53 Tumor protein 53
PBS Phosphate buffered saline
PBST PBS with Tween 20
PCR Polymerase chain reaction

PDH Prolyl hydroxylases
PFG Protein-folding gene
PI Propidium iodide
PI3K Phosphatidyl inositol-3 kinase
Rb Retinoblastoma
qRT-PCR qualitative real-time PCR
RNA Ribonucleic acid
RNAi RNA interference
RNase Ribonuclease
RT-PCR Reverse transcriptase PCR
SDS Sodium dodecyl sulphate
s seconds
siRNA Short interfering RNA
SOD1 superoxide dismutase 1
Sp1 Specificity protein 1
STAT3 Signal Transduction And transcription
TNF Tumour necrosis factor
TRAP1 TNF receptor associated protein 1
TSP Thrombospodin
VEGF Vascular endothelial growth factor
VHL von Hippel-Lindau

CHAPTER 1
INTRODUCTION

1.1 Heat Shock Proteins

Heat Shock Proteins (HSP) are products of several distinct gene families required for cell survival during stress and named according to their relative molecular mass ranging from HSP10 to HSP110. HSPs are involved in controlling cellular metabolism, regulating mitogenesis and cell cycle progression and protection from programmed cell death (Calderwood, Khaleque et al. 2006). Their cellular functions that deem them as molecular chaperones involve protein holding and protein folding (Buchner 1999, Wegele, Muller et al. 2004). The principal HSPs involved in protein holding and the most studied are the family of HSP70 and 90 (Calderwood, Khaleque et al. 2006).

In their role of protein holding, HSPs bind unfolded sequences of polypeptide substrates during 1) mRNA translation to prevent premature self -association as nascent proteins; 2) during heat shock when proteins become partially unfolded; and 3) constitutively, which happens when HSP 90 binds to proteins with unstable tertiary structures(Pratt and Toft 2003, Wegele, Muller et al. 2004, Calderwood, Khaleque et al. 2006). HSP70 and 90 function in large protein complexes in association with accessory proteins that assist the primary chaperone in substrate selection and the series of associations and dissociations that occurs between the primary chaperone and selected substrate (Pratt and Toft 2003, Mayer and Bukau 2005).

The protein folding function of chaperone proteins is subsequent to release of protein substrates by the holding protein and usually involves the HSP60 family also referred to as the

chaperonin. These chaperonin self-associate to form large folding chambers in which substrate proteins can undergo the appropriate intramolecular interactions required to attain its correct tertiary structure (Spiess, Meyer et al. 2004, Young, Agashe et al. 2004).

However a folding function is not exclusive to HSP60, HSP70 and HSP90: HSP27 participates in the folding function but with a different mechanism (Arrigo 2005).

1.2 HSPs and Cancer

In normal cells protein denaturation and aggregation trigger intense HSP upregulation which exerts a powerful anti apoptotic effect via its cryoprotective properties, while buying time for proteosomal repair (Beere 2004, Nylandsted, Gyrd-Hansen et al. 2004). Unfortunately, just as malignant cells can hijack normal cell functions for adaptive survival, the cytoprotective holding and folding properties of HSPs are also co-opted during malignant progression, taking prime advantage of the upregulated HSPs to facilitate tumor cell growth and survival (Ciocca and Calderwood 2005, Calderwood, Khaleque et al. 2006).

1.2.1 Mechanism of Increased HSP expression in Cancer

Increase of HSPs in cancer follows en suite with basic oncogenic pathways. A primary mechanism for HSP regulation in normal cells involves the tumor suppressor p53 and related protein p63 that acts to repress HSP genes (Taira, Sawai et al. 1999, Wu, Osada et al. 2005). In human malignancies one of the most frequently mutated genes is p53 that usually reverses its suppressive effect on HSP, which in turn contributes to cancer enhanced transcription of HSPs,

especially HSP70 (Agoff, Hou et al. 1993, Tsutsumi-Ishii, Tadokoro et al. 1995, Madden, Galella et al. 1997, Ghioni, Bolognese et al. 2002).

In some cancers, such as head and neck, there is expression of a p63 isoform ΔNp63α, which acts as a dominant-negative inhibitor of the wild-type p63. In effect, this also reverses the suppressive effect of p63 on HSP expression in cancer, allowing increased HSP expression (Wu, Osada et al. 2005).

In addition to reversal of P53's repressive effect, the upregulation of HSPs in tumors is further incited via the signalling circuitry of the heat shock response pathway. During heat shock response, a massive increase in HSP gene expression occurs due to the interaction of heat shock factor protein 1 (HSF1) with heat shock regulatory element in the promoter region of the HSP genes triggering a massive production of HSPs (Lindquist and Craig 1988, Georgopoulos and Welch 1993, Wu, Osada et al. 2005).

Also since human malignancies frequently have mutated p53 this could be another source of increased HSP expression in malignancies since HSP tends to preferentially bind mutant p53 than wild type p53. In support of this are studies showing HSP90 accumulation in large amounts in cancer cells in association with mutant p53 (Calderwood, Khaleque et al. 2006).

Finally, it is also possible that an HSP increase could be induced by the microenvironmental stress imposed by the tumor milieu (Folkman 2002). The premise behind this being that response to unfolded protein in the tumorigenic environment automatically triggers a stress response up regulating HSPs (Calderwood, Khaleque et al. 2006).

1.2.2 HSP's Role in Formation of Malignant phenotype

According to Hanahan and Wienberg (Hanahan and Weinberg 2000, Hanahan and Weinberg 2011), as a normal cell progressively evolves to a neoplastic state it acquires a succession of hallmark capabilities (figure 1) during a multistep process of human tumor pathogenesis. These hallmark traits categorized into six essential alterations in cell physiology include: Sustaining Proliferative Signaling/Self sufficiency; Evading growth suppressors; Resisting Cell Death; Activating invasion and metastasis; Inducing angiogenesis; Enabling replicative immortality and Development of resistance to cytotoxic therapies. The upregulation of HSP expression participates in many of these cancer developmental stages and is successively described below.

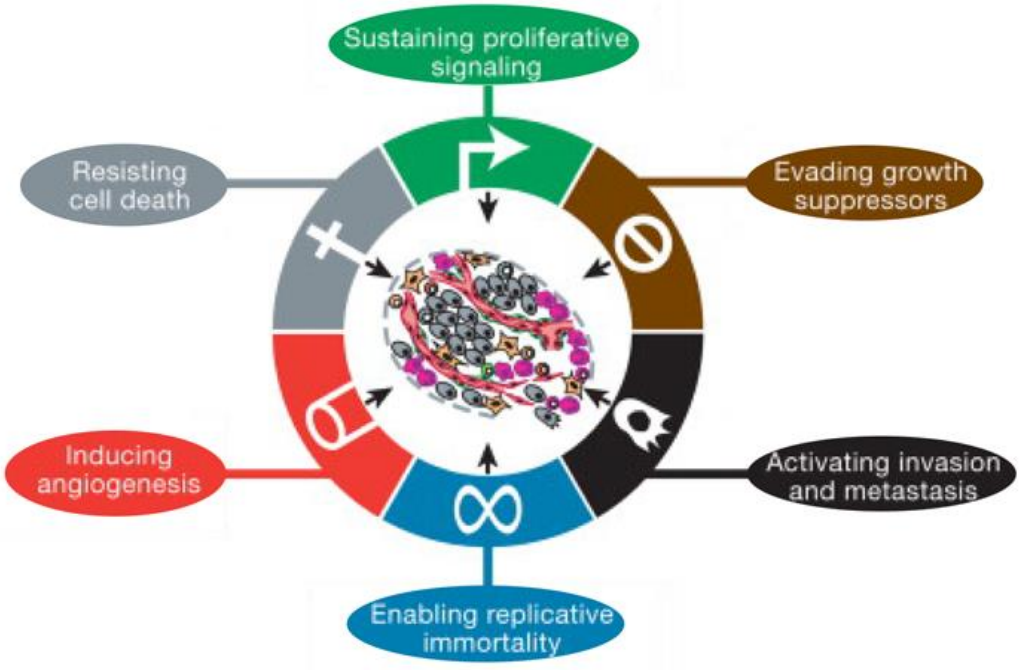

Figure 1.1.Formation of malignant phenotype. Figure adapted from Hanahan et al 2011-Hallmarks of Cancer: The next generation (Hanahan and Weinberg 2011).

1.2.2.1 HSP and Self Sufficiency/ Proliferative Signaling and Growth

HSP is crucial in this step of self-sufficiency particularly with their holding and folding role. This chaperoning function of HSP allows stabilization of and refolding of mediators and signal transduction proteins like receptors and protein kinases contributing to transformation in cancer cells. Nuclear factor κB (NFκB) and mitogen-activated protein kinase (MAPK) are examples of cell signaling molecules folded with the assistance of HSP90 and co-chaperone CDC37 (Basso, Solit et al. 2002, Chen, Cao et al. 2002, Lange, Rebollo et al. 2002). Just before the inception of transformation, cell signaling is dependent on a normal growth pathway and cuing but as the cell progressively deviates from normal, the self sufficiency characteristics begin to emerge and the cancer cells hijack and transform normal cell function to an overdrive production and mutation of crucial molecules which become highly dependent on HSPs (Neckers and Lee 2003, Calderwood, Khaleque et al. 2006). HSPs facilitate this deviant behavior by stabilizing and folding these mutated molecules and in effect contribute to the emergence of a polymorphism that supports the evolution of resistant clones. HSP90 for instance stabilizes the conformations of mutant proteins that arise from translocations such as Bcr-Abl responsible for chronic myelogenous leukemia (Nimmanapalli, O'Bryan et al. 2001, Neckers and Ivy 2003).

1.2.2.2 HSP and Insensitivity to Growth Inhibition

Insensitivity to growth inhibition is mainly due to the arrest of tumor suppressor gene function. Growth inhibitory signals inhibit cellular proliferation by driving cells into the quiescent G0 state or by inducing terminal differentiation. Both Rb and P53 play important roles in these mechanisms which are highly modulated by HSPs. HSP70 and HSP90 are able to bind potent

tumor suppressors such as p53 (Pinhasi-Kimhi, Michalovitz et al. 1986, Lane, Midgley et al. 1993). Additionally there have been evidence of an up-regulation of HSP70 and HSP90 in cancer cells being associated with p53 mutations (Pinhasi-Kimhi, Michalovitz et al. 1986, Lane, Midgley et al. 1993).

1.2.2.3 HSP and Resistance to cell death

The two main HSPs involved in inhibiting cell death are HSP70 and HSP27 (Gerner and Schneider 1975). These two HSPs are up-regulated in human cancers and exert such profound resistance to programmed cell death in cancer that inactivation or knockdown of HSP70 or HSP27 leads to spontaneous activation of programmed cell death that has not been observed in tissues of normal origin (Beere 2001). In order to completely abrogate programmed cell death, several pathways are required to be subverted, which include the c-myc pathway and p53, in order to successful contribute to the emergence of cancer cells (Hanahan and Weinberg 2000, Nelson and White 2004).

The exact relationship of HSP27 and HSP70 to the p53 and BCL2 pathways remains unclear (Beere 2001, Jaattela 2004). Additionally, HSP inhibition of programmed cell death can lead to a default to cell death via necrosis however it is not clear whether necrosis is as efficient as other death pathways in eradicating deviant/cancer cells. Necrosis also causes release of cell content into the tumor microenvironment that triggers inflammation, angiogenesis and, possibly, metastatic propagation (Proskuryakov, Konoplyannikov et al. 2003, Nelson and White 2004, Viatour, Merville et al. 2005).

1.2.2.4 HSP and Replicative Immortality / Inhibition of senescence

The up-regulation of HSPs in tumors has a potent effect in increasing longevity in several cell types hence suggesting increased HSP involvement in resistance to senescence in Caenorhabditis elegans(Tatar, Khazaeli et al. 1997, Hsu, Murphy et al. 2003). To escape senescence and undergo unlimited growth, tumor cells must bypass the crisis point at which telomeres on chromosomes have been shortened to their limit and suppress further cell division. This is attained in cancer in part due to the fact that their p53-sensitive expression of the enzyme telomerase is sufficient to bypass this crisis point and permit unlimited growth in cells (Campisi 2005). HSPs' contribution to this is the requirement of HSP90 to stabilize the telomerase protein, further indicating the importance of HSP90 in inciting transformation and neoplastic formation (Workman 2004).

Rohde et al. have demonstrated that high levels of HSP70 in breast cancer also inhibit the onset of senescence. HSP70-2 (a member of the HSP70 family) antagonizes engagement of the senescence pathway by decreasing both p53 dependent and independent mechanisms (Rohde, Daugaard et al. 2005).

Additionally, studies have shown that knockdown of Mortalin, an HSP70 family member induces cell senescence (Wadhwa, Taira et al. 2002), while an overexpression of a mortalin homologue in *Caenorhabditis elegans* resulted in an extension of its lifespan (Yokoyama, Fukumoto et al. 2002). It is thought that Mortalin inhibits senescence and pushes increased cell division by inhibiting p53 activity (Calderwood, Khaleque et al. 2006)

1.2.2.5 HSP and Angiogenesis

Angiogenesis in cancer is highly dependent on HIF1α, the primary sensor of tumor cell hypoxia. HIF1α is regulated by HSPs at the level of protein stability. In hypoxia HSP90 and HSP70 are required to mediate stabilization and accumulation of HIF1α(Zhou, Schmid et al. 2004). Hypoxia facilitates cell mobility via HIF1α induced activation of vascular endothelial growth factor (VEGF) and nitric oxide synthase (NO) (Neckers and Ivy 2003, Sun and Liao 2004, Pfosser, Thalgott et al. 2005, Calderwood, Khaleque et al. 2006). Also both VEGF and NO require HSP90 for their induction and stabilization in vascular endothelial cells (Neckers and Lee 2003, Sun and Liao 2004, Pfosser, Thalgott et al. 2005). Additionally, it has been shown that angiogenesis is enhanced by the overexpression of HSP90 and inhibited by the HSP90-targeted drug 17-demethoxygeldamycin 17 AAG- an analogue of geldamycin (17AAG) in a rabbit hindlimb ischemia model (Sun and Liao 2004, Pfosser, Thalgott et al. 2005).

1.2.2.6 HSP and Chemotherapy Evasion

Up-regulation of HSP70 and HSP27 has been shown to increase resistance to chemotherapy. HSPs' role in therapy resistance might be through the evasion of cell death that results from high HSP expression which has evolved to permit cell populations to survive toxic environmental stresses until protein repair occurs. Ultimately, this mechanism became co-opted by cell tumors to override the barriers to programmed cell death and senescence (Vargas-Roig, Gago et al. 1998, Calderwood, Khaleque et al. 2006). Also HSP75 over-expression is one of the protective mechanisms adopted during tumor progression and is closely related to the multi-

drug resistance commonly found in cancer cells (Gatenby and Gillies 2004, Montesano Gesualdi, Chirico et al. 2007).

1.2.2.7 HSP and Oncogenic and Non-oncogenic addiction

In addition to the six multistep mutagenic hallmarks of onset and progression of cancer as outlined by Hanahan and Weienberg (Hanahan and Weinberg 2000, Hanahan and Weinberg 2011) more hallmarks have been proposed based on genetic analyses of cellular cancer phenotypes (Luo, Solimini et al. 2009). The up-regulation of HSP is evidence of tumors exhibiting and counteracting proteotoxic stress (Whitesell and Lindquist 2005) because this increases toxic unfolded protein aggregation which places additional burdens on the protein folding and degradation machineries (Whitesell and Lindquist 2005, Denoyelle, Abou-Rjaily et al. 2006). Increasing HSP activity can inadvertently uphold and refold oncogenic proteins further contributing to cancer progression. Tumors can in turn get highly dependent on this HSP assisted oncogenic activity as tumor maintenance depends upon the continued activity or overexpression of certain oncogenes, the so called Oncogenic addiction (Weinstein 2002). Oncogenic addiction has been demonstrated in transgenic mice using inducible MYC oncogenes showing that MYC driven lymphoma and skin papillomas respectively can be reversed upon withdrawal of the MYC oncogene (Felsher and Bishop 1999)(Pelengaris, Littlewood et al. 1999, Luo, Solimini et al. 2009). A similar evidence is accumulating in in vitro‘ models of human pancreatic cancer cell lines carrying mutant K-ras, but not wild type K-ras, being inhibited by an antisense K-ras oligonucleotide (Aoki, Yoshida et al. 1997). Also in vivo, a subset of oncogenes whose inhibition can lead to tumor cell death, differentiation and arrest have also proven successful as targets for therapy such as BCR-ABL (imatinib/Gleevac),

EGFR (gefitinib/Iressa), and HER2 (trastuzumab/Heceptin) (Druker 2002, Sharma, Yang et al. 2005, Roberts and Der 2007).

Additionally there is non-oncogenic addiction, a phenomenon that involves genes and pathways that are not necessarily oncogenic nor are required to the same degree for the viability of normal cells, but are essential to support the oncogenic phenotype of cancer cells (Solimini, Luo et al. 2007, Luo, Solimini et al. 2009). By token of being needed to refold denatured oncogenic proteins, HSP plays the role of a non-oncogene which tumors get heavily dependent on, because of the tumors' addiction to the oncogene that the HSP refolds (Solimini, Luo et al. 2007, Luo, Solimini et al. 2009).

1.2.3 HSPs as targets for treatment

The increase in activity of HSPs in malignant cells (Whitesell and Lindquist 2005, Kang 2012) and their role as possible non-oncogenic addictive agents required for malignant growth render them effectively targets for cancer treatment (Solimini, Luo et al. 2007, Luo, Solimini et al. 2009). It might appear counter intuitive that proteins which have functional roles in both normal and malignant cells could be useful in cancer treatment but in practice targeting HSPs has demonstrated benefits for cancer patients. For instance the loss of HSP chaperoning functions induces mitochondrial membrane permeabilization followed by immediate cell death in many neoplastic cells but not in normal, implying that much of the chaperoning network operates in a cancer specific manner possibly being the Achilles heel of many cancer cells (Kang and Altieri 2009, Kang 2012). It has been observed that tumor cells are selectively sensitive to the anti–HSP90 reagent, 17-(Allylamino)-17-demethoxygeldanamycin (17AAG) of the ansamycin family of drugs (Kamal, Thao et al. 2003, Neckers and Lee 2003, Workman 2004) that interestingly are protective under some circumstance in normal cells. These anti-

HSP90 drugs target a diversity of proteins required for cell growth and are showing promising results in phase 1 and II clinical trials (Neckers and Ivy 2003, Workman 2004, Banerji, Walton et al. 2005).

1.3 The HSP90 family– Hsp90 and Hsp75 (TRAP1)

1.3.1 HSP90

HSP90 activity in various organisms reflects their relative complexity, as it is a molecule that is highly conserved from bacteria to mammals (Bardwell and Craig 1987). It is best known for its association with a variety of signal transduction systems such as those forming complexes with steroid hormone receptors (Joab, Radanyi et al. 1984, Sanchez, Toft et al. 1985). Inhibition of HSP90 results in destabilization of the complexes and its protein substrate is then usually targeted for degradation, in effect compromising the intracellular signaling of its substrate. This implies that HSP90 is specialized particularly for aiding in maturation of signal transduction proteins (Nathan, Vos et al. 1997). However further studies have confirmed its additional role as a molecular chaperone, having been found to suppress aggregation of non-native proteins (Jakob, Lilie et al. 1995) and promoting the refolding of substrates in cooperation with HSP70 (Schumacher, Hansen et al. 1996).

In the formation of complexes, HSP90 acts in cooperation with its co-chaperones, Hop, p23 and HSP70 (Felts, Owen et al. 2000). The co-chaperone Hop has the ability to bind both HSP90 and HSP70 and seems to be the link that brings the two chaperones together. The p23 co-chaperone binds HSP90 and stabilizes it. Additionally HSP90 has ATP-binding activity through its N-terminus domain (Grenert, Sullivan et al. 1997, Prodromou, Roe et al. 1997,

Felts, Owen et al. 2000). HSP90 ATP binding and hydrolysis are also associated with its ability to interact with substrate proteins and its co-chaperones Hop and p23 (Grenert, Sullivan et al. 1997, Obermann, Sondermann et al. 1998, Prodromou, Siligardi et al. 1999). Importantly HSP90 needs to bind ATP in order to form a to complex with its co-chaperone p23, which is a crucial step in enabling HSP90 to carry out its function (Felts, Owen et al. 2000).

1.3.2 HSP75 (TRAP1)

It is widely reported that HSPs are frequently up-regulated in malignant cells (Chant, Rose et al. 1995) which is an implication of the high demand for protein refolding in a tumorigenic environment of acidosis, nutritional deprivation, severe hypoxia and oncogenic mutations (Chen, Chen et al. 1996, Whitesell and Lindquist 2005, Kang 2012). However in gene micro-array studies from our laboratory, we made a surprising observation of a down regulation of certain HSP/protein folding genes mRNA in some non-small cell lung cancers when compared to normal lung samples (Hu personal communication). One such down-regulated HSP in this study was HSP75 (TRAP1).

TRAP1 has been shown to assist in the refolding of denatured Retinoblastoma (Rb) to a protease-resistant state (Chen, Chen et al. 1996). In the mammalian cell the relationship between Rb and TRAP1 comes into play when they form a complex under two specific conditions: 1) during the M phase when the membrane separating the nucleus from the cytoplasm breaks apart and 2) in the event of heat shock when TRAP1 translocates from the cytoplasm to the nucleus where it potentially refolds denatured Rb to its active conformation (Chen, Chen et al. 1996). Since the Rb pathway is central to human cancer we began to

investigate the significance of TRAP1 expression in cancer and how its expression or lack of it affects cell cycle and growth.

TRAP1 is primarily localized in the mitochondria (Felts, Owen et al. 2000). It was first identified as a protein that interacted with the intracellular domain of type 1 tumor necrosis factor receptor 1 (TNFR1) (Song, Dunbar et al. 1995), making it a significant protein in its signal transduction pathway. It has also been shown to be involved in protecting cells from cyclophillin D mediated apoptosis (Masuda, Shima et al. 2004, Kang, Plescia et al. 2007) and oxidative stress (Montesano Gesualdi, Chirico et al. 2007, Neckers, Kern et al. 2007). An open reading frame of the longest TRAP1 cDNA extracted via the yeast two-hybrid system using retinoblastoma as bait, coded for a protein with substantial sequence homology to the HSP90 family (Chen, Chen et al. 1996). Just like HSP90, TRAP1 is also an ATP-binding protein with ATPase activity that can be inhibited by geldanamycin, hence securing TRAP1's position in the HSP90 protein family (Felts, Owen et al. 2000). However TRAP1 does not form stable complexes with the classic HSP90 co-chaperones Hop and p23 which are required for HSP90 chaperoning functions. Studies have shown that the c-terminal region of HSP90 required to bind co-chaperones do not exist in TRAP1 (Chen, Sullivan et al. 1998). Additionally TRAP1 does not inhibit HSP90 dependent reconstitution of PR-hormone binding nor does it substitute for HSP90 in this system. TRAP1 has very little activity in luciferase refolding assays that utilize HSP70, HSP90 and Hop, implying that its chaperoning function is different from that of HSP90 (Johnson, Schumacher et al. 1998).

TRAP1 may play an oncogenic role by way of inhibiting apoptosis and oxidative stress (Masuda, Shima et al. 2004, Kang, Plescia et al. 2007) but in the event of a shock such as hypoxia, TRAP1 may have a tumor suppressor effect by maintaining Rb1 in its active

conformation (Chen, Chen et al. 1996). However no studies have yet investigated how TRAP1 regulates the Rb1/E2F pathway.

Data from our laboratory demonstrated that following induction of hypoxia, TRAP1 moves to the nucleus and binds to Rb1. If TRAP1 is silenced, the total amount of Rb1 is diminished and following hypoxia, Rb1 fails to bind to E2F1; as a consequence, more cells enter S phase. Re-establishment of TRAP1 expression reverses this effect. This effect however appears to be, at least in vitro, transient and disappears after the first 24 hours (Hu et al. Manuscript submitted). Additionally work demonstrated that TRAP1 holds Rb in the hypophosphorylated state to enable RB-E2F1 complex formation(Tan, Pezzella et al. 2007). Loss of TRAP1 reduced Rb-E2F1 complex formation significantly in hypoxia and deregulated the G1 restriction point control with a significant increase in S phase fraction but this did not occur in normoxia.

Hypoxia induces G1 arrest in cells (Raleigh, Calkins-Adams et al. 1998, Webster, Hodgkiss et al. 1998) and is associated with hypophosphorylated Rb (Ludlow, Glendening et al. 1993). Tan speculated that, during the first 24 hours of hypoxia, loss of TRAP1 reverses the hypoxia-induced Rb1-driven G1 arrest. In the first hours of hypoxia induction, in absence of it chaperone TRAP1, Rb would fail to remain properly folded and would therefore be inactivated. Its inactivation leads to loss of Rb-mediated repression of E2F1 which then would allow maintenance of cellular proliferation in spite of a low oxygen tension. This was the premise of the hypothesis that TRAP1 loss in some cancers may favors a more aggressive phenotype that continues to proliferate even under hypoxia conditions (Tan 2007).

However more recent experiments “in vitro” looking at cell cultures over a five days period, show that in hypoxia the accumulation of TRAP1 in the nucleus, where it chaperones Rb1,

stops after the first 24 hours and then the also the nucleus levels of TRAP1 start to diminish after approximately 48 hours, while cytoplasmic TRAP1 remains steady in normoxic cells. Hypoxia and slower proliferation are associated with loss of cytoplasmic TRAP1 while normoxia and high proliferation are associated with steady cytoplasmic levels. (Agoreta et al manuscript in preparation).

1.4 Junctional mediating protein (JMY)

As discussed above, work done in our laboratory suggested that TRAP1, while having a tumor suppressor effect in the first 24 hours following a shock, by transiently moving to the nucleus and maintaining RB1 in an active conformation, could have, in the longer term, an oncogenic effect possibly by promoting cell proliferation (Agorreta et al manuscript in preparation). This hypothesis was supported by micro array studies done to identify genes and pathways associated with TRAP1 (Liu, Hu et al. 2010). TRAP1 expression is directly associated with transcription of genes promoting cell proliferation but inversely associated with expression of genes promoting metastasis and cell motility. TRAP1 appears to regulate cell proliferation both in normoxia and hypoxia via pathways activated by TNF and by genes such as those coding for G protein coupled receptors. In contrast, it upregulates genes promoting cell-cell/cell matrix adhesion, tight junctions and cadherins but inhibits transcription of genes involved in metastasis including one gene which one appeared to us to be of particular interest: the Junctional Mediating and regulator protein (JMY)(Liu et al., 2010).

JMY was originally identified as a CBP/p300 co-factor regulating p53 response in the nucleus: upon DNA damage, it was observed that JMY formed a complex with Strap and p300 that recruits PRMT5 into a co-activator complex that drives the p53 response (Coutts, Weston et al.

2009). According to Coutts et.al, JMY's functional role in p53 response is evident in JMY's increase of p53-dependent transcription and apoptosis. A transcriptional co-factor role of JMY is observed in its ectopic expression without altering p53 protein levels (Coutts and La Thangue 2005). Also studies have shown JMY to be an MdM2 target for ubiquitination and degradation through which MDM2 regulates p53 activity. Consistent with its role as a p53 cofactor upon DNA damage, JMY is released from MdM2 allowing it to contribute to the p53 response (Coutts and La Thangue 2005).

JMY localizes primarily in the nucleus in HL60 cells (Zuchero, Coutts et al. 2009) and shuttles between the nucleus and cytoplasm (Roadcap and Bear 2009). Metastasis is facilitated by increased cell motility, allowing tumors to invade and colonize surrounding as well as distant tissues. In addition to its effect on p53, JMY has also another very interesting effect, it enhances cell motility (Coutts, Weston et al. 2009). JMY contains a series of WH2 domains that promote actin nucleation or elongation enabling it to promote cell motility (Paunola, Mattila et al. 2002, Coutts, Weston et al. 2009). Other studies have shown that JMY nucleates actin in vitro and induces actin filament formation in vivo as a consequence of its inherent WH2 domain series (Coutts, Weston et al. 2009, Zuchero, Coutts et al. 2009). Via its WH2 domain, JMY is also able to down-regulate E-cadherin, an adherens junction protein required for cell-cell adhesion that is known to be lost during the course of tumor progression (D'Souza-Schorey 2005, Jeanes, Gottardi et al. 2008). This loss of E-cadherin also favors cell motility, metastasis and invasion. This in effect supports our hypothesis generated by our micro array study showing an inverse relationship between JMY and TRAP1: hypoxia leads to slower proliferation and decreased TRAP1 with increased JMY which in turn, promote cell motility in order to escape the hypoxic environment.

Interestingly Coutts et al have demonstrated that when JMY shuttles into the nucleus to facilitate transcriptional control of P53 in response to DNA damage, JMY's contribution to cell motility becomes limited (Coutts, Weston et al. 2009). This implies that JMY is playing a dual role. It is then important to reconcile the involvement of JMY in the two different cellular processes of transcriptional and actin dynamic regulation and their role in tumorigenesis.

1.4.1 JMY and Cell Motility

Actin filaments provide the structural basis for cell motility and are critical to numerous physiological processes such as morphogenesis, wound healing, migration and membrane transport as well as metastasis (Roadcap and Bear 2009). Actin filament formation occurs either via branching of already existing actin filament or alternatively via de-novo nucleation of actin monomers (Roadcap and Bear 2009). Spontaneous assembly and nucleation of actin trimers and dimers are kinetically unfavorable so to counteract this obstacle cells use actin nucleators and nucleation promoting factors (NPF) to jump start actin nucleation and filament formation. Actin formation via branching is usually facilitated by the actin nucleator 'Actin related protein 2/3 complex' (ARP2/3). ARP2/3 is activated by NPFs via their 'Wiskott Aldrich Syndrome protein (WASp) homology-2' domain (also known as WH2 domain), which are actin binding motifs that enable assembly of actin monomers (Campellone and Welch 2010). The de-novo nucleation however is produced by nucleators such as 'Spire' that themselves contain WH2 domains and do not require activation by NPFs (Coutts, Weston et al. 2009, Campellone and Welch 2010).

Zuchero et al (Zuchero, Coutts et al. 2009) demonstrated that purified JMY biochemically activates actin polymerization in a dose dependent fashion. Additionally they demonstrated that

JMY inherently possessed WH2 domains and was able to catalyze new filament formation in a Spire-like fashion, in the absence of Arp2/3 activity. This implies that JMY is capable of producing both forms of biochemical actin filament formations (Zuchero, Coutts et al. 2009). Having both forms of biochemical actin polymerization would also imply importantly that JMY's contribution to cell motility is via its nucleation filament and that JMY can promote rapid assembly of a new actin network by harnessing its ability to first nucleate new mother filaments and then activate Arp2/3 to branch off these filaments. Also the duality of JMY localization and functions between the cytoplasm and nucleus might be a gained evolutionary advantage of JMY in lieu of its ability to promote actin polymerization in a different cellular context either in the cytoplasm in the presence of Arp2/3 or in the nucleus in the absence of Arp2/3 (Roadcap and Bear 2009, Zuchero, Coutts et al. 2009).

1.4.2 JMY and Metastasis

Metastasis is facilitated by increased cell motility allowing tumors to invade and colonize surrounding as well as distant tissues and JMY is known to enhance cell motility "in vitro'. The ability of JMY to influence cell motility is dependent in part on its control of cadherin expression and in part its WH2 series function and their role in promoting actin nucleation and elongation (Coutts, Weston et al. 2009).

Cadherins such as E and N cadherins are adherens junction proteins responsible for cell-cell adhesion (Coutts, Weston et al. 2009), with E-cadherin being the major cadherin molecule expressed by epithelial cells (Nam, Ino et al. 2004). Cell –cell adhesion is intimately connected to cell migration, invasion and tumor progression. At cell-cell junctions, cadherin proteins from one cell form transmembrane contacts with cadherin proteins in neighboring cells, while the

cytoplasmic domain associates with cytosolic catenins. All together this complex is functionally linked to the actin cytoskeleton via alpha catenin (Syed, Mak et al. 2008). The main body of evidence now favors the view that dysfunction of the E-cadherin mediated cell adhesion system playing a role in cancer invasion and metastasis. As a matter of fact down-regulation of E-cadherin has been reported in various human carcinomas and further shows a close relationship to metastatic ability in clinical cases (Hirohashi 2000, Nam, Ino et al. 2004). JMY is also able to down-regulate E-cadherin: studies by Coutts et al have demonstrated that depletion of JMY resulted in decreased cell motility and alteration of cell morphology that correlates with alteration of cellular adhesion. Additionally they also show a marked up-regulation of E-cadherin in JMY siRNA treated MCF7 cells, while simultaneous depletion of JMY and E-cadherin or N-cadherin rescued the decrease of cell motility upon JMY depletion. This suggests that JMY could increase the metastatic ability of one cell on one side by increasing cell motility and on another side via a mechanism that modulates cadherin stability (Coutts, Weston et al. 2009, Wang 2010).

1.4.3 JMY and Hypoxia

Hypoxia triggers adaptive response and is an important physiological stress that is relevant in tumor progression (Harris 2002). Human cancer frequently has areas of necrosis in which cancer cells have died due to inadequate oxygenation while the cells closest to a perfused blood vessel remain viable as are exposed to relatively higher O2 concentration. Although such oxygen concentration gradients exist in normal tissues they are much steeper in tumors to the extent of the oxygen concentration dropping to zero which ultimately leads to necrosis in these regions (Semenza 2010). So as the size of a tumor increases, oxygen tension continues to decline creating a hypoxic state (Harris 2002, Coutts, Pires et al. 2011). Oxygen concentration

regulates HIF 1, a hetero-dimeric complex of HIF 1 α and HIF1β(Wang, Jiang et al. 1995). HIF-1α is stabilized in hypoxia (Harris 2002, Semenza 2010). The HIF-1 complex acts in the nucleus where it binds to hypoxia response elements of HIF regulated genes coding for proteins crucial for adaptation and survival of the cell under hypoxic stress (Semenza 2010, Coutts, Pires et al. 2011).

JMY is a stress and hypoxia responsive protein and is sensitive to oxygen tension (Coutts, Pires et al. 2011). JMY is up-regulated during hypoxia as its transcriptional regulation is hypoxia responsive, HIF1α dependent and possesses an HRE that recruits HIF1α to its promoter (Coutts, Pires et al. 2011). Evidence for this is reflected in an experiment with an MCF7 cell line depleted of HIF1α (HIF1α siRNA) and exposed to hypoxia by treatment with desferoxamine [DFO] (an iron chelator whose effects mimic certain properties of hypoxia) that failed to upregulate JMY. The same cells treated only with DFO showed both JMY and HIF1α upregulation whereas co-treatment with DFO and HIF1α inhibitor resulted reduced HIF 1α and JMY upregulation. Also in vivo data is consistent with this in vitro data by showing a HIF1α dependent JMY upregulation in hypoxia in anti-VEGF treated tumors (Coutts, Pires et al. 2011).

Hypoxia facilitates increased cell motility and is a driving force for cancer metastasis inciting tumors to seek out a more oxygenated environment and in effect invade and colonize surrounding as well as distant tissues (Coutts, Weston et al. 2009, Coutts, Pires et al. 2011). The adaptation to hypoxia promotes many key aspects of cancer progression mainly because cancer cells co-opt adaptive responses in which normal feedback mechanisms have been disrupted by somatic mutation and epigenetic changes (Semenza 2010). This would also imply

that JMY, a hypoxia responsive protein, is vital in the promotion of hypoxia induced metastasis via a HIF1α dependent pathway. JMY depletion in MCF7 cell lines demonstrated that there was a marked decrease in the ability of these cells to migrate into newly formed wounds (where the ability to do so is a litmus test for cell migration), with a 17% wound closure after 24 hour, while the control cells showed a higher migration rate with a 37% wound closure in the same amount of time. Similar results were also observed in 2 other cell types (Coutts, Pires et al. 2011). This indicates that JMY is crucial for cell motility and invasion during hypoxia possibly facilitated through its ability to foster actin nucleation.

This interplay between JMY and HIF1α uncovers another novel facet in cell motility regulation under hypoxic conditions. JMY's ability to mobilize cancer cells facing a severe hypoxic microenvironment and in effect facilitating metastasis deems it a putative metastatic marker that could be targeted clinically as a cancer treatment.

1.5 Angiogenesis versus non-angiogenesis

1.5.1 Introduction

This final theme of the thesis addresses the prospect of a novel pathway for cancer progression. A genomic data analysis of TRAP1 in non-small cell carcinoma lead us to the discovery of a difference in tumor growth that may be either angiogenic or non-angiogenic. Additional personal observations also suggested an association between cytoplasmic p53 and non-angiogenic tumors. So I set out to further characterize the angiogenic and non-angiogenic cancer phenotypes

For many years there has been controversy about tumor growth and neovascularization. Early workers often regarded blood vessels as sub-ordinate in potential clinical interest to the tumor cells themselves. Goldman (Goldmann 1908)regarded an increase in vascularity seen in and around tumors as a host reaction while others dismissed it as inflammation. Around the 1940's it was observed that tumors could themselves stimulate vascular proliferation and that the characteristic hyperemia seen around tumors was related to tumor proliferation (Coman and Sheldon 1946). However it wasn't until 1970 that Judah Folkman and co-workers established that study of tumor vasculature was of itself a vital part of tumor research and that angiogenesis was fundamental to tumor growth. Importantly, it was suggested that tumor vessels could be deliberately targeted and destroyed by specific drugs, which could potentially lead to the regression of the entire tumor (Folkman, Cole et al. 1966, Folkman 1972).

1.5.2 How Do Tumors Gain Blood Supply

All tumors clearly require a blood supply in order to flourish. In early experiments it was noted that small tumor spheroids suspended in soft agar with growing medium grew no larger than 1-2mm (Folkman 1995) and a clinical parallel was observed in the numerous miniscule tumors that classically 'seed' intra-peritoneally from certain tumor types. It was hypothesized that these remained small, white and inactive due to a lack of vessels (Folkman 1985). Animal models of angiogenesis were developed with tumor cells seeded into avascular areas such as the cornea (Gimbrone, Cotran et al. 1974), the anterior eye chamber (Gimbrone, Leapman et al. 1972) or an artificial tumor window chamber which showed a small (< $2mm^3$), initially avascular, aggregate of cells that failed to grow larger until vascularized (Gimbrone, Leapman et al. 1972). Angiogenesis (later defined as the development of new blood vessels following the proliferation of the endothelial cells from pre-existing vessels) was proposed to be an

absolute requirement for tumor growth beyond a critical size of 2-3mm^3 (related to the theoretical diffusion distance for oxygen) (Carlsson, Stalnacke et al. 1979).

It was demonstrated that the tumor cells themselves could induce the in-growth of new vessels by means of the production and secretion of an angiogenic factor (Shing, Folkman et al. 1984). Many other pro- and anti-angiogenic molecules were subsequently identified, produced both by tumor and other cells and the circumstances affecting their relative balance and the consequent initiation or inhibition of angiogenesis (the 'angiogenic switch') studied (Folkman 1995). Angiogenesis is now regarded as one of the six major hallmarks of tumor development described by Hanahan and Weinberg in 2000 (Hanahan and Weinberg 2000) and is still considered pivotal in the recently updated 'Hallmarks of Cancer: The next generation' (Hanahan and Weinberg 2011). Important related research has identified mechanisms by which hypoxia is sensed and responded to, including angiogenesis initiation (Pezzella, Pastorino et al. 1997, Azam, Mehta et al. 2010, Bridges and Harris 2011, Potente, Gerhardt et al. 2011). As already discussed in the previous paragraphs, in response to hypoxia HIF1α gets stabilized, binds to its dimer HIF1β and translocates into the nucleus. Here the HIF heterodimer transcriptionally activates hypoxic response genes particularly Vascular Endothelial Growth Factor (VEGF) that is an essential factor for neovascularization and angiogenesis (Teodoro, Evans et al. 2007, Carmeliet and Jain 2011).

1.5.3 Anti-Angiogenic Therapy

Many pro- and anti-angiogenic molecules have been identified and translated into clinical use allowing the anti-angiogenic treatment of cancer to advance from theory to a therapeutic option. The anti-VEGF antibody Bevacizumab [Avastin]in combination with chemotherapy

was reported in 2006 to produce an increased overall survival in metastatic colorectal cancer (Potente, Gerhardt et al. 2011). It became the first FDA approved anti-angiogenic drug. It was later approved in combination with chemotherapy or cytokine therapy for several other advanced metastatic cancers, including non-squamous non-small cell lung cancer and renal cell cancer (RCC). Also based on a randomized phase II trial, bevacizumab monotherapy has been approved for recurrent glioblastoma cancer (Potente, Gerhardt et al. 2011) Four multitargeted pan-VEGF receptor tyrosine kinase inhibitors (RTKIs) have also been approved: Sunitinib [Sutent] and Pazopanib [Votrient] for metastatic RCC, Sorafenib [Nexavar] for metastatic RCC and unresectable hepatocellular carcinoma, and Vandetanib [Zactima] for medullary thyroid cancer (Potente, Gerhardt et al. 2011) Sunitinib has also been recommended for treatment of advanced pancreatic neuroendocrine tumors (PNET) (Naresh, Nerurkar et al. 2001). However there have been numerous failures with these treatments. Anti-angiogenic drugs as anti-VEGF antibody and RTKIs have slowed metastatic disease progression in some patients, leading to increased progression-free survival (PFS). However, the results are more modest than predicted by preclinical testing and the benefits in PFS are often not accompanied by increased overall survival (Ebos and Kerbel 2011). The list of potential pitfalls in anti-angiogenic treatment is long with several mechanisms proposed for different malignancies and tumors at various stages of development (Bridges and Harris 2011). Consequently, finding predictive markers in anti-angiogenic therapy is highly desirable but so far no predictive marker has been established in a clinical setting.

1.5.4 Non-angiogenesis

Several recent reviews have focused on the potential pitfalls of anti-angiogenic treatment and offered different explanations for drug resistance (Azam, Mehta et al. 2010, Carmeliet and Jain 2011, Ebos and Kerbel 2011, Potente, Gerhardt et al. 2011). An alternative tumor blood supply to angiogenesis has been proposed as one of many potential explanations why anti-angiogenic treatment has been less effective than expected. There is growing evidence that in certain situations tumors can obtain sufficient blood supplies from pre-existing vascular beds to grow without angiogenesis. This form of neoplastic growth has been termed non-angiogenec tumor progression (Pezzella, Pastorino et al. 1997, Holash, Maisonpierre et al. 1999, Pezzella, Harris et al. 2001, Adighibe, Micklem et al. 2006). It has also been described as a tumor blood supply in which tumor cells hijack the existing vasculature and tumor cells migrate along the vessels of the host organ: these co-opted vessels are fully mature as indicated by both morphology and vessel phenotype (Passalidou, Trivella et al. 2002). This form of tumor growth challenges the universality of the hypothesis that angiogenesis is an absolute requirement for tumor growth and suggest that the vasculature of human tumors is more complicated than initially anticipated (Adighibe, Micklem et al. 2006).

Non-angiogenesis has been described in both humans and animals. In our laboratory it has been described in non-small cell cancer lung tumors as neoplastic cells filling the alveolar spaces with no evidence of vascularization but a co-option of pre-existing pulmonary blood vessels. These non-angiogenic cases were also observed to be more aggressive clinically than the predominant angiogenic tumors(Pezzella, Harris et al. 2001).

Colpaert et al (Colpaert, Vermeulen et al. 2003) have described it as ‘an infiltrative‘ growth pattern in non-angiogenic breast cancer metastases to the skin. The tumor infiltrated without destroying dermal structures, including blood vessels, which were seen incorporated into the tumor. Endothelial cell proliferation, a marker of angiogenesis, was significantly reduced in comparison with the aggressive ‘desmoplastic’ pattern. The same growth patterns, with preservation of architecture in ‘non-angiogenic replacement’ type tumors, were seen in lymph node metastases from ductal breast carcinoma and in liver metastases from colorectal and breast carcinomas (Colpaert, Vermeulen et al. 2003). In animals, non-angiogenic progression has been described in artificially induced melanoma metastasis in mouse brain (Kusters, Leenders et al. 2002) and in a rat glioma model (Holash, Maisonpierre et al. 1999)

In addition to ‘pure’ non-angiogenic tumors a mixed phenotype is often observed (Pezzella, Pastorino et al. 1997, Offersen, Pfeiffer et al. 2001, Funai, Yokose et al. 2003) suggesting that non-angiogenic tumors, rather than being distinct subtype, are probably only one extreme of a fairly widespread process occurring in many tumors. In these mixed cases the vessel co-option component is often observed at the actively growing edges, with the more mature centre showing a switch to an angiogenic phenotype.

1.5.5 Characterization of angiogenic and non-angiogenic tumors

Micro vessel density count is one of the techniques used as a surrogate to evaluate angiogenesis. It is based on counting vessel density in a tumor with so-called hot spots being representative of major angiogenic regions. A drawback with this technique is that it does not account for the potential presence in a tumor of co-opted mature vessels. For instance, a non-angiogenic tumor growing by co-opting a densely vascular bed would by MVD be described as

a highly angiogenic region (Hlatky, Hahnfeldt et al. 2002, Vermeulen, Gasparini et al. 2002). The fraction of proliferating endothelial cells, highlighted by double-immunostaining with endothelial cell associated antibodies such as CD34 or Factor VIII and proliferation associated antibodies such as Ki67 or PCNA, has therefore been proposed as a more reliable measure of ongoing angiogenesis than MVD (Sardari Nia, Colpaert et al. 2004, Arnes, Stefansson et al. 2011).

Another technique is by characterizing the vascular phenotype of angiogenic tumors versus that of non-angiogenic specimens. Angiogenic vasculatures are predominantly immature whilst the non-angiogenic involve co-opting vasculature from normal or already existing blood vessels and are more mature blood vessels. Mature blood vessel are surrounded by pericytes and characterized by markers such as smooth muscle actin (SMA) and LH39 making immunostaining for these markers a potential means of differentiating angiogenic from non-angiogenic tumors. Passilidou et al demonstrated that LH39 was expressed by all vessels in normal and non-angiogenic tumors but on only a small minority of angiogenic tumors (Passalidou, Trivella et al. 2002).

Finally, I have demonstrated the different morphological patterns between these two tumors with a comparative 3Dimensional reconstruction of the tumor and its vasculature. This involved selecting 200 serial sections of normal lung, angiogenic and non-angiogenic tumors respectively, staining the serial sections with antibodies to vessel wall antigens coupled with secondary fluorescent markers and photographing them under a fluorescence microscope. The images were then reassembled digitally into a 3-dimensional stack that could be rotated. The angiogenic tumor vessels showed an abnormal branching convoluted morphology while in the non-angiogenic tumor the integrity of the lung architecture was retained while these alveolar

entrapped neoplastic cells continue to thrive without producing new vessels of their own. While too technically demanding to be used to identify non-angiogenic tumors routinely it provides a clear picture of vessel morphology and of the essential differences between a neo-angiogenic and a co-opted blood supply (Adighibe, Micklem et al. 2006).

1.5.6 Non-angiogenic tumors: Incidence and survival

1.5.6.1 Incidence

Tumors with a co-opted blood supply form a significant minority of a range of tumor types, both primary and metastatic, and even a majority in some rare tumors. Table 3 summarizes the proportions of tumors with co-opted blood supplies reported in published studies.

Table 1.1. Reported incidences of tumors with vessel co-option

Reference	Non-angiogenic tumor type	Number of cases	Number co-option tumors	Percentage ofco-option tumors
(Party 2000)	Lung metastases from breast	26	5	19%
(Funai, Yokose et al. 2003)	Peripheral squamous cell carcinoma of the lung	109	5 (+ 50 mixed type)	4.6%
(Guedj, Couvelard et al. 2004)	Mucinous bronchioloalveolar lung carcinoma	3	3	100%
(Mattern, Koomagi et al. 1999)	Squamous cell lung carcinoma	87	17	19.5%
(Offersen, Pfeiffer et al. 2001)	Non small-cell lung carcinoma	143	17 (+ 18 mixed)	12%
(Passalidou, Trivella et al. 2002, Passalidou, Stewart et al. 2003)	Non-small cell lung carcinoma	113	9	8%
(Pezzella, Di Bacco et al. 1996, Pezzella, Harris et al. 2001)	Metastatic tumor to lung	36	8	22%
(Pezzella, Pastorino et al. 1997)	Non-small cell lung carcinoma	500	80	16%
(Stessels, Van den Eynden et al. 2004)	Liver metastases from primary breast cancer	45	43	96%
(Vermeulen, Colpaert et al. 2001)	Liver metastases from primary colorectal adenocarcinomas	26	3	12%
(Sardari Nia, Colpaert et al. 2008)	Non small-cell lung carcinomaNSCLC	239	45	19%

1.5.6.2 Prognostic studies

Studies of primary tumors and their metastases have shown that non-angiogenic tumors, far from representing an early stage in tumor progression, are able to metastasize, probably via invasion of blood vessels. Interestingly, the vascular phenotype of metastases does not necessarily reflect that of the primary since angiogenic tumors can produce non-angiogenic metastases (2000). A significant adverse difference in survival and time of recurrence was identified in the original study of non-small cell lung tumors, most markedly in the stage pT1N0 (Pastorino, Andreola et al. 1997) A study by a different group, while identifying the non-angiogenic pattern in lung carcinoma cases, did not find the correlation with diminished survival, although no differentiation was made between 'mixed' and purely non-angiogenic cases (Offersen, Pfeiffer et al. 2001). However, a further study (Sardari Nia, Colpaert et al. 2004) has confirmed the adverse prognosis on disease-free and overall survival of non-angiogenic growth in NSCLC tumors (hazard ratio=1.8, 95% confidence interval=1.1-2.9, p=0.016).

Table 1.2. Summary of survival data for vessel co-option non-small cell lung tumor

Study	Association of vessel co-option growthpattern with survival	p-value	Number ofco-option cases	Number of angiogenic cases	Stage
(Pastorino, Andreola et a 1997)	Decreased survival (adverse independent prognostic factor)	Relative Risk =1.91, p=0.04	10	84	pT1N0
(Mattern, Koomagi et al 1999)	Decreased survival	P=0.04 log-rank	17	70	I-IIIa
(Offersen, Pfeiffer et al. 2001)	Increased survival	P=0.007, log-rank	17	108	I-III
(Funai, Yokose et al. 2003)	Increased survival		5	49	I
(Sardari Nia, Colpaert et al. 2004)	Decreased survival (adverse independent prognostic factor)	Hazard ratio=1 p=0.016	45	196	I-III
(Sardari Nia, Colpaert et al. 2008)	Decreased survival (adverse independent prognostic factor)	p=0.002, log rank	45	161	I-III

1.5.7 Characteristics of Angiogenic versus Non-angiogenic tumors

Together with inflammation, changes in energy metabolism have been introduced as a new hallmark of cancer (Hanahan and Weinberg 2011). cDNA microarray analysis has been carried out in our laboratory to compare non-angiogenic with angiogenic lung tumors(Hu, Bianchi et al. 2005)and tumors with co-opted blood supplies had higher levels of genes coding for proteins involved in mitochondrial metabolism. This finding suggests a more effective regulation of the intracellular respiratory chain in these tumors. Further, non-angiogenic tumors expressed a panel of hypoxia-related proteins in a manner comparable to angiogenic tumors. We hypothesized that hypoxia induces metabolic re-programming in tumors co-opting the vessels that compensates for the diminished oxygenation and allows neoplastic growth without triggering angiogenesis. In angiogenic tumors, there were higher levels of expression of genes coding for membrane vesicles, angiogenesis and remodeling and inflammation-related pathways supporting this finding is the observation that there is a significant lack of fibrosis or desmoplasia and a reduction in inflammation in tumors with co-opted blood supplies in comparison to angiogenic tumors. This study also found a differential expression of six genes involved in the regulation of apoptosis. The pattern of expression observed suggests that more apoptosis occurs in angiogenic tumors and tumors with a co-opted blood supply have reduced inflammation, decreased apoptosis and a more efficient mitochondrial metabolism (Hu, Bianchi et al. 2005).

In the last decade research related to angiogenesis has been massive, but the investigation on vessel co-option as an alternative blood supply for tumor growth has been more limited. Study of ‘non-angiogenic’ tumor growth is likely to be of particular interest to investigators

developing clinical trials of drugs that target angiogenesis and for the development of new approaches to the study of tumor angiogenesis. Reliable identification of these tumors is essential for the accurate assessment of anti-angiogenic drugs in the most suitable tumors.

As I made an observation suggesting an association between cytoplasmic p53 and non-angiogenic tumors I set out to investigate if p53 and JMY/TRAP1 had any relational correlation to these forms of tumor growth.

The aim of this thesis were:

I) To investigate how the TRAP1 expression affects cell growth ‘in vitro‘ and how this relates to apoptosis, proliferation and hypoxia using spheroid as a 3 dimensional model

II) To raise a characterize a monoclonal antibody specific for JMY to perform both “in vitro” and clinical studies

III) To verify our hypothesis that TRAP1 regulates the expression of JMY, a putative regulator of cell motility and metastatic spread.

IV) To better characterize the immunophenotype of angiogenic and non-angiogenic forms of non-small cell lung carcinoma.

1.6 Plan of investigation

In chapter 3, the effects of TRAP1 expression on the growth of spheroids was investigated.

This technique allows cell growth in 3 dimensions up to a diameter of hundreds of microns, mirroring the state in tissues better than a cultured monolayer. This arrangement allows development of a gradient from normoxia (external surface) to hypoxia (central areas). The growth rate can be assessed by calculating the spheroid volume.

In chapter 4, a monoclonal antibody against JMY was produced and characterized. Furthermore the role of JMY in cancer and its relationships to cell motility/metastasis and its tumor suppressive effect in regards to its association to p53 was investigated.

In chapter 5, since JMY was found in our micro array data to be inversely related to TRAP1 I decided to verify the micro-array results of any relationships or links between JMY and TRAP1.

In chapter 6, I characterized the distinct difference between the two phenotypes of angiogenic and non-angiogenic tumors. I utilized both three dimensional reconstructions and immunophenotyping with a comprehensive panel of markers for this study.

CHAPTER 2
MATERIALS AND METHODS

2.1 Tissue specimens

Clinical specimens were obtained from patients who had received treatment at the John Radcliffe Hospital, Oxford. This collection had ethical committee approval (study number C02.216 – The pathophysiology of human neoplasia). Tissues were fixed in formalin, processed and embedded in paraffin. Tissue microarrays were constructed using the Beecher Instrument manual arrayer MTA-1. Up to four suitable areas of suitable tumor were chosen from a slide stained with Hematoxylin and Eosin (H&E) (Sigma-Aldrich, St. Louis, MO, USA). Areas of necrosis were avoided. From the corresponding tissue block, a 1mm diameter core was extracted and placed in a recipient block.

2.2 Immunohistochemical studies

2.2.1 Immunostaining of tissue sections

4μm sections were cut from paraffin blocks and mounted on slides. Slides were first

Heated at 60^{o}C for 12 mins to melt the wax, dewaxed by immersing in citroclear twice, (6 mins each time) and then rehydrated in graded ethanol solutions (100% ethanol twice, then 50% ethanol once, 5 mins each time). Slides were rinsed in distilled water before antigen retrieval, if indicated. Antigen retrieval was performed by pressure-cooking in either 10mM citrate pH 6.0 (for composition of solutions see Appendix A) or in Tris-EDTA pH 8.0, usually for 1.5min. Slides were allowed to cool for at least 30mins before proceeding further. 0.3% hydrogen peroxide (VWR BDH, Leicestershire, UK) was applied for 5 mins at room temperature to quench any intrinsic tissue peroxidase activity that would falsely enhance the peroxidase

reaction in the final step since the secondary antibody being used is conjugated with horseradish peroxidase. Non-specific binding was blocked by incubating with 2.5% normal horse serum (Vector Laboratories, Burlingame, CA, USA). Primary antibody was then applied. Details of all antibodies used are in Table 1. Substitution of the primary antibody with phosphate-buffered saline (PBS) served as a negative control. Slides were then washed in PBS thrice before the secondary antibody was applied for 30 mins. In general, the Envision kit (Dako) was used. Slides were again washed in PBS thrice before DAB was applied for 8 mins. Slides were immersed in distilled water to stop the reaction and then immersed in H&E for 20 seconds. Coverslips were mounted with aqueous mountant and then left to dry. Frozen tissue sections were stained using a similar protocol, with omission of dewaxing and rehydration and antigen retrieval steps.

The slides were scored simultaneously by two observers. Intensity was scored on a scale of 0 to 3; where 0 = no staining, 1 = weak staining, 2 = moderate staining. 3= strong staining. The percentage of cells staining positively was recorded in absolute numbers. The subcellular location of positive staining was also recorded: nuclear, cytoplasmic, membranous, as was the presence of positive staining in the stroma, vessels and infiltrating inflammatory cells. Disputed scores were discussed and a consensus reached. For tissue microarrays, cores which did not contain tumor tissue or which were more than 50% incomplete were excluded.

Table 2.1. Antibodies used in immunohistochemical studies

Antibody	Source	Species/Clonality /Isotype	Antigen retrieval method	Antibody Dilution	Incubation period
CAIX	Pasterova M75	Mouse/ Monoclonal/ IgG1	None	1:50	0.5h
Caspase 3	R&D System , USA	Rabbit /Polyclonal	Citrate pH6.0	1:1500	1h
HIF-1α	BD Transduction Laboratories	Mouse/ Monoclonal/IgG	Tris/EDTA pH9 pressure cook 1.5min	1:100	16h
JMY	NDCLS, Oxford , UK	Mouse/ Monoclonal/IgG	Tris/EDTA pH9 1.5h pressure cook	Neat	1h
P53	Dako A/S, Glostrup, Denmark	Mouse/ Monoclonal/IgG2b	Tris/EDTA pH9 1.5min pressure cook	1:50	overnight
MIB1	Dako A/S, Glostrup, Denmark	Mouse/Monoclonal/ IgG1	Citrate pH6.0; pressure cook 1.5min	1:50	2.5h
Rb	Dako A/S, Glostrup, Denmark	Mouse/ Monoclonal (IF8)/IgG1	Citrate pH6.0; pressure cook 1.5min	1:50	2.5h
TRAP1	Labvision , Fremont, CA, USA	Mouse/ Monoclonal/ IgG1	Citrate pH6.0; pressure cook 1.5min	1:400	2.5h

2.2.2 Scoring

There are two different method used to score immunostained slides samples

I Sections can be scored as the number of cells (as percent of the total number of neoplastic cells) positive in cytoplasm and in nucleus. Intensity of staining was scored as 0 in negative cells and as 1 for low intensity, 2 intermediate and 3 high. Data were summarized independently for nuclear and cytoplasmic staining as IPS Intensity Percentage Score obtained multiplying the percent of positive cells by the intensity. Therefore such a score is from 0 (a negative case) to 300 (100% of cells with 3 of intensity).

II Angiogenic and Non-angiogenic immunostainings were scored for cytoplasmic and nuclear localization and, for some proteins, membrane staining. Tumors were evaluated for percentage of positive cells (on a scale from 0 to 4) and intensity of staining (from 0 to 3); these two values were then multiplied to provide a score called the "Intensity Percentage Grade" (IPG), the maximum score being 12.

2.3 Procedures for handling RNA

2.3.1 General Techniques

All solutions were prepared using nuclease-free, DEPC-treated water (Ambion).Work surfaces were cleaned with absolute ethanol and RNaseZap (Ambion). All tipsand tubes used were RNAase-free.

2.3.2 Total RNA extraction from cultured cells

The PARIS kit (Ambion) was used according to the manufacturer's instructions toobtain total RNA and protein from the same sample. Cells (numbers ranging from $10^2$to 10^7) grown in monolayers were harvested with PBS containing 3mMethylenediaminetetraacetic acid (EDTA), pelleted and washed once with PBS. Thecell pellet was lysed with 400µl to 600µl of ice-cold Cell Disruption Buffer (PARISkit, Ambion). Protease inhibitors (1 tablet EDTA-free protease inhibitor cocktailtablet per 10ml lysis buffer and 1.5mM Pefabloc SC Plus® (Roche, Basel,Switzerland)) were added to the buffer. Half the lysate volume was used for RNAextraction and the other half was saved for protein analysis. The lysate volume wasadded to an equal volume of 2x Lysis/Binding solution, containing β-mercaptoethanol(Sigma) and mixed gently by inverting the tube 4 to 6 times. An equal volume of100% ethanol was then

added andmixed gently. The mixture was transferred to asilica-membrane column and centrifuged at 17,000xg for 1min. The adsorbed RNAwas washed once with 700µl of Wash Solution 1, and a further 2 times with 500µL of Wash Solution 2. The column was centrifuged for another 30s to remove any residual ethanol from the wash solution. RNA was eluted from the column with a total of 40µlof Elution buffer (pre-heated up to 95°C). The elution step was done twice to maximize the recovery of RNA from the silica membrane. RNA could be stored at -80°C for up to a week before proceeding further.

2.3.3 DNase Treatment

Total RNA extracted was subjected to DNase-free treatment (Ambion) to remove contaminating DNA to levels below the limit of detection of routine PCR. With the RNA extraction protocol in the previous section (2.4.2), RNA concentrations of between 200ng/µl to 300ng/µl were routinely obtained. As such, 1µl of DNAase(2U/µl) and 5µl of 10x DNase I Buffer were added to 44µL of RNA sample and incubated at 37°C for 30min. The reaction was terminated by the addition of 5µl of DNase Inactivating Reagent and the sample was incubated at room temperature for2mins with occasional mixing. Samples were centrifuged at 17,000xg for 1.5 minutes. The supernatant was transferred to a new RNase-free tube without disturbing the pellet containing the DNase Inactivating Reagent. RNA yield was analyzed by spectrophotometry at 260nm. RNA could be stored at -80°C for up to a week.

2.3.4 Spectrophotometric quantitation of nucleic acids

Both DNA and RNA were quantified by measuring the UV absorbance at 260nm(A_{260}) using the ND-1000 spectrophotometer (Nanodrop Technologies, Wilmington,DE, USA) supported with NanoDrop version 3.0.1 software. The ND-1000 was cleaned with distilled water before every use. A 1.2µl sample of distilled water was placed on the sample pedestal to initialize the

machine, as suggested by the manufacturer. A fresh 1.2µl sample of distilled water was used to blank the ND-1000 prior to sample measurement. The sample pedestal was wiped after every sample with a clean Kim Wipe (Kimberly-Clark, UK). A 1.2µl sample of either DNA or RNA was pipetted onto the sample pedestal and a reading taken. All readings were printed out and stored for record. DNA was quantified used the DNA-50 presets and RNA was quantified using the RNA-40 presets. Assuming the weight of a nucleotide pair is 660Da, the following formula was used: 1 unit A_{260} was equivalent to 50µg/ml for double-stranded DNA and 40µg/ml for RNA. The purity of DNA or RNA was assessed by the ratio of A_{260} to A_{280} values, and should be between 1.8 to 2.1.

2.3.5 Reverse transcription (RT)

cDNA was synthesized by reverse transcription of total RNA using the RetroScript kit(Ambion). Generally 1µg of RNA was reverse transcribed in each reaction. 1µg ofRNA was added to 2µl of oligo(dT) primers and made up to a final volume of 12µlwith DEPC water. The tube was gently flicked to mix the components and briefly spun down at 17,000xg. The reaction was heated to 85°C for 3min and then removed onto ice. A mastermix comprising of 2µl 10x RT buffer, 4µl dNTP mix, 1µl RNaseinhibitor and 1µl MMLV-RT per reaction was prepared. Eight microliters of the mastermix was added to each PCR reaction tube. Reactions were then placed in a Peltier Thermo Cyler (MJ Research,Waltham, MA, USA) and incubated under the following conditions: 44°C for 1h and 92°C for 10min. cDNA was then diluted with DEPC-treated water to achieve a final concentration of 5ng/µl and stored at -20°C until PCR analysis.

2.3.6 Quantitative real-time PCR (art-PCR)

2.3.6.1 Primer sequences

Primers for art-PCR were designed using the web-based Universal Probe Library Assay Design Center (Roche Applied Science, www.roche-applied-science.com). The primers were synthesized by Operon Biotechnologies (Cologne, Germany) and probes were supplied by Roche.

Table 2.2 . Primers used

Gene Name	Accession Number	Forward Primer	Reverse Primer
β-actin	NM_001101	cccagcacaatgaagatcaa	cgatccacacggagtacttg
JMY	NM_152405.4	gtagagcttttggacttg	tctgatctgctcgcatcc
TRAP1	ENST00000246957.2	agaccaatgccgagaaagg	tcctgtgtcatcccgatacc

2.3.6.2 Quantitative real-time PCR (qRT-PCR)

qRT-PCR was performed using primers and specific PCR probes as described in the preceding section (2.3.6.1)(Pfaffl 2001, Kruhoffer, Jensen et al. 2005). The analysis was performed on the Rotor Gene 3000® qPCR System (Corbett Research, Sydney,Australia) using the ABSOLUTE® qPCR Master Mix (ABgene, Epsom, UK). Each sample was run in triplicate, therefore to evaluate gene expression of 1 sample, amaster mix was made up consisting of 12.5µl of ABSOLUTE qPCR Master Mix, 1µleach of forward and reverse primers, 0.25µl PCR probe and 5.25µl of nuclease-freewater. To this was added 5µl (25ng) of cDNA. Conditions for the PCR reaction were2 min at 50°C, 10 min at 95°C and then 40 cycles, each consisting of 15 seconds at 95°Cand 1 min at 60°C. The housekeeping genes (HKGs) were screened and

selected from a panel of 12 commonly used HKGs as previously described (Vandesompele etal., 2002). The reaction efficiency for each gene was calculated after obtaining standard curves for each PCR reaction by making 10-fold serial dilutions covering the range equivalent to 50 to 0.5ng of RNA.

Relative quantification of expression of the gene of interest was derived using the normalization factor calculation based on geometric mean of multiple HKGs as previously reported(Vandesompele, De Preter et al. 2002). Briefly, threshold cycle (Ct) values from all samples for each gene of interest (GOI) and HKG were converted to raw expression values. Next, GOIs were then normalized to a factor based on the geometric mean of the raw expression values of the HKGs for a given sample. Normalized GOI expression values could then be rescaled according to any internal control samples. Though error propagation was calculated as standard deviation (SD)throughout calculations, final results were reported with standard error (SE) in order to reflect the multiple measurements upon which results are based. For qRT-PCR using clinical specimens, relative quantification of gene expression was done using the method described by Pfaffl et al (Pfaffl 2001).The relative ratio of gene expression was calculated as [(Etarget) $^{\Delta CtTARGET (mean\ comparator\ -mean\ sample)}$] ÷ [(Eref) $^{\Delta CtREF(mean\ comparator\ -\ mean\ sample)}$], where Etarget is reaction efficiency of the gene of interest; Eref, reaction efficiency of the reference gene; and ΔCt, the cycle difference between the comparator and the sample. All calculations were based on the mean value of PCR reactions done in triplicate.

2.4 Cell Culture

2.4.1 General Growth Conditions

Cells were grown in tissue culture incubators in a humidified atmosphere of 5% CO_2,95% filtered atmospheric air, and maintained at a temperature of 37°C. Cells were cultured on

sterile, tissue-culture grade polystyrene, non-pyrogenic plastic ware including 75cm2 and 175cm2 flasks with vented cap, 150 x 25mm; 100 x 20mm and60 x 15mm dishes and 6-well and 24-well tissue culture plates (Sarstedt, Nu¨mbrecht,Germany) (Table 3).

Table 2.3.Details of culture vessels used.

Culture vessel	Surface area(mm^2)	Seeding density	Volume ofEDTA (ml)	Volume ofgrowth medium(ml)
10cm dish	7,854	2.2 X 10^6	5	10
15cm dish	17,671	5.0 X 10^6	10	20
6-well plate	962	0.3 X 10^6	2	3
75cm^2 flask	7,500	2.1 X 10^6	5	10
175cm^2 flask	16,000	4.6 X 10^6	10	20

2.4.2 Recovery of Cryo-preserved Cells

20ml of warm (37°C) culture medium was prepared in advance in a sterile falcon tube

(BD Biosciences, San Jose, CA, USA). A vial of cryo-preserved cells was retrievedfrom the nitrogen tank (vapor phase) and rapidly thawed in a 37°C water bath, swirling the tube constantly to ensure even thawing. As soon as the cells appeared to have thawed completely, they were transferred to the prepared falcon tubes with a sterile disposable Pasteur pipette (Sarstedt). The cells were centrifuged at 1,300rpmfor 3min and the supernatant aspirated and discarded. The cell pellet was then resuspended in warm culture medium and transferred to a 75cm^2or a 175cm^2flask.

2.4.3 Sub-culturing of cells

Cells were sub-cultured when 80% to 90% confluent. IMR90, MRC-5 and MCF10Acells were routinely split 1 in 5, HEK293 and MDA231 cells 1 in 20. The rest of the cells were sub-cultured at a 1 in 10 ratio. Culture medium was aspirated and discarded

and cells were detached from the flasks using pre-warmed (37°C) 3mM EDTA in PBS. The flasks were incubated at 37°C for 3min to 5min (up to 15min for MCF10A cells) to allow for complete detachment. An equal volume of culture medium was then added to neutralize the EDTA. The cell suspension was then transferred to a 50ml sterile falcon tube, and centrifuged at 1,300rpm for 3min. The medium was aspirated and discarded and the cell pellet re-suspended in fresh culture medium and transferred to a new tissue culture flask.

2.4.4 Preparation of Cell Stocks (Cryopreservation)

Only cells in the log phase of growth were used for cryopreservation. Cells were detached and centrifuged as in section 2.5.3. The cell pellet was re-suspended in freezing medium (about 5 million cells per ml), and transferred into 2ml Corning round-bottomed cryogenic vials (Fisher Scientific, Waltham, MA, USA). Freezing medium was made up with 10% dimethylsufloxide (DSMO) (Sigma), 40% FCS(Sigma), and 50% cell culture medium. The cryovials were incubated on ice for about1 hour before being stored overnight at -80°C in an isopropanol-bath freezing container. Cryovials were transferred to nitrogen tank (vapor phase) for long-term storage.

2.4.5 Cell lines

All cells were free from Mycoplasma contamination.

Cell Line name	Short Description	Growth Medium
A549	Human lung adenocarcinoma	DMEM supplemented with 10% FCS
Hela	Human cervical cancer	DMEM supplemented with 10% FCS
MCF7	Human breast adenocarcinoma	DMEM supplemented with 10% FCS
MDA-MB-231	Human breast adenocarcinoma	DMEM supplemented with 10% FCS
SUDHL1	Human lymphoma	DMEM supplemented with 10% FCS

Table 2.4 Cell lines used

FCS: Foetal calf serum; DMEM: Dulbecco's modified Eagle medium

2.5 Transient transfection of cultured cells

2.5.1 Transfection with RNAi duplexes TRAP1 Eurogenetic (Oligofectamine)

A lipid-mediated transfection protocol was used to introduce double-stranded siRNAinto cultured mammalian cells. siRNA duplexes against TRAP1 were designed and synthesized by Eurogentec (Eurogentec, Liège, Belgium). Two sequences were designed against 2regions of the TRAP1 gene. The first sequence starts from position 248: 5'-ggguuccacuuccaaacau-3' and 5'-auguuuggaaguggaaccc-3'. The second sequence starts from position 689: 5'-ccaguggcuuucagauggu-3' and 5'-accacucugaaagccacugg-3'. Negative control duplex sequence was also obtained: 5'-auguuuggaaguggaauag-3'and 5'-uaggguguacccguaauag-3'. The duplexes were supplied desalted and fully deprotected and were re-suspended in DEPC water provided to give a 20μM working solution 24 hours prior to transfection, cells were seeded at the appropriate density to achieve a 40% to 50% confluency on the day of transfection and less

than 90% confluency on the day of harvest (usually 48 hours after transfection). Cells were transfected using Oligofectamine (Invitrogen) (Elbashir et al., 2001). siRNA duplex concentrations used ranged from 5nM to 200nM for optimization, but for most experiments, a 50nM concentration was used. For transfection of a 6cm dish, a mixture of 20µM siRNA (Refer to Table 3 for concentration) duplex and OptiMEM to achieve the desired siRNA concentration (Tube A) and a mixture of 4.5µl of oligofectamine and 150µl OptiMEM serum-free medium (Invitrogen) (Tube B) were incubated separately for 10min at room temperature. Both mixtures were then combined and incubated at room temperature for 25 minutes. During this time, cells were washed twice with 3ml of OptiMEM to ensure a serum-free environment for maximum transfection efficacy. 285µl of OptiMEM was then added to the lipid /siRNA mixture to yield a final volume of 1000µl that was added dropwise to the cells. After a 4-hour incubation at 37°C, 100µl of 10% FCS and 4ml of complete growth medium were added to the cells. Transfected cells were grown at 37°C for typically72h prior to further manipulation.

2.5.2 Transfection with RNAi duplexes Quagen (Using Lipofectamine)

One day before transfection, cells were plated in 6cm dish in 5 mL of growth medium without antibiotics such that they were *30–50% confluent* at the time of transfection. 6µl of 10µM siRNA oligomer was diluted in 500µl Opti-MEM® I Reduced Serum Medium without serum and mixed gently. In another tube, 10µl of Lipofectamine RNAiMAX was diluted in 500µl of Opti-MEM and mixed gently. Both tubes were incubated at room temperature for 5minutes. After the 5-minute incubation, the diluted siRNA oligomer was combined with the diluted Lipofectamine® RNAiMAX Transfection Reagent, mixed gently and incubated for 30 minutes at room temperature. Meanwhile the plated cells were washed twice with Opti-MEM, then replenished with 5ml Opti-MEM. After 30minutes of incubation the oligomer-Lipofectamine® RNAiMAX complexes was added dropwise to dish containing cells and medium, mixed by

gently rocking the plate. Cells were then incubated at 37°C in a CO2 incubator for 72hours after which cells were harvested.

2.6 Protein Analysis

2.6.1 Harvesting of cultured cells

Cells were harvested as cell pellets for subcellular fractionation studies and when RNA extraction was not to be performed immediately. Growth medium was aspirated and the cell monolayer washed with ice-cold PBS. Cells were scrapped from the dish and transferred to a clean 1.5ml eppendorf tube. Cells were centrifuged at 13,000rpmfor 1min, washed once with ice-cold PBS and centrifuged again at 13,000rpm foranother 1min. The PBS was aspirated dry and the cell pellet either snap frozen or lysed with the appropriate lysis buffers. All samples were stored at -80^{o}C.

Adherent cells were lysed directly in ice-cold Cell Disruption buffer (Ambion),particularly when higher protein yields were essential (e.g. for immunoprecipitation assays). Growth medium was aspirated from the dishes and adherent cells were washed once with ice-cold PBS. The PBS wash was aspirated completely and 200µlto 600µl of Cell Disruption Buffer (Ambion) was directly added to the cells in the dish (at least 300µl of buffer was used if there were more than 10^{6} cells). Cells were scraped from the dish and transferred to a pre-chilled 1.5ml Eppendorf tube on ice. Samples were vortexed to completely lyse the cells and obtain a homogenous lysate. Samples were incubated on ice for 5 to 10min to allow for complete lysis before protein assay. Samples were stored at -80°C if not used immediately. Special attention was given to cells subjected to hypoxic treatment in order to minimize changes in protein levels

upon re-oxygenation. Cells were harvested on ice and centrifuged at 4°C. Ice-cold PBS was used. The entire procedure was completed within 10min.

2.6.2 Subcellular Fractionation

The PARIS kit (Ambion) was used for subcellular fractionation studies. Actively growing cells were harvested as in section 2.6.1. Cells were gently re-suspended in300µl to 500µl of ice-cold Cell Fractionation Buffer and incubated on ice for 7 mins. The Cell Fractionation Buffer lyses the cell membranes but leaves the nucleus intact. Vigorous handling was avoided in order to minimize partial nuclear lysis. Lysates were centrifuged at 500xg for 3min at 4°C. The supernatant containing cytoplasmic components was aspirated without disturbing nuclear pellet and transferred into afresh eppendorf tube. The nuclear pellet was lysed with 300µl to 500µl of ice-cold Cell Disruption Buffer and incubated on ice for 5min before BCA protein assay. Nuclear fraction lysates obtained from several breast cell lines were sonicated to reduce the viscosity.

2.6.3 BCA Protein Assay

The BCA Protein Assay (Pierce, IL, USA) is a detergent-compatible formulation based on bicinchoninic acid (BCA) for the colorimetric detection and quantitation of total protein. This method combines the well-known reduction of Cu+2 to Cu+1 by protein in an alkaline medium (the biuret reaction) with the highly sensitive and selective colorimetric detection of the cuprous cation (Cu+1) using a unique reagent containing bicinchoninic acid.1 The purple-colored reaction product of this assay is formed by the chelation of two molecules of BCA with one cuprous ion. This water-soluble complex exhibits a strong absorbance at 562 nm that is nearly linear with increasing protein concentrations over a broad working range (20-2,000 µg/ml). The BCATM method is not a true end-point method; that is, the final color continues to

develop. However, following incubation, the rate of continued color development is sufficiently slow to allow large numbers of samples to be assayed together.

Standard curve was set-up using 0 µg/ml, 25 µg/ml, 125 µg/ml, 250 µg/ml, 500 µg/ml, 750 µg/ml, 1,000 µg/ml, 1,500 µg/ml, 2,000 µg/ml of bovine serum albumin (BSA). Working reagent was prepared by mixing 50 parts of BCATM Reagent A with 1 part of BCATM Reagent B (50:1, Reagent A:B). 25 µl of each standard or unknown sample replicate was pipetted into a microplate well (working range = 20-2,000 µg/ml). Then 200 µl of the working reagent was added to each well and mixed thoroughly by shaking the plate. The plate was covered and incubated at 37°C for 30 minutes, then allowed to cool at room temperature. Absorbance was measured at 562 nm on a plate reader. A standard curve was created in Microsoft Excel by plotting the average Blank-corrected 562 nm measurement for each BSA standard vs. its concentration in µg/ml. The standard curve was used to determine the protein concentration of each unknown sample.

2.6.4 Co-immunoprecipitation studies

2.6.4.1 Co-immunoprecipitation using Dynabeads Protein A

Co-immunoprecipitation was performed using Dynabeads Protein A system (Invitrogen) which uses a magnet format. Dynabeads was completely resuspended by rotating on a roller for 5 min.50 µl of Dynabeads was then transferred to a tube, place on magnet and supernatant was removed. Dynabeads was then removed from magnet and resuspended in 200 µl Ab Binding &Washing Buffer containing antibody of choice (typically 1 - 20 µg of antibody is the optimal amount needed but will depend on the individual antibody being used) and incubate 10 minutes

with rotation at room temperature. Tube was then placed on magnet and supernatant removed. Tube was then removed from magnet and the Dynabeads-antibody complex was washed by resuspending in 200 µl antibody Binding & Washing Buffer, replaced in magnet and supernant was removed. Then antigen containing sample (typically 100 - 1,000 µl) was added to the Dynabeads-antibody complex and gently resuspend by pipetting. Mixture was incubated overnight with rotation at 4^{o}C. The next day tube was placed in magnet, supernant was removed, then the Dynabeads-antibody-antigen complex was washed 3 times, using 200 µl Washing Buffer for each wash, mixing gently by pipetting. The Dynabeads-antibody-antigen complex was resuspended in 100 µl Washing Buffer and the suspension was transferred to a clean tube. Tube was placed on magnet and supernatant was removed. The Dynabeads-antibody-antigen complex was gently resuspended in 20 µl Elution Buffer plus 10 µl NuPAGE® LDS Sample Buffer and incubated 10 minutes at 70°C. Then place on magnet and collect supernatant. 30 µl of collected supernatant was then loaded onto 10% SDS-PAGE gel for electrophoresis

Table 2.5. Antibodies used in immunoprecipitation

Antibody	**Source**	**Species/Isotype**	**Clonality**	**Antibody Concentration**
TRAP1	Santa Cruz, CA, USA	Mouse/IgG_{2a}	Monoclonal	2µg per 1mg protein
E2F1	Santa Cruz, CA, USA	Mouse/ IgG	Monoclonal (KH95)	4µg per 1mg protein
JMY	NDCLS lab	Mouse/IgG	Monoclonal	300µl per 1mg of protein
JMY	Santa Cruz, CA, USA	Goat/IgG	Polyclonal	2µg per 1mg protein
Normal IgG	Upstate, Billerica, MA, USA	Mouse/IgG	NA	2µg per 1mg protein

2.7 Production of Anti-JMY Antibodies.

JMY monoclonal antibody was raised by conventional techniques. Peptide sequences were chosen from 3 different locations: the C-terminal, the middle of peptide sequence and from the N-terminal. Three JMY peptides (RPHVFDEREKHKFVC; KREKLHDEEERKSAC and CPDTDPLTRSIHEALRRIKEASPE) were synthesized by solid-phase techniques (Weatherall Institute of Molecular Medicine). After cleavage and deprotection, peptides were coupled to Keyhole limpet hemocyanin (KLH) from Imject Maleimide activated mcKLH kit purchased from Pierce (Rockford, IL USA). Peptide to protein ratio were determined for all conjugates by amino acid analysis.

Balb/c mice were immunized subcutaneously with a mixture of 15 ug of each KLH conjugated peptide (a total of 45ugs) in PBS in Titremax Gold (Stratech Scientific Ltd) adjuvant using the recommended protocol, followed by 3 further intraperotoneal injections using the same dose in PBS without adjuvant at intervals of 10 days. Mice splenic lymphoid cells were fused with mouse myeloma NS0 using conventional technique 3 days after the final immunizations. The resultant hybridomas were screened via ELISA on the JMY-KLH peptides and unrelated peptide-KLH. Samples positive only on the JMY peptide conjugate were further screened for ability to distinguish JMY protein by immunostaining on formalin fixed inducible JMY cell pellets and on cells with and without JMY. Five antibodies were further tested for further validation using western/immunoblotting.

2.8 Immunoblotting

2.8.1 SDS-PAGE electrophoresis

SDS-PAGE electrophoresis was used to separate proteins according to molecular weight. The polyacrylamide gels were prepared according to the method of Laemmli (Laemmli, 1970). The apparatus (Mini Protean 3) used for this procedure was obtained from Bio-Rad (Hercules, CA, USA). 1.5mm 8 x 10cm gels were cast. The gels were made in two parts, the resolving gel and the stacking gel. The resolving gel was prepared with 30% acrylamide, 0.4% bisacrylamide stock (Protogel, National Diagnostics, Atlanta, GA, USA) to give a final concentration of 5-10% acrylamide, 0.1% SDS and 0.375M Tris-Cl. 10% ammonium persulphate (APS) (Sigma) and TEMED (Sigma) were added as polymerization catalysts. A 10% acrylamide resolving gel was generally used, particularly when analyzing proteins smaller than 50kDa and when intending to visualize the hyper- and hypophosphorylated forms of Rb as separate bands. A 7.5% acrylamide gel was used when proteins between 50kDa to 150kDa (composition of 7.5% and 10% resolving gels detailed in Table 9). The resolving gel mix was poured between two clean glass gel plates to within 2cm of the top and overlaid with 200µl of isobutanol while the polyacrylamide polymerized. The isobutanol was then poured away and blotted dry with absorbent paper. The stacking gel mix (Appendix A) was poured to the top of the gel plates and a 1.5mm comb(either 10 or 15-lane) was inserted. After the stacking gel had polymerized, the comb was removed and the gel inserted into the electrophoresis tank and covered with 1xSDS running buffer.

Table 2.6.Composition of 7.5% and 10% resolving gels.

	7.5% resolving gel (sufficient for 2 gels)	10% resolving gel (sufficient for 2 gels)
Acrylamide (ml)	5.63	11.25
0.375M Tris-Cl / SDS, pH 8.8(ml)	5.63	8.45
Distilled water (ml)	11.25	14.06
10% APS (µl)	150	225
Temed (µl)	30	45

Each sample typically contained 20µg to 50µg of protein mixed with 6x Laemmlibuffer (Appendix A). For a 10-lane gel, 35µl of protein solution was mixed with 7µlof 6x Laemmli buffer, boiled at 95$_o$C for 5min and briefly centrifuged. 40µl was loaded into each well. The high-range rainbow marker (Amersham Biosciences,Buckinghamshire, UK) served as a protein standard. A current of 100V was applied for 1.5h.

2.8.2 Semi-dry protein transfer

Proteins separated by SDS-PAGE electrophoresis were transferred onto nitrocellulose membrane using a semi-dry transfer method. 6 pieces of 3M filter paper and 1 piece of Hybond C Extra nitrocellulose membrane (Amersham Biosciences) were soaked in transfer buffer (Appendix A) for at least 20min. The gel was then removed from the electrophoresis tank. Three pieces of the 3M filter paper were stacked on the bottom screen of the semi-dry transfer apparatus (the anode) (Hoefer SemiPhor Transfer Unit,Amersham Biosciences), followed by the membrane, the resolving portion of the gel and finally the three remaining pieces of 3M paper. The stack was compressed to remove any bubbles that might interfere with a uniform transfer of the protein from the gel onto the nitrocellulose membrane. A constant current of 35mA gel was applied for 3 hours for complete transfer of proteins to the nitrocellulose membrane.

2.8.3 Primary antibodies application

After the 3h transfer, the nitrocellulose membranes were blocked for 1h on a shaking platform with 5% non-fat milk (Marvel) in PBS containing 0.1% Tween20 (PBST) to reduce non-specific antibody binding. Membranes were then cut horizontally according to the appropriate molecular weight of the desired protein if more than 1 protein was being probed on the same membrane. The antibodies used for immunoblotting are detailed in Table 10. β-actin and β-tubulin antibodies served as loading controls. Membranes were placed protein side up in 10cm culture dishes with about 10ml of primary antibody diluted in blocking buffer and incubated overnight on a shaking platform at 4$_{o}$C to ensure uniform exposure of the entire membrane. The next morning, membranes were washed three times in 0.1% PBST for 15min each. Membranes were then incubated with the appropriate secondary antibody for 1h on a shaking platform at room temperature. The secondary antibodies used were either goat anti-mouse (Dako) or goat anti-rabbit (Dako) conjugated with horseradish peroxidase (HRP). This was again followed by 3 15-min washes in 0.1% PBST.

2.8.4 Detection of Protein bands

ECL Plus detection kit (Amersham Biosciences) was used to detect the protein bands. Antibody-conjugated HRP converts a lumigen PS-3 acridan substrate to an acridiniumester intermediate which reacts with peroxide in alkaline conditions and emits light detectable by autoradiography. The ECL Plus kit consists of 2 solutions: Solution A(substrate solution containing Tris buffer) and Solution B (acridan substrate solution in doixane and ethanol) which are mixed in a 40:1 ratio and applied over the protein side of the membranes for 5min at room temperature. Excess ECL was tipped off and the membranes placed into an X-ray film cassette. In a dark room, X-ray film(Biomax MR Film, Kodak) was placed over the membranes

and exposed for between30s to 20min. Exposures were timed to avoid signal saturation. The ECL Advance Plus detection kit (Amersham Biosciences) was at times used to give a stronger signal. The radiographs were scanned and imported into Adobe Photoshop (Adobe Systems Incorporated, USA).

Table 2.7. Antibodies used in immunoblotting

Antibody	Source	Species/Isotype	Clonality	Primary Antibody dilution used
TRAP1	Santa Cruz, CA, USA	Mouse/IgG_{2a}	Monoclonal	1:1000
E2F1	Santa Cruz, CA, USA	Mouse/ IgG	Monoclonal (KH95)	1:200
JMY	NDCLS lab	Mouse/IgG	Monoclonal	1:10
JMY	Santa Cruz, CA, USA	Goat/IgG	Polyclonal	1:1000
HIF-1α	BD Transduction Laboratories, San Jose , CA, USA	Mouse/IgG1	Monoclonal	1:200
Rb	Novocastra, Newcastle Upon Tyne, UK	Mouse/IgG1	Monoclonal	1:50

2.9 Growing Spheroids

2.9.1 TRAP1 stable knockdown in A549 cells

A549 TRAP1 Stable knockdowns were produced by Dr Jackie Agorreta. Single stranded oligos were annealed to generate double stranded oligo at 95°C. Then resultant double stranded (ds) oligos were cloned into pCDNA 6.2-GW GFP vector, ligation as done at room temperature. The ds oligo/ vector ligation was then transformed into competent TOP10 Ecoli bacteria. Transformants were then spread on LB agar containing Spectinomycin and incubated overnight at 37°C. The next day 5-10 Spectinomycin-resistant colonies were picked and cultured overnight in 1ml LB containing Spectinomycin and as well streaked plate also containing

Spectomycin and incubated overnight. The next day the streaked plate was put in the cold room 4degrees, while plasmid DNA was isolated from the LB and purified on miniprep (QIAprep Mini system, Qiagen)and use for a quick check of correctness of orientation of the ds oligo insert. The expression clone was transfected with oligofectamine into A549 cells to test its efficiency in inhibition.

Then a stab of colony of streaked plate in cold was put in glycerol and also colony was taken and grown in 500ml LB. Then a midiprep was done to obtain DNA, some DNA was sent for sequencing, the remaining DNA was linearized by digesting with EagI restriction enzyme, inserted into plenti6/V5-dest vector and then transformed into Ecoli bacteria. Plasmid was purified by midiprep and sequenced, then appropriate clone were transfected into 293FT cell with lipofectamine protocol. Transfection efficiency was checked by viewing GFP positive cells under a fluorescence microscope. Medium was collected, ultracentrifuged at 19500 for 2 hours at 12°C. Finally A549 cells were transfected with virus in presence of polybrene (6μg/ml). Positive cells were selected in presence of Blasticidin (6μg/ml).10 days after viral transfection cell were checked under fluorescence microscope for GFP positivity.

Figure 2.1. Schematic representation of the pLenti6/V5-DEST® Gateway® Vector (Invitrogen datasheet)

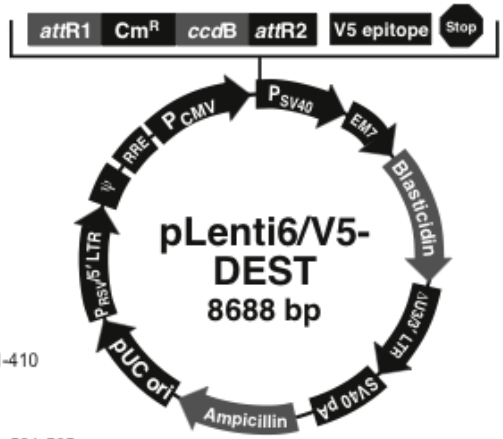

Comments for pLenti6/V5-DEST
8688 nucleotides

RSV/5′ LTR hybrid promoter: bases 1-410
RSV promoter: bases 1-229
HIV-1 5′ LTR: bases 230-410
5′ splice donor: base 520
HIV-1 psi (ψ) packaging signal: bases 521-565
HIV-1 Rev response element (RRE): bases 1075-1308
3′ splice acceptor: base 1656
3′ splice acceptor: base 1684
CMV promoter: bases 1809-2392
*att*R1 site: bases 2440-2564
Chloramphenicol resistance gene (Cm^R): bases 2673-3332
*ccd*B gene: bases 3674-3979
*att*R2 site: bases 4020-4144
V5 epitope: bases 4197-4238
SV40 early promoter and origin: bases 4293-4602
EM7 promoter: bases 4657-4723
Blasticidin resistance gene: bases 4724-5122
ΔU3/3′ LTR: bases 5208-5442
ΔU3: bases 5208-5261
3′ LTR: bases 5262-5442
SV40 polyadenylation signal: bases 5514-5645
bla promoter: bases 6504-6602
Ampicillin (*bla*) resistance gene: bases 6603-7463
pUC origin: bases 7608-8281

Invitrogen™
life technologies

2.9.2 TRAP1 restoration in MDA-MB-231 cells

2millions Ampho Phoenix packaging cells were plated in 6cm dish with 4 ml of E4 and 10%FCS medium. The next day, the plated cells had reached 50-70% confluency and were transfection with (10 ug) plasmid DNA using Ca/POH and incubated at 37°C for 24 hours. Then medium was changed with fresh medium containing 2ug/ml puromycin. The next day, medium was changed and cells were split into 10-cm dish (8ml) and cultured in fresh medium containing 2ug/ml puromycin for another day. 24 hours later, medium was removed and fresh medium without puromycin was added and allowed to grow overnight. The next day medium was replaced with 8ml Optimen (serum-free) medium and transfer to a 37°C incubator for 24 hours. The following day the Optimem (serum-free) medium was collected and filtered through a 0.45um filter then polybrene was added to a final concentration of 4 ug/ml. Then MDA-MB-231 cells at 40-50% confluency in 10cm dish were infected with the filtered supernatant containing polybrene and allowed to incubate at 37°C for 3-6 hours. Then further diluted (1:3) with fresh medium with polybrene and allowed to incubate overnight. After 24 hours, the culture was replaced with fresh medium and allowed to incubate overnight. After 24 hours cells were looked at under UV-light of an inverted microscope for green color.

2.9.3 Spheroid Growing Technique I

The original protocol used to grow the spheroid was by transferring exponential growing A549 cells into spinner culture flasks containing 250ml DMEM media (FCS10%, Glut 1%, Pen/Strep1%) that mechanically induced the cells to aggregate and form spheroids. The spheroids were allowed to grow in the spinner flasks for up to 24 days with media changed every other day by gradually aspirating out 150ml of media and replenishing with a fresh 150ml of media.

2.9.4 Spheroid Growing Technique II

2.9.4.1 Plate preparation

Multicell spheroids were grown in standard 96-well tissue culture plates. Initially the plates must be prepared with agarose gel constituting a solid surface onto which the spheroids form. This prevents the spheroids from adhering to the lower surface of the well. After pouring, the agarose set to form a meniscus, at the bottom of which the spheroid would develop.

Preparing 10 x 96 well plates:

100ml Medium (without glutamine or FCS) 1.5g Agarose (Sigma A9539) resulting in 1.5% agarose solution and one plate would use approximately 10mls. The agarose powder was added to the medium and dissolved using a magnetic stirring hotplate. A beaker within another larger beaker of water on the verge of boiling was used for this.

Once the agarose had dissolved it was left for a further 20 minutes in the boiling water to kill any pathogenic contamination. The agarose containing beaker was then transferred to the tissue culture hood, and a multi-pipettor was used to fill the wells with 100µl aliquots. This was done as rapidly as possible as the agarose solidified on cooling. After aliquoting the agarose mixture, the plates were left with the lids partially removed to prevent them from sticking onto the top of the plates as the agarose solidified. When the plates have cooled and the agarose set, they could either be used immediately or stored in their original packaging at 4°C. If refrigerated they would need to be brought up to room temperature before use.

2.9.4.2 Initiating Spheroids

Lung adenocarcinoma cell line A549 was obtained from Clare Hall Laboratories (London, UK) and regularly screened for the presence of mycoplasma. Cells were cultured as monolayer in Dulbecco's Modified Eagle's Medium (DMEM) supplemented with 10% heat-inactivated FCS,

100 units/ml penicillin, and 100 μg/ml streptomycin at 37°C in a humidified atmosphere of 5% CO_2. Cells grown in monolayers at the exponential growth phase were used for initiating spheroids.

The cells were seeded at a concentration of 2000 cells/well. 200μl of medium was used per well and the cells were counted with a haemocytometer and diluted appropriately. Approximately 20mls of media cell suspension was required per 96 well plate. The cells were diluted in an autoclaved 100ml beaker and the cell suspension was dispensed into the well using an Eppendorf multi-pipettor on setting '2' which could dispense 200μl with the 5 ml tip (1=100μl). Once the culture had been initiated, it was incubated at 37°C and not disturbed for 2 days as movement would disaggregate the newly forming spheroids.

2.9.4.3 Feeding spheroids

The spheroid cultures were usually fed three times per week (Monday, Wednesday & Friday). 100μl of medium was aspirated from each well. This could be done using a Pasteur glass pipette connected to a suction line such as a venturi type pump, connected to a water tap. The pipette was held at an angle so as not to disturb the spheroid. Once the plate had been aspirated, a multi-channel pipette was used to replenish an equivalent volume (100μl) of aspirated medium.

2.9.4.4 Spheroid Measurement *In vitro*

Spheroid growth was measured *in vitro*, and also histometrically. The progress of spheroid growth could be assessed in-vitro by measuring spheroid diameters using a Axio Zeiss camera interfaced with an inverted microscope. The pixels measurement of the camera was calibrated

against a stage micrometer scale (Graticules Ltd.) on the inverted microscope at various magnifications, at 10x magnification 1120 pixels is equivalent to 1mm.

2.9.4.5 Spheroid Collection, Embedding and Processing

Collection of spheroids is possible at about day 7 after the initiation of spheroid growth and spheroids can then be collected every 2 days. A Pasteur pipette was used to collect the individual spheroids from their wells, transferred into a cryovial, making sure to pipette out any culture medium that might be transferred with the spheroid. Then 10% formalin is added and allowed to fix over night. The fixed spheroids were then transferred to a small plastic hemisphere made from the rounded end of a cryovial, also making sure to remove any formalin that might have been transferred along with the spheroid. The hemisphere is then filled with molten agar/10% formalin mixture and immediately placed on ice to cool and set. The resulting lens of solid agar was removed from the hemisphere with a hypodermic syringe needle and placed in a tissue cassette. The cassette was then sealed and placed in formalin before being processed through graded alcohols, xylene and hot liquid paraffin wax. The embedding process was performed by the personnel of the Cellular Pathology Laboratory at the John Radcliffe Hospital, Oxford, using an automatic tissue processor. Following processing the paraffin embedded lens, containing the spheroids at its apex, was then formed into a solid wax block prior to cutting into 5μm thick microtome sections.

2.10 Statistical analysis

Correlation between biomarkers and the various clinic pathological parameters was evaluated using the t test. Analysis of markers of the angiogenic and non-angiogenic tumors was evaluated using the t test (Mann Whitney test) - A non-parametric statistical tests used to compare continuous variables between groups, as these assume no underlying distribution in the data. For example, in order for a t-test to be valid, asymmetrically normal distribution must be assumed. The unpaired t-test then tests the assumption that the means of two groups are equal. The non-parametric version of this test is the Mann-Whitney U-test. In this test, the observations are ranked sequentially and the hypothesis tested is that the underlying distribution of the two groups is the same. Since this test compares ranks rather than absolute values it is resistant to outliers. Relapse free survival curves were calculated using tumor recurrence (defined as the first appearance of tumor at any site following definitive treatment) as the endpoint. All univariate and survival analysis were performed using GraphPad Prism version 4.00 for Windows, (GraphPad Software San Diego California USA, www.graphpad.com).A 2-tailed P value test was used in all analyses and a P value of less than 0.05 was considered statistically significant.

CHAPTER 3
TRAP1 EFFECT ON PROLIFERATION IN SPHEROID GROWTH

3.1 Introduction

Genetic and epigenetic alterations that activate oncogenes and silence suppressor genes are important in the initiation of cancer. However alternative mechanisms exists, for instance, up regulation of heat shock proteins (HSP) which could facilitate tumorigenesis by maintaining wild type oncogenes in an active oncogenic conformation (Ciocca and Calderwood 2005, Solimini, Luo et al. 2007). By comparing tumor versus normal tissue mRNA expression profiles in 25 sets of DNA microarray data in non-small cell lung cancer, we found that some HSPs, however, are significantly down-regulated in tumors. A novel observation was that 12 of these HSPs are chaperones to tumor suppressor proteins (Pezzella F et al manuscript in preparation) and one of these HSPs is TRAP1. This suggests yet another oncogenic mechanism in which tumor suppress protein can be inactivated in absence of its appropriate chaperone.

TRAP1, a member of the Hsp90 family (Song, Dunbar et al. 1995)is located in mitochondria (Felts, Owen et al. 2000). Two functions are known to be associated with TRAP1:In the event of heat shock it relocates into the nucleus, where it refolds denatured Rb1 back to its active conformation (Chen, Chen et al. 1996) and, secondly, it protects the cell from apoptosis (Masuda, Shima et al. 2004, Neckers, Kern et al. 2007) and oxidative stress (Montesano Gesualdi, Chirico et al. 2007, Neckers, Kern et al. 2007).

There appears to be tissue specificity to TRAP1's regulation in cancer since some studies have reported up regulation of TRAP1 in stomach, prostate, and colorectal adenocarcinomas but a down regulation in bladder transitional cell, renal cell and hepatocellular cell carcinomas (Kang, Plescia et al. 2007, Ramasamy, Mondry et al. 2008, Liu, Hu et al. 2010). This is intriguing enough to question why this protein would have such a dichotomy in various cancers. Possibly, the answer to this lies in the various roles of TRAP1 and the effect of its expression on cell biological processes. TRAP1 has a putative tumor suppressive role due to its inherent possession of a unique LxCxE motif that allows its binding to Rb during mitosis or in the event of stress such as heat shock /hypoxia where it serves to refold and keep Rb in its active conformation (Liu, Hu et al. 2010). Also TRAP1 could have an oncogenic role by way of its function as an HSP in cancers (Calderwood, Khaleque et al. 2006) as well as its potential ability to inhibit oxidative stress induced mitochondrial apoptosis (Masuda, Shima et al. 2004, Montesano Gesualdi, Chirico et al. 2007, Neckers, Kern et al. 2007, Leav, Plescia et al. 2010).

Data from our laboratory on *in vitro* cell cultures demonstrated that during the first 24 hours of hypoxia, TRAP1 moves to the nucleus and binds to Rb1. Following hypoxia and in absence of TRAP1, Rb1 fails to bind to E2F1 and as a consequence more cells enter S phase. Re-establishment of TRAP1 expression reverses this action. However this effect appears to be, at least in vitro, transient and disappears after the first 24 hours when TRAP1 relocates back to the cytoplasm and the amount of nuclear TRAP1 diminishes again (Hu et al. Manuscript submitted).

More recent experiments monitoring growth in cell culture (2 dimensional growth) of the A549 cell line via manual, automated cell counting (with Coulter Z2 particle count) and clonogenic assaying suggest that in normoxia, after five days of growth in culture, the number

of TRAP1 positive cells is double that of the TRAP1 negative cells; and further increases to almost quadruple that of the TRAP1 negative cells by the 7th day. This increase in cell number in TRAP1 positive cells was observed to be mostly due to increased proliferation in these TRAP1 positive cells rather than by inhibition of apoptosis as proposed by Leav et al and Neckers et al (Neckers, Kern et al. 2007, Leav, Plescia et al. 2010). Additionally, in hypoxia, a state known to down regulate TRAP1 (Tan, Pezzella et al. 2007), there was no observable difference of the number of cells in TRAP1 positive and TRAP1 negative cell lines as hypoxia decreased the level of TRAP1 in the TRAP1 positive cell and attenuated these cells' proliferative potential (Agorreta et al., manuscript in preparation). This result was in effect suggesting a strong correlation between TRAP1 presence and increased cell proliferation.

The above results were obtained from cell cultures in Petri dishes hence were mainly 2 dimensional studies. To follow up on this work, I sought to investigate the effect of TRAP1 loss on cell growth "in vitro" as it relates to proliferation, apoptosis and hypoxia in an "in vitro" 3 dimensional spheroid model. Tissues and tumors grow in 3 dimensions and cell-cell interactions affect the rate of response and growth (Dufau, Frongia et al. 2012). Hence a spheroid model was ideal for this study as it is the closest model to a xenograph that best emulates tumor growth in reality. Spheroids allow cell growth in 3 dimensions up to a diameter of hundreds of microns, mirroring the state in tissues better than a cultured monolayer. Additionally, this model allows development of a gradient from normoxia (external surface) to hypoxia (central areas) (**Figure 3.1**). With this model, the effect of normoxia and hypoxia can be monitored in tandem. Also, the growth rate of the spheroids can be assessed by a calculation of the spheroid volume.

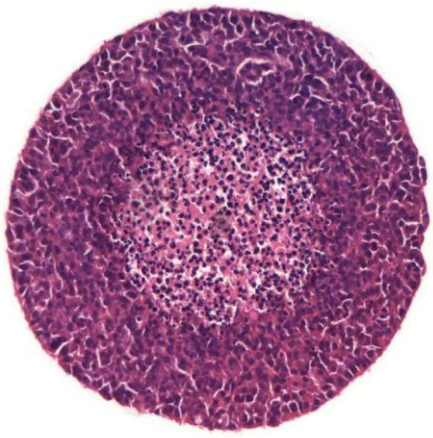

Figure 3.1 Section of spheroid stained with heamatoxylin and eosin (H&E).
The purple stain of H&E stains viable cells while the pink stains dead cells. The primarily purple H&E stained external portion of the spheroid is the well oxygenated portion of spheroid, while the predominantly pinked stained central core of the spheroid has becomes increasingly hypoxic as the spheroid grows and eventually necrosis develops. Picture obtained from Dr Russell Leek, Nuffield Department of Clinical Laboratory Sciences.

3.2 Results

3.2.1 TRAP1 in cell growth and proliferation

3.2.1.1 Creating stable TRAP1 knockdowns and overexpression in cell lines

I intended to monitor the effect of TRAP1 in cell growth and to compare the growth rate in cells with and without TRAP1 over the course of 20-30 days. The use of TRAP1 siRNA treated cells or plasmid transfected cells was not feasible for this experiment since siRNA and the plasmid effect in cells last for approximately 7 days and would not be adequate for the duration that I intended to observe the effects on cell growth. It was imperative to create a virally transduced cell line with a stable TRAP1 knockdown and TRAP1 overexpression that would

keep TRAP1 down-regulated and over-expressed respectively through the long 30days duration of the growth monitoring in these cells. I also had comparable respective scrambled and mock transfected cells as controls.

For the TRAP1 knockdown experiments, I chose A549 lung cancer cell as these are rich in TRAP1(Tan, Pezzella et al. 2007). While for TRAP1 over-expression experiments I chose MDA-MB-231 metastatic breast cancer cells that are deficient in TRAP1(Tan, Pezzella et al. 2007). The A549 TRAP1 knockdown experiment was performed by Dr Jacqueline Agorreta (procedure in material and method chapter) while I performed the MDA-MB 231 TRAP1 over-expressions as described in Chapter 2 Materials and Methods.

The experiments produced significant TRAP1 knock down and TRAP1 over-expression in the A549 and MDA-MB-231 respectively, capable of keeping TRAP1 down regulated or over-expressed after 6 passages (15 days of culture growth) as represented in Figure 2by a Western blot of a protein extracts respectively from; A549 TRAP1 knock down and control and MDA-MB-231 TRAP1 over-expression and control resolved in 10% SDS-PAGE electrophoresis and immunoblotted with an anti-TRAP1 antibody.

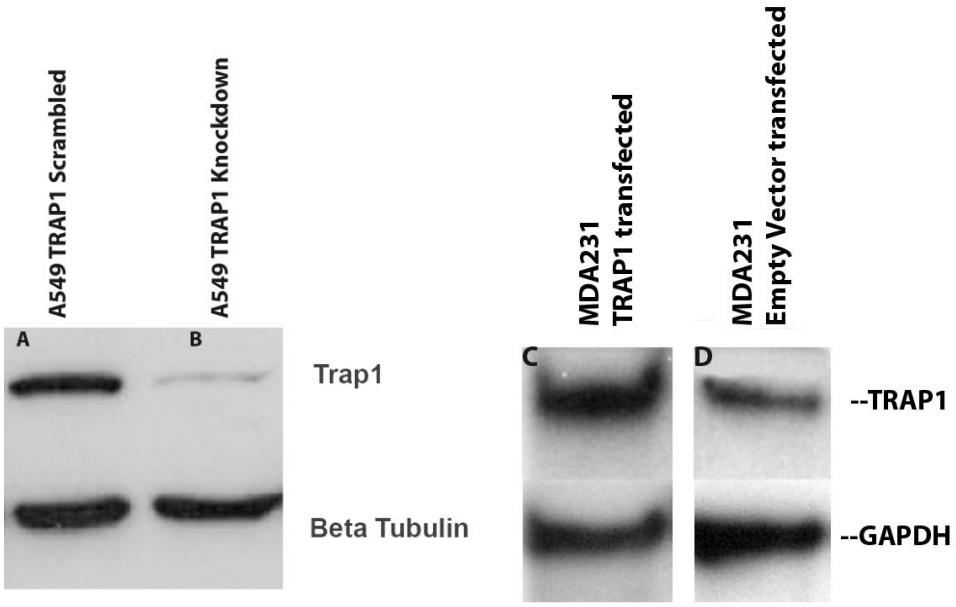

Figure 3.2 Western blot showing a permanent TRAP1 knockdown after 15 days

(A) A549 scrambled. (B) A549 TRAP1 knockdown, the knockdown is one of 3 clones of A549 TRAP1 knockdown. Total cell lysate with a significant decrease of TRAP1 protein in the knockdown extract compared to the scrambled. Beta tubulin used for loading control in A549. (C) MDA231 TRAP1 transfected (TRAP1 overexpression). (D) MDA231 transfected with empty vector. GAPDH used for loading control in MDA321 western blotting. Blot C and D were run in the same on the same western gel but several lanes apart so were cut out and juxtaposed to each other in this figure.

3.2.1.2 Optimization of spheroid growth

Spheroids were grown as described in Chapter 2 according to a method previously described in our laboratory (Leek et al., 2005 thesis). Before I could study the effect of TRAP1 on growth and proliferation I had to optimize a method of growing these spheroids to allow for accurate measurement within the parameters that I needed to observe. My first attempt of growing spheroids was an effort to ascertain if the cells to be used for the study, A549 and MDA-MB-

231, would form spheroids. I grew my initial spheroids using the wild-type form of these cells and using a batch spinner flask spheroid induced method where I transferred exponential growing cells into spinner culture flasks containing 250ml DMEM media(FCS10%, Glut 1%, Pen/Strep1%). The spinning of the spindle in the flask mechanically induced the cells to aggregate and form spheroids. These spheroids were allowed to grow in the spinner flasks for up to 24 days with media changed every other day by gradually aspirating out 150ml of media and replenishing with a fresh 150ml of media.

3.2.1.3 Characteristic of Spheroids grown using the batch spinner induced method.

Spheroids grown with the above technique were collected between day 15 and 35 of growth (collection of spheroids started on the 15th day of growth because that is when they were big enough to be collected from the spinner flask). To assess the integrity of the spheroids, they were harvested and fixed in formalin at intervals of 3 days. After formalin fixation, the spheroids were embedded, processed into paraffin blocks, and sectioned into 4 microns histological sections. These sections were then stained with H&E (as described in chapter 2) Figure3.3. Pictures of spheroids were taken with a Nikon 'CoolPix" camera interfaced with an Olympus light microscope.

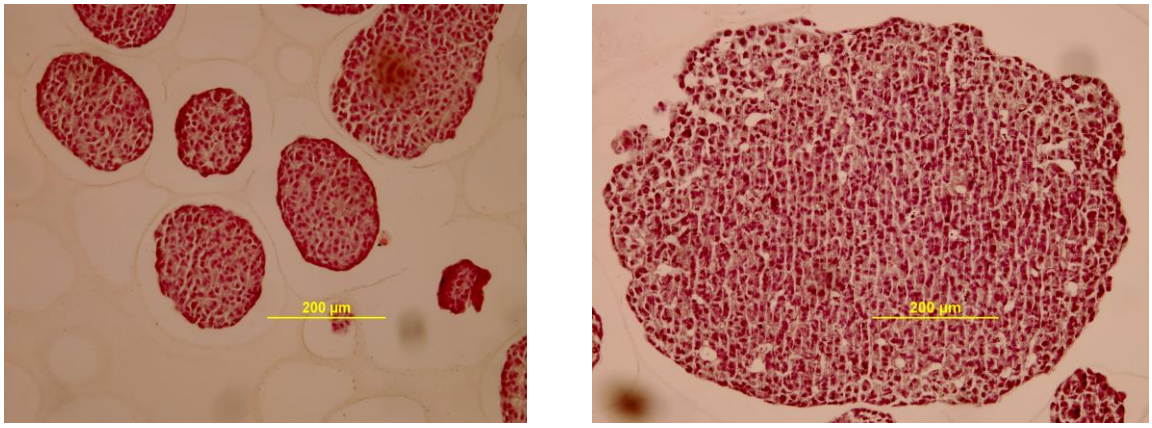

Figure 3.3Haematoxylin/Eosin staining of A549 wild-type spheroids.
(A) Day15 of spheroid growth cells are still intact and cohesive. (B) Day 35, spheroid has grown to t point where the cells are not properly oxygenated and have become necrotic.

Additionally, to investigate the progression of decreased oxygen penetration and proliferation through the course of the spheroid growth, histological sections of these spheroids were also immunostained with antibodies for CA9, MIB1 and TRAP1.

CA9.

Immunostaining for CA9 was performed to demonstrate the pattern of progressive decreased oxygen penetration of the spheroid's core between days 15 and 35 of growth. By day 15 there was a low degree of CA9 staining that was relatively and uniformly sparse through the nodule. By day 35 CA9 staining was largely concentrated in the core of the nodule with less oxygen penetration (Figure 3.4).

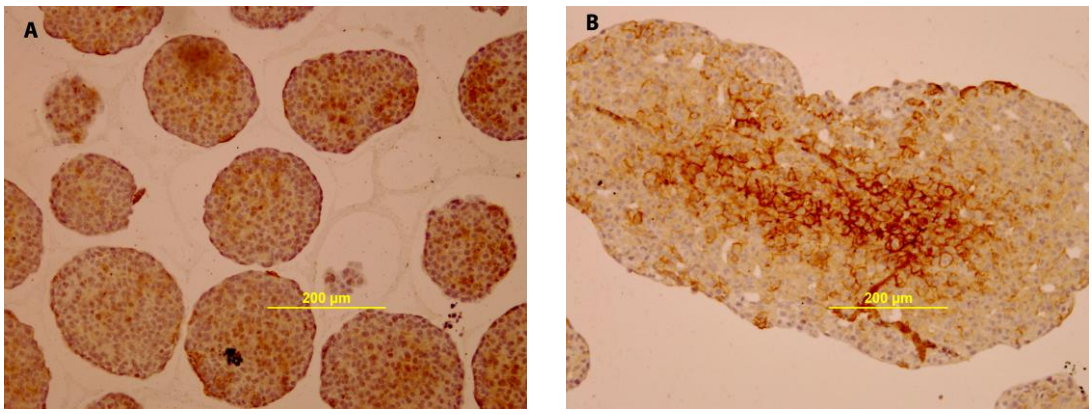

Figure 3.4 CA9 staining.

(A) Day 15 there is a relatively low degree of CA9 staining generally sparsed throughout t spheroid. (B) Day 35, the degree of CA9 staining had intensified, particularly in the core regi where there is severe deprivation of oxygen and nutrients such that the cells in this core regi have become necrotic.

MIB1.

Immunostaining for MIB1 was undertaken to demonstrate the pattern and areas of proliferation in the spheroid between days 15 and 35 of spheroid growth. On the 15th day the cells of the spheroid nodule continued to have access to full oxygenation and the whole nodule remained proliferative. However by day 35, the proliferation of the nodule was concentrated in the well oxygenated periphery and almost absent in the less oxygenated core of the nodule (Figure 3.5).

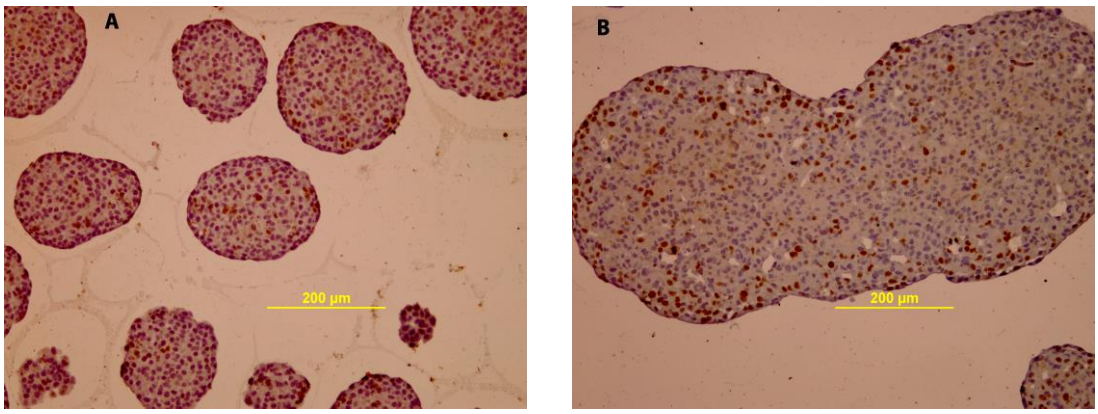

Figure 3.5 MIB1 staining.

(A) At day 15, proliferation as marked by the MIB1 presence, is scattered relatively throughout the spheroid nodule. At this point of growth the spheroid is still small and uniformly well oxygenated. (B) By day 35 most of the proliferation is more concentrated at the periphery of the spheroid where it is better oxygenated, while the core of the spheroid is becoming hypoxic and has less proliferating cells as indicated by the decreased presence of MIB1 positivity in the core.

TRAP1.

Immunostaining for TRAP1 was to correlate proliferation and hypoxia to TRAP1 expression. There is a strong expression of TRAP1 throughout the nodule at day 15. By day 35 TRAP1 is down-regulated or switched off in the nodule core though it remained strongly expressed around the well oxygenated periphery of the nodule.

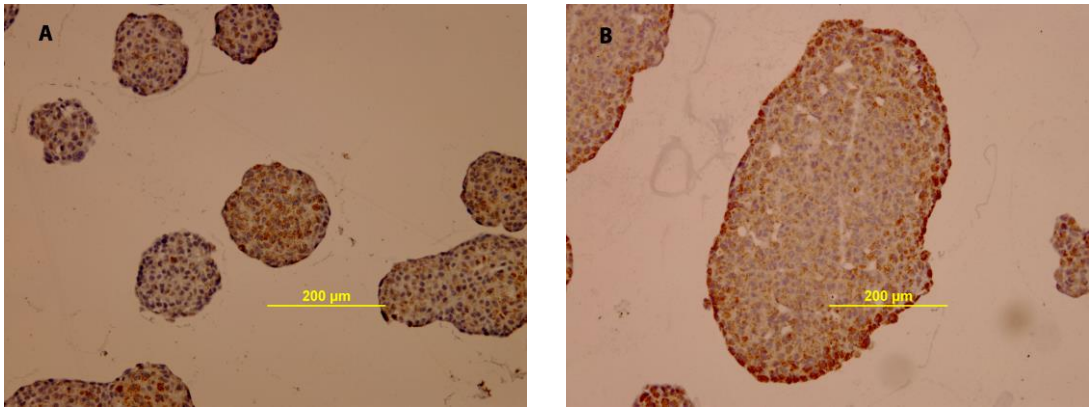

Figure 3.6 TRAP1 staining.

(A) TRAP1 immunostain at day 15 showing TRAP1 spread throughout the whole spheroid while it still relatively well oxygenated. (B) By day 35 there appears to be a switch off of TRAP1 in the cen where the spheroid is becoming more hypoxic as well as the spheroid getting bigger. TRAP1 consequently more concentrated at the peripheral rim of the spheroid that is less hypoxic.

3.2.1.4 Disadvantage of the Spinner Induced Spheroid Method.

The disadvantage of the spinner-induced spheroid growing technique was that it does not differentiate between cells growing due to clonal expansion or due to spinner induced cell aggregation. Which meant that any observed spheroid enlargement was not always necessarily purely due to cellular proliferation. This in effect creates a bias in the monitoring of the

spheroid growth since their exponential growth may not be accurately recorded using this spheroid growing technique. In order to address this problem I decided to grow individual spheroids in culture plates as described in the material and methods. With this method a specific number of cells were seeded in respective wells and then subsequent growth was monitored. This ensures that any resultant spheroid growth that occurred was purely due to clonal expansion of the specifically seeded cells and this allowed for a more accurate monitoring of spheroid growth. Additionally, spinner induced spheroid do not form distinct necrotic cores as demonstrated in the model spheroid of figure 3.1, hence this spheroid will not allow for proper comparism of well oxygenated external layer to less oxygenated necrotic core.

3.2.1.5 Optimization of the Individual Spheroid Growing Technique

Using the individual spheroid growing technique, I was able to grow spheroids for up to 28 days and demonstrated by measuring the spheroid volume a progressive increase in size over the course of 20 days.

With the first set of spheroids growing experiments utilizing the individual growing technique, in an effort to further optimized this technique by investigating the number of cells most appropriate to initiate spheroid growth, I seeded the cells as follows: A549 wild-type cells - 1500 cells; the scrambled A549 cells - 2000 cells and A549 TRAP1 knock down cells - 1500 cells. Series of these spheroids were collected at various intervals and measured as shown in Figure 3.7.

A549 Wild-type

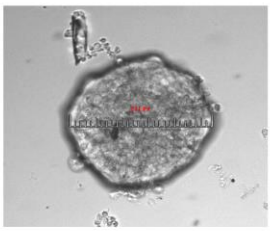

10 days growth

Diameter: 0.241mm

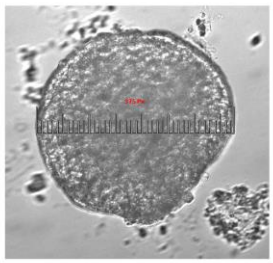

18 days growth

0.335mm

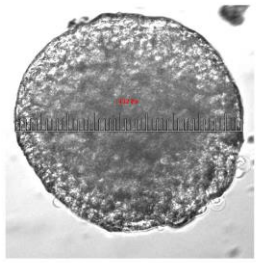

20 days growth

0.386mm

A549 Scrambled

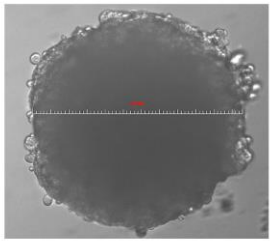

7 days growth

Diameter: 0.485mm

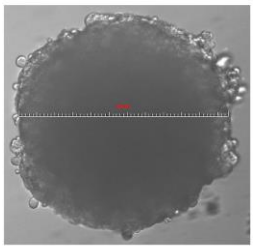

11 days growth

0.517mm

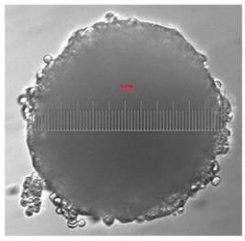

13 days growth

0.545mm

A549 TRAP1 knockdown

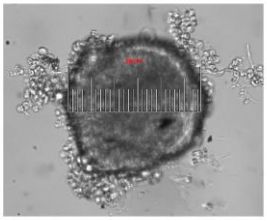

10 days growth

Diameter: 0.255mm

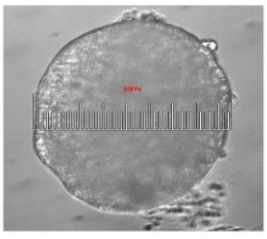

18 days growth

0.382mm

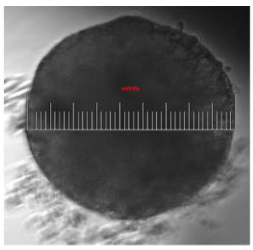

20 days growth

0.400mm

Figure 3.7. Spheroid measurements

Progressive measurement and optimization of growing spheroids; A549 wild-type, scrambled and TRAP1 knockdowns. Scrambled spheroids have rougher outer cores and numerous blebs while the TRAP1 knockdown spheroid is smoother. Growth was assessed in-vitro by measuring spheroid diameters using an Axio Zeiss camera interfaced with an inverted microscope. The pixel measurement of the camera was calibrated against a stage micrometer scale (Graticules Ltd.) on the inverted microscope at 10x magnification, 1120 pixels is equivalent to 1mm.

By recording spheroid growth and morphological integrity over the course of their development as shown in Figure 7, I determined that the most appropriate number of cells to initiate spheroid growth via the "individual spheroid growing technique" was 2000 cells.

3.2.1.5 Effect of TRAP1 knockdown in A549 cell line spheroid growth

Having optimized the individual spheroid growing method as the best technique for monitoring spheroid growth, I then proceeded to use the technique to explore the effect of TRAP1 knockdown on spheroid growth. I grew spheroids from the A549 cell lines with a stable TRAP1 knockdown and along side A549 cell lines transfected with a scramble sequence as a control, over the course of 28 days. The spheroid media was changed every 2 to 4 days as described in the methods. The spheroid images were captured via an inverted microscope interfaced with an axiovert camera. ImageJ software was used to determine the area of the spheroid and the volume of the spheroids were calculated from this parameter and rendered graphically. Each bar of graphical rendition is representative of an average of 8-10 spheroid volumes.

Figure3.8 is representative of three independent experiments and show that for the first 7 days the scramble transfected spheroids (SCR) and the TRAP1 knock down spheroids (TRAP1 KD) were of equal size at onset, but by day 10 the SCR spheroids had begun to outgrow the TRAP1 KD spheroids. By day 16, the SCR spheroids were about 50% larger than the TRAP1 KD spheroids and from this point onwards, continued to grow larger and faster than the TRAP1 KD spheroids.

A.

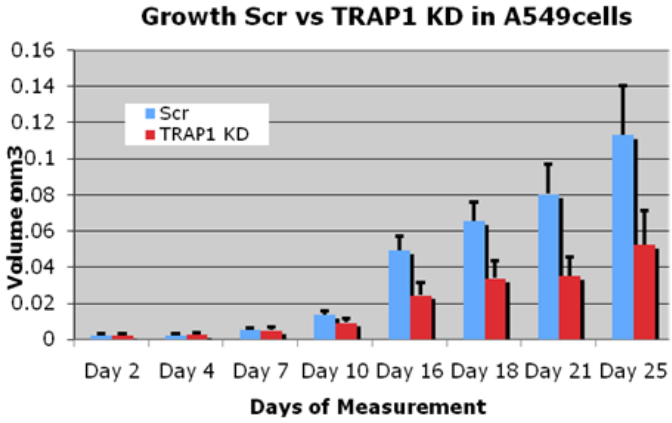

B.

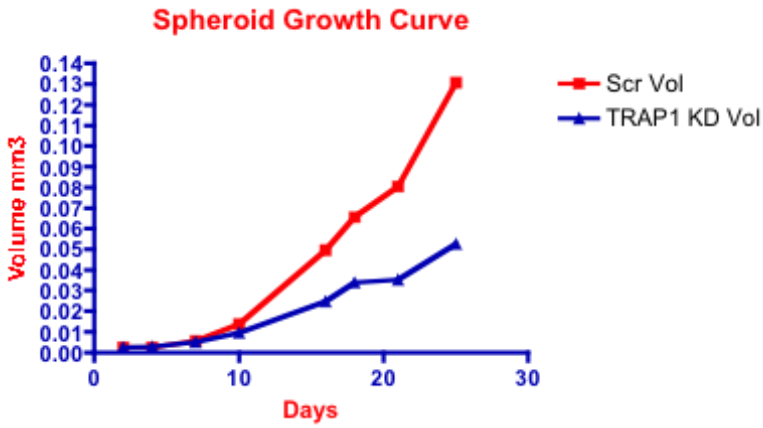

Figure 3.8 Effect of TRAP1 knockdowns in spheroid growth.

Comparing mock transfected A549 spheroid (SCR) to the TRAP1 knockdown spheroids (TRAP1 KD). The SCR (TRAP1 positive) spheroids outgrew the TRAP1 KD (TRAP1 knockdown spheroids). (A) Bar graph of spheroid volume measurement in mm^3 (y-axis) versus the days of spheroid measurement (x-axis) of A549 SCR and TRAP1 KD spheroids. Each bar is representative of the average volume of 8-10 spheroids. The error bars represent the standard deviations. (B)Spheroid growth between the SCR and TRAP1 KD in form of a Growth curve each point representing the average volume measurement of 8-10 spheroids through the course of 28 days of growth. P value = 0.0078 (Wilcoxon signed ranked test) for spheroid growth between the mock transcfected A549 and TRAP1 knock down spheroid.

3.2.1.6 Effect of TRAP1 over-expression on MDA-MB-231 cell growth.

The breast cancer cell line MDA-MB-231 expresses very low levels of TRAP1 so I stably restored TRAP1 in this cell line via viral transfection for TRAP1 over expression and also

created a mock viral transfected MDA-MB-231 as a control (as described in Chapter 2). I confirmed the efficiency of transfection with Western blotting and then proceeded to use these cells for spheroid production. Spheroids were initiated in 96 well plates as described above. Spheroid areas were measured every 3-5 days and the volumes were calculated from the area measurements and rendered graphically. MDA-MB-231 spheroid measurements were initiated on day 11 due to their slow rate of growth and degree of spheroid formation. Day 11 is the point during their course of growth that they were recognizable as definite cohesive spheroids.

Figure 3.9 is representative of 3 independent experiment with each bar or point on growth curve representing the average volume of 8-10 spheroids. From the graph in Figure 9 it can be seen that by the 11^{th} day of growth, the MDA-MB-231 TRAP1 positive spheroids (TRAP1 UP) had began to outgrow the mock transfected spheroids and this remained the pattern of growth up until the final day of spheroid measurement. An additional observation was that the mock transfected MDA-MB-231 spheroids (SCR) appeared to have minimal growth, plateauing between days 16 to day 26, while the TRAP1 positive spheroids seemed to grow exponentially within the course of those days such that by day 26 the TRAP1 positive spheroids were approximately six times the size of the mock transfected MDA-MB-231 spheroids.

As MDA-MB-231 cells were slow in forming spheroids, they ultimately produced very small spheroids that were measurable with aid of a microscope but could not be manipulated for formalin fixation and wax processing.

A.

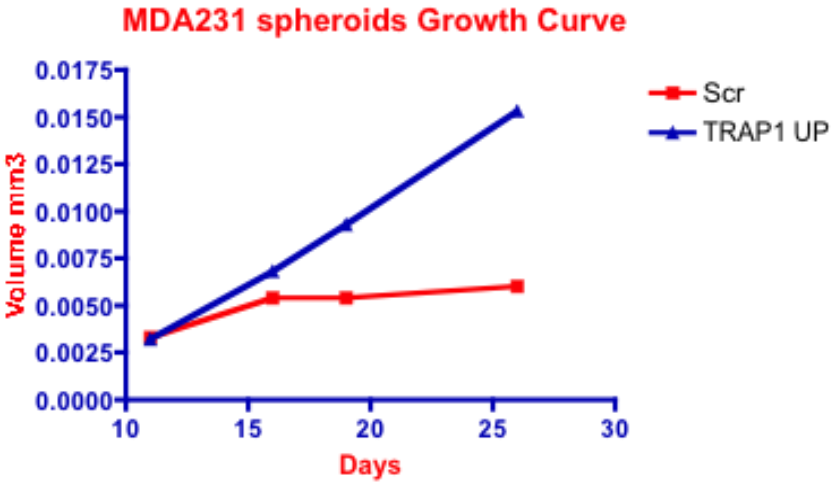

B

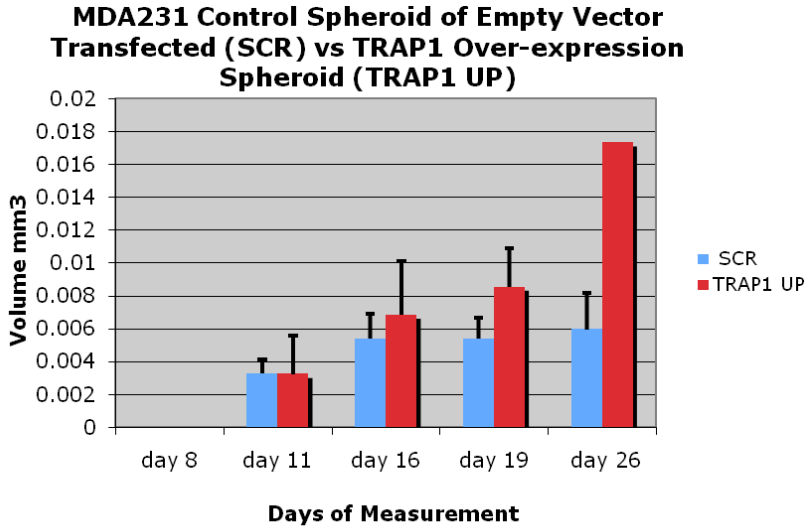

Figure 3.9 Effect of TRAP1 over-expression on MDA-MB-231 cell growth.

Comparison of MDA-MB-231 TRAP1 positive spheroids equivalent to TRAP1 overexpression (represented in legend as TRAP1 UP) and **empty vector control** transfected equivalent to TRAP1 depleted spheroids (represented in legend as SCR). Figure shows the MDA-MB-231 TRAP1 overexpression spheroids exponentially outgrowing the MDA-MB-231 TRAP1 depleted spheroids.(A) Bar graph of MDA-MB-231 SCR versus TRAP1 UP spheroid volume in mm^3 versus days of volume measurement with each bar representing the average volume of 8 to 10 spheroids. The error bars represent the standard deviations. (B) Growth curve of MDA-MB-231 SCR versus TRAP1 UP spheroids with each point representing the average volume measurement of 8-10 spheroids through the course of 28 days of growth. p= 0.0083 (Wilcoxon signed ranked test).

3.2.1.7 Deciphering the TRAP1 Pathway by immunostaining A549 Scrambled and TRAP1 knockdown Spheroids.

The scrambled and TRAP1 knockdown spheroids were collected at intervals of 2 to 3 days, with collection initiated on the 15th day of growth up to 28th day. Spheroids collected is an amalgam of 3 sets of spheroids set up independently.

Spheroids were fixed in formalin, processed into wax blocks and sectioned for immunohistochemistry staining (as described in Chapter 2) . Sections of formalin fixed paraffin embedded reactive tonsils were used as positive controls for the immunostaining of TRAP1, MIB1 and Caspase3. A lung tumor was the positive control for CA9.

The immunostainings were evaluated by 2 different techniques to minimize result biases. Immunostained sections of the spheroids were first blindly, manually scored by me and 2 other senior pathologist for thoroughness. Manual scores were given in the form of intensity percentage score (IPS) with a possible minimum score of 0 and possible maximum score of 300. The sections were then further analyzed by image analysis using Q-imaging Micropublisher 5 RV camera interface with a Ziess Axioskop microscope and Photoshop software which generated numerical values for the degree of staining intensity from images captured. The results of each the various studied markers obtained by both techniques are depicted graphical below preceded by their respective corresponding table reflecting the manual IPS and image analysis' average intensity scores.

TRAP1 immunostaining of spheroids

TRAP1 immunostaining				
	Manual Scoring		**Image Analysis Scoring**	
Days	A549 SCR IPS	A549 TRAP1 KD IPS	A549 SCR Intensity	A549 TRAP1 KD Intensity
15	180	40	55.2	55.5
17	180	20	59	51
19	140	50	53.7	46.7
21	160	30	57	42.2
24	140	30	39	35.8
28	160	30	49.5	16.5
	Unpaired t test, P value <0.0001		Unpaired t test, P value = 0.114	

Table 3.1.Results of TRAP1 immunostain analysis via manual and image analysis scoring. Data from table confirming TRAP1 knockdown in the TRAP1 KD spheroid as compare to the sequence transcfected (SCR) spheroid, with a statistically significant difference ($p<0.0001$) between the TRAP1 KD and SCR from the manual scoring.

TRAP1 immunostaining was done for confirmation of efficient TRAP1 silencing in the TRAP1 knockdown spheroids (TRAP1 KD) compared to the spheroids with scramble transfection (SCR). The presence of TRAP1 was mostly localized in the cytoplasm when observable. Results obtained from the **manual scoring** of the spheroids reflect adequate TRAP1 silencing in the TRAP1 knockdown spheroids with significant p value of 0.0001, compared to the spheroids with scrambled sequence transfection (Table 1; Figure 10A). The **image analysis** did as well reflect a degree of TRAP1 silencing however not a significant TRAP1 knockdown, P value = 0.114 (Table 1; Figure 10B)

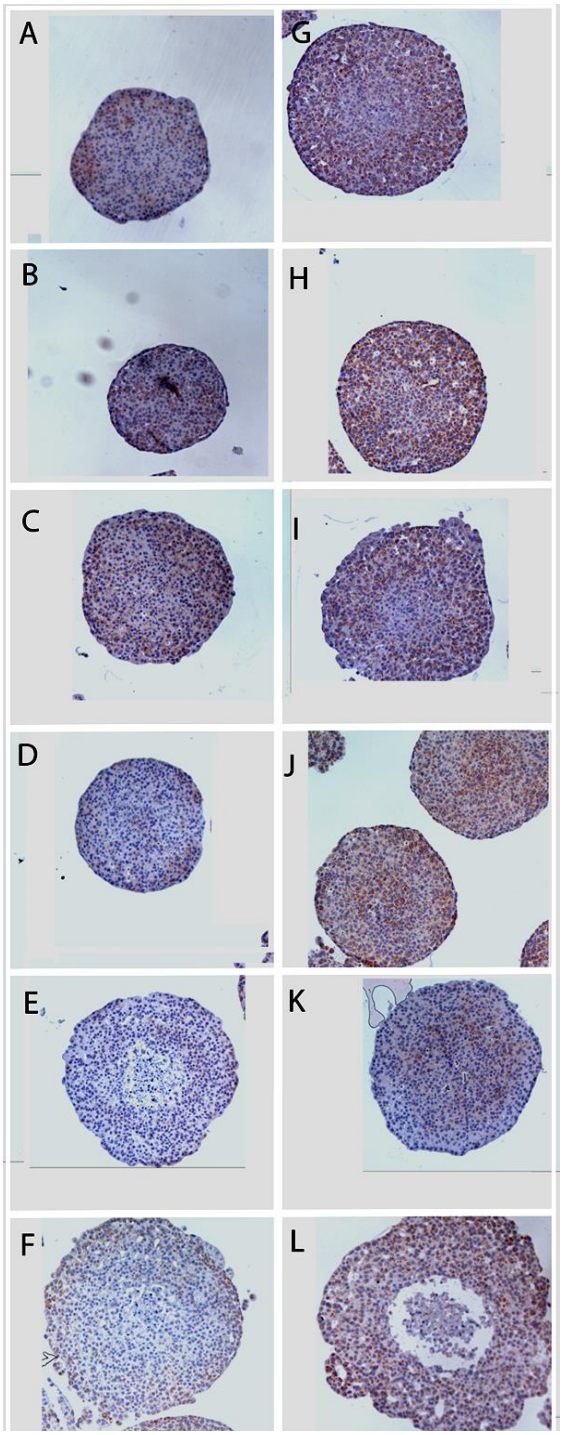

Figure 3.10 TRAP1 staining of spheroids.

A to F are TRAP1 KD spheroids of days 15, 17,19, 21, 24, 28 respectively. G to L are SCR spheroids of days 15, 17, 19, 21, 24, 28 respectively. Figure shows progressive increase in size from day 15 to day 28, with the SCR spheroids consistently larger than the TRAP1 KD spheroids. The SCR spheroids also have more roboust TRAP1 staining indicative of TRAP1 presence than the TRAP1 KD spheroid with TRAP1 silencing.

TRAP1 and Proliferation (MIB1 immunostaining of spheroids)

MIB1 immunostaining				
	Manual Scoring		**Image Analysis Scoring**	
Days	A549 SCR IPS	A549 TRAP1 KD IPS	A549 SCR Intensity	A549 TRAP1 KD Intensity
15	20	30	34.33	57
17	50	30	49	61.25
19	20	15	35.3	22.75
21	15	40	39.33	74.4
24	5	5	26	32.25
28	5	5	20.2	21.8
	Unpaired t test, P value =0.86		Unpaired t test, P value = 0.306	

Table 3.2.Results of MIB1 immunostain analysis via manual and image analysis scoring. MIB1 staining of the sequence transfected and TRAP1 knock down spheroid, though not statistically significant p= 0.306, image anaylsis reflects high MIB1 expression in the TRAP1 knockdown, while manual scoring reflects generally equal degree of MIB1 expression in both spheroids.

MIB1 expression in spheroids when observed was mainly nuclear. While assessing for proliferative potential in the spheroid using MIB1 markers, it was evident from a physical observation stand point (Figure 3.11) that through their course of growth between days 15 to 17, both the scrambled and TRAP1 knockdown spheroids had significant MIB1 positivity. By day 21, the scrambled sequence transfected spheroids (SCR) were much larger, had more peripheral zoning pattern and prominent necrotic cores deficient of MIB1 positive cells; while the smaller TRAP1 knockdown spheroids (TRAP1 KD) still had MIB1 positive cells scattered throughout the whole nodule. Between days 24 to 28 the SCR spheroids had progressively become very necrotic and had little to no observable MIB1 positive cells, while the TRAP1 KD spheroids retained a substantial degree of peripheral cells positive for MIB1 during this time course. However, the manual and image analysis scoring did not show any significant difference between the SCR and TRAP1 KD spheroids' MIB1 expression.

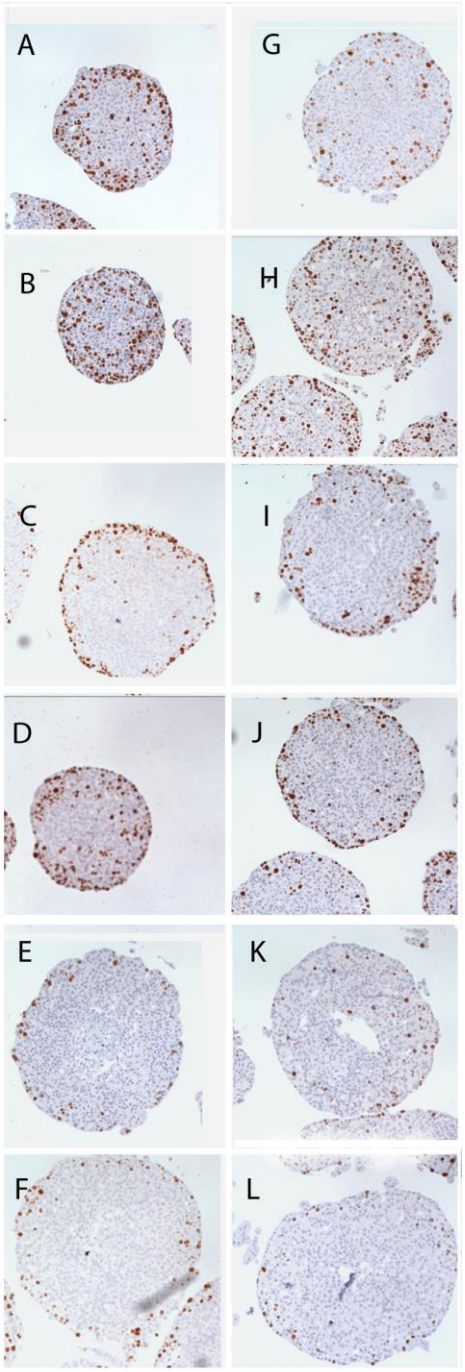

Figure 3.11MIB1 staining of spheroids.

A to F are TRAP1 KD spheroids of days 15, 17,19, 21, 24, 28 respectively. G to L are SCR spheroids of days 15, 17, 19, 21, 24, 28 respectively. Figure shows progressive increase in size from day 15 to day 28, with the SCR spheroids was generally larger developing necrotic core earlier than the TRAP1 KD spheroids. Both the TRAP1 KD and SCR spheroids demonstrated equal MIB1 positivity.

TRAP1 and Hypoxia (CA9 immunostaining of spheroids)

CA9 immunostaining				
	Manual Scoring		**Image Analysis Scoring**	
Days	A549 SCR IPS	A549 TRAP1 KD IPS	A549 SCR Intensity	A549 TRAP1 KD Intensity
15	225	240	132.4	111.8
17	150	60	108.2	82.5
19	210	270	122	112.5
21	270	150	101.7	101.3
24	270	270	131.3	116.8
	Unpaired t test, P value =0.67		Unpaired t test, P value = 0.23	

Table 3.3.Results of CA9 immunostain analysis via manual and image analysis scoring.
Table shows CA9 staining of both sequence transfected and TRAP1 knockdown with no statistically difference of CA9 expression in either the sequence transfected or TRAP1 knockdown spheroid.

Positive CA9 was mostly membranous with only occasional weak cytoplasmic staining. By day 15, 75-80% of both the SCR and TRAP1 KD spheroids cells were positive for CA9, though from physical observation the SCR spheroids appeared to have a quicker and more intense onset of CA9 expression than the TRAP1 KD spheroid. Manual and image analysis did not demonstrate any statistical significant difference in CA9 expression between both the SCR and TRAP1 KD spheroids.

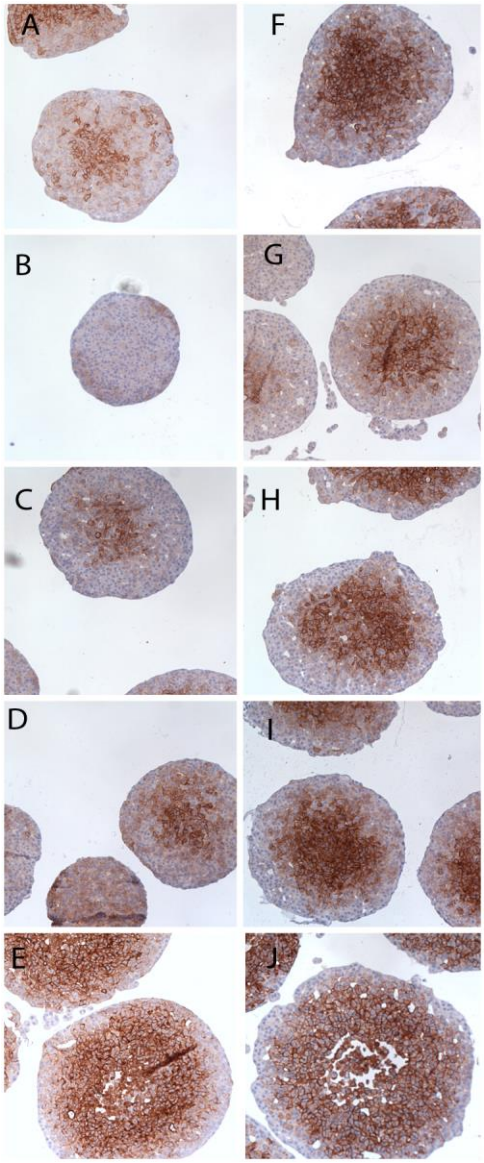

Figure 3.12 CA9 staining of spheroids.

A to E are TRAP1 KD spheroids of days 15, 17,19, 21, 28 respectively. F to J are SCR spheroids of days 15, 17, 19, 21, 28 respectively. Figure shows progressive increase in size from day 15 to day 28, with the SCR spheroids consistently larger and having stronger CA9 positivity than the TRAP1 KD spheroids.

TRAP1 and Apoptosis (Caspase 3 immunostaining of spheroids)

Caspase 3 immunostaining				
	Manual Scoring		**Image Analysis Scoring**	
Days	A549 SCR IPS	A549 TRAP1 KD IPS	A549 SCR Intensity	A549 TRAP1 KD Intensity
15	210	150	93.2	68.8
17	270	270	112.5	88.4
19	210	210	115	100.5
28	300	240	121.8	104
	Unpaired t test, P value =0.41		Unpaired t test, P value = 0.10	

Table 3.4. Results of Caspase 3 immunostain analysis via manual and image analysis scoring.

Table shows relatively equal degree of Caspase 3 staining in both the scramble transfected (TRAP1 SCR) and TRAP1 knockdown (TRAP1 KD) spheroids via both scoring methods, results not statistically significant.

Caspase 3 when present was primarily nuclear. From observation (Figure 17), by day 15 the SCR spheroids had about 70% Caspase 3 positive cells while TRAP1 KD spheroids had only about 50% Caspase 3 positive cells. Based on the manual and Image analysis scoring, between days 17-28, both the SCR and TRAP1 KD spheroids had attained relatively equal degree of Caspase 3 positivity.

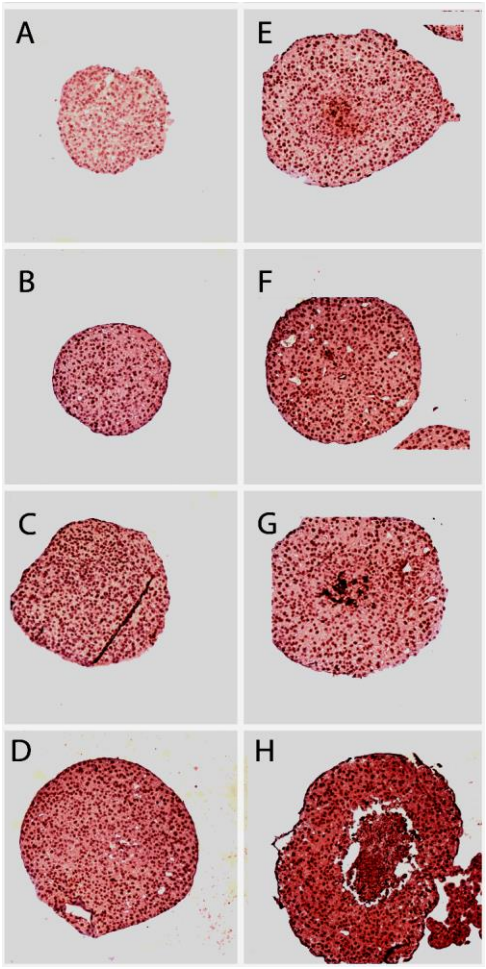

Figure 3.13. Caspase 3 staining of spheroids.

A to D are TRAP1 KD spheroids of days 15, 17, 19, 28 respectively. E to H are SCR spheroids of days 15, 17, 19, 28 respectively. Figure shows progressive increase in size from day 15 to day28, with the SCR spheroids consistently larger than the TRAP1 KD spheroids. Both SCR and TRAP1 KD have equal caspase 3 positive nuclei.

Correlation between TRAP1 and Rb expression

Rb immunostaining		
	Manual Scoring	
Days	**A549 SCR IPS**	**A549 TRAP1 KD IPS**
15	40	5
17	60	20
19	60	30
21	150	90
24	100	20
28	120	75
	Unpaired t test, P value =0.05	

Table 3.5.Results of Rb immunostain analysis via manual scoring.
Table shows decreased Rb in the TRAP1 knockdown (TRAP1 KD) spheroids from days 15 to 28 when compared to the scramble sequence transfected spheroids with a statistically significant p value of 0.05.

Due to the prominent blue color of the 3,3' Diaminobenzidine (DAB) counter stain, Rb immunostaining was unable to be analyzed by image analysis and hence was only scored manually. Rb staining was observed predominantly in the nucleus. Rb staining pattern appeared to correlate with the absence or presence of TRAP1. The TRAP1 positive SCR spheroids on day 15 had about 30-40% positive Rb cells, while the TRAP1 negative TRAP1 KD spheroids had about 5 % Rb positive cells. Between days 17-28 there was an increase in Rb positivity to about 30% in the TRAP1 knockdown spheroids though there was twice this degree of Rb positivity in the scrambled sequence transfected spheroids. Overall there was a higher degree of Rb staining in the scrambled sequence transfected spheroids than in the TRAP1 knockdown spheroids.

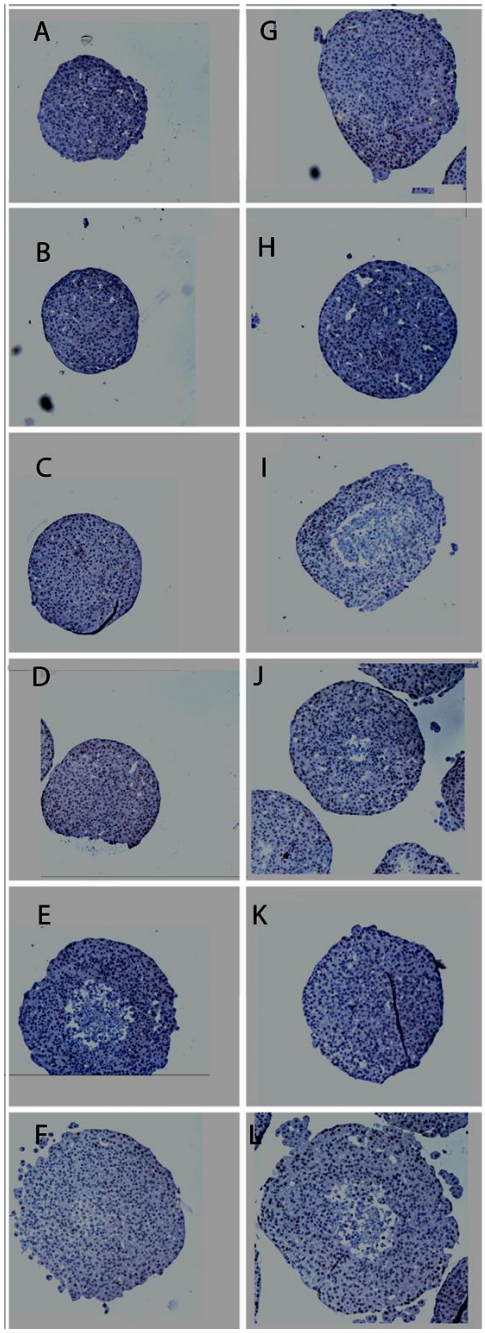

Figure 3.14. Rb staining of spheroids.

A to F are TRAP1 KD spheroids of days 15, 17,19, 21, 24, 28 respectively. G to L are SCR spheroids of days 15, 17, 19, 21, 24, 28 respectively. Figure shows progressive increase in size from day 15 to day 28, with the SCR spheroids consistently larger than the TRAP1 KD spheroids. The SCR spheroids with TRAP1 present was more positive for Rb staining than the TRAP1 KD spheroid with silenced TRAP1.

3.3 Discussion

TRAP1 is a chaperone to Rb (Chen, Chen et al. 1996), a role that produces a transient inhibitory role in cell proliferation in the event of heat shock when TRAP1 moves into the nucleus, however this effect is transient as after 24 hours, nuclear levels of TRAP1 diminish again (Hu et al Submitted). TRAP1 was originally identified in association with TNFR1 (Song, Dunbar et al. 1995). It has also been demonstrated that in both normoxia and hypoxia TRAP1 expression is associated with an mRNA signature consistent with activation of proliferation via the TNFR pathway (Liu, Hu et al. 2010).

In 2D cell culture, we observed that in normoxia TRAP1 positive cells doubled in number quicker than TRAP1 negative cells. This cell doubling was determined to be due to increased cell proliferation in the TRAP1 positive cells rather than a result of apoptosis inhibition. We also determined that hypoxia down-regulates TRAP1 hence in hypoxia, TRAP1 positive and negative cells grew and multiply at similar rates (Agoretta et al., manuscript in preparation).

As these were result from 2D cell culture, it became necessary to access this information in 3D "in vitro" spheroid models which better emulate tumor characteristics than 2D cell culture. The spheroid model allowed me to get a better idea of how these results could relate to real tumors since growing spheroids display a gradient of proliferating cells from the outer cell layers and quiescent cells located more centrally. When deprived of oxygen and glucose, the central cells die and a necrotic core is formed. This spheroid cell heterogeneity is similar to that found in avascular regions of tumors (Mellor, Ferguson et al. 2005, Dufau, Frongia et al. 2012). As an abnormal or inadequate vasculature is often found within solid tumors to affect their micro-environment (Mellor, Ferguson et al. 2005), the 3D model would capture this characteristic and

in tandem allow the monitoring of the effect of TRAP1's presence or absence in this micro-environment .

The A549 cell growth curve of the spheroid (Figure 3.8) showed that the TRAP1 positive cells, transfected with a scrambled sequence (SCR), out grew the TRAP1 knockdown (TRAP1 KD) spheroids through the entirety of their growth in culture. Concomitantly, when TRAP1 was restored in the TRAP1 deficient MDA-MB-231 spheroids, a similar effect was observed whereMDA-MB-231 spheroids with restored TRAP1 (TRAP1 over-expression) consistently grew faster than the vector control transfected MDA-MB-231 spheroids. These observations emphasize the significant role played by TRAP1 in proliferation and growth.

Additionally, from morphological observation of the spheroids, comparing the scramble sequence transfected (SCR) to the TRAP1 knockdown (TRAP1 KD) spheroids, the former were larger in size (Figures 3.10-3.13), had very rough external outer surfaces with numerous blebs (Figure 3.7) and developed necrotic cores early on. The TRAP1 knockdown spheroids generally looked healthier, had smoother outer rims (Figure3.7) and had a larger percentage of viable cells with at most only a minimal necrotic core. These characteristics imply that the scrambled sequence transfected spheroids were most likely proliferating rapidly and at the same rate using up their nutrients and oxygen, an inherent feature that was most likely facilitating their rapid aging and necrosis.

Immunostaining for MIB1 was used to assess proliferation in these spheroids (Figure 3.11, Table 3.2). The scrambled-sequence transfected spheroids having developed a significant necrotic core as early as day 17 showed a zoning pattern with the MIB1 marker at this time, with much of its proliferative potential at the periphery of the nodule and by last date of

measurement had less proliferative cells than the TRAP1 knockdown spheroid. This as well points to the rapid proliferative rate of the TRAP1 positive spheroids.

The scrambled-sequence-transfected spheroid's large size in turn also contributes to its rapid hypoxia development as its size limits proper oxygen and nutrient penetration of the entire nodule. Since that demand is not adequately met, the scrambled sequence transfected spheroids' succumb to hypoxia quicker, as physically observed with the CA9 marker studies (Figure 3.12), which also contributed to a decline in their proliferative ability. As a result, they falls apart quicker which further explains the observed roughness and blebs around their surface(Figure 3.7).

Its has been previously described in our lab that TRAP1 protein does play a contributory role in driving cell proliferation via its participation in the TNF pathway (Liu, Hu et al. 2010). Results from present study confirms this as it can be seen (Figures 3.10) that TRAP1 knockdown A549 cells which had decreased TRAP1 protein produced smaller spheroids when compared to the scrambled sequence transfected A549 spheroids which are TRAP1 positive and grew faster and larger.

Extrapolating this result to real life, the smallness of a TRAP1 knockdown spheroid could be one of the advantages that tumors like non-small cell lung cancer that down-regulate their TRAP1 protein (Pezzella, Pastorino et al. 1997) possess. These TRAP1 negative tumors probably proliferate slower, are more efficient in oxygen and nutrient consumption and as a result they remain viable longer. This as well, will suggest that TRAP1 negative tumors could be one of those tumors that grow for many years before they fully develop and become detectable. While, TRAP1 positive real life tumors may be equivalent to the rapidly

proliferating scrambled sequence transfected spheroids which has been demonstrated by this present study to be marked by their prolific consumption of oxygen and nutrients, and in effect facilitate rapid hypoxia onset and early necrosis. As hypoxia is a catalyst for metastasis (Mellor and Harris 2007, Semenza 2010), such tumors are hence very likely proned to rapid metastasis.

With consideration to the above speculation, it would be worth investigating and confirming if tumors that down-regulate their TRAP1 proteins are always slower growing and conversely if most slow growing tumors have a reduced or no TRAP1 presence. Additionally, it would also be interesting to investigate if most rapid metastatic tumors tend to over-express TRAP1.

Since TRAP1 is a chaperone for Rb, a gene central to many human cancers, I wanted to investigate how loss of TRAP1 affected Rb expression. It was consistently observed that the TRAP1 knockdown spheroids were less positive for Rb than the scrambled sequence transfected spheroids.

It also corroborates the role played by TRAP1 as a chaperone to Rb (Chen, Chen et al. 1996). The following conclusions are reflected in the Rb staining patterns: 1) When TRAP1 positivity decreased in the spheroid, Rb positivity also decreased. 2) Hypoxia is known to switch off TRAP1 (Liu, Hu et al. 2010), so as the spheroids got larger and hypoxia ensued, there was a corresponding decrease in TRAP1 in both the scrambled sequence transfected and TRAP1 knockdown spheroids. This TRAP1 decrease was more significant in the latter which had: 1) depleted TRAP1 2) the impact of the onset of hypoxia switching off whatever residual TRAP1 it still had available. This in turn affected the Rb which was observed to have an equivalent decreased expression in association with a decreased TRAP1 expression (Figure 3.11). The Rb decrease was as well more prominent in the TRAP1 knockdown spheroids especially between

days 21-28 (Figure 3.14) when hypoxia had reached optimum and further limited the capability of TRAP1 to refold any denatured Rb. The consequence of this is increased advancement into the cell cycle and ultimately, increased proliferation. This implication also corroborates Hu et al's finding (manuscript submitted) showing that when TRAP1 is silenced the total amount of Rb diminishes and following hypoxia there is an absence or failure of Rb to bind to E2F1 and consequently more cells than usual enter the S phase and proliferate.

Caspase 3 was used to assess apoptosis in these spheroids (Figures 3.13). Analysis of these spheroids showed no difference in the pattern or intensity of Caspase 3 between both the scrambled and TRAP1 knockdown spheroids. Both had the same degree and intensity of Caspase 3 staining through the whole nodule. This then implies that both the TRAP1 knockdown and scrambled spheroids were experiencing apoptosis at the same rate. Also, it further affirms the conclusion made from the analysis of the MIB1 marker that though the scrambled sequence transfected spheroids were generally larger than the TRAP1 knockdown spheroids, this was primarily due to TRAP1 induced rapid proliferation in the scrambled sequence transfected spheroids and not as a result of TRAP1's inhibition of apoptosis. This also further confirms Agoretta et al's (manuscript submitted) finding in 2D cell culture showing no significant observable difference in apoptosis between the TRAP1 positive and negative A549 cells.

3.4 Conclusion

In conclusion TRAP1 appears to be a cancer related double edge sword where both its presence and absence could play out to the advantage of a cancer. Using the spheroid model, I have demonstrated that TRAP1 is involved in tumor proliferation, which is evident in the growth

curves where TRAP1 positive cells steadily grew faster than TRAP1 negative cells. Also, due to rapid proliferation in TRAP1 positive cells hypoxia rapidly ensued which when correlated to real tumors indicates a poor prognosis for a patient.

Additionally, I have shown here that TRAP1's link to the Rb pathway correlates to its function as a chaperone to Rb. A compromise of TRAP1/TRAP1 absence is a detriment to Rb as this will facilitate rapid progression into cell cycle and ultimately favor cell proliferation. This could be a possible adaptive mechanism with which TRAP1 negative tumors on the other hand promote cell proliferation and tumor growth.

Furthermore, I confirmed colleagues' work of there being no clear association between TRAP1 presence and inhibition of apoptosis, hence implying that TRAP1's oncogenic role lies more in its promotion of cell proliferation than in inhibition of apoptosis. These results support a role for TRAP1 as a possible therapeutic target in cancer treatment, which has been emphasized in a recent clinical review (Kang 2012).

CHAPTER 4
JMY PROTEIN EXPRESSION IN NORMAL AND NEOPLASTIC TISSUES

4.1 Introduction

The gene coding for JMY (junction-mediating and regulatory protein) was cloned in 1999 and identified as a p300-binding protein helping to regulate the p53 response and promoting apoptosis (Shikama, Lee et al. 1999). Alongside three other pro-apoptotic p53 cofactors, JMY expression was discovered to be up-regulated by E2F1, linking in this way the Retinoblastoma (Rb) pathway to p53 regulation (Hershko, Chaussepied et al. 2005). This link was further supported by the finding that JMY is targeted and degraded by Mdm2, as part of the inhibitory action that this protein has on p53 (Coutts, Boulahbel et al. 2007).

It was later on, with the discovery of its protein sequence homology to actin regulators and nucleators (Zuchero, Coutts et al. 2009)that its involvement with actin came to attention. JMY's capacity to regulate actin dynamics lies with its possession of WH2 domains that can either independently initiate actin filament formation in SPIRE-like fashion or activate actin nucleators such as ARP 2/3 (Campellone and Welch 2010). Experiments using the myeloid lineage HL60 have shown that JMY is mostly nuclear in these cells but when differentiation into neutrophils is induced, some JMY protein moves to the cell edge were it co-localizes with actin. JMY over-expression has also been found to be associated with increased speed of cellular migration (Zuchero, Coutts et al. 2009). Finally JMY expression and cytoplasmic co-localization with actin is increased under HIF1 stimulation (Coutts, Pires et al. 2011).

Actins filaments help facilitate physiological processes such as cell motility and migration, morphogenesis and immune response. Hence aberrant regulation and control of actin filament dynamics is vital in the process of tumor dissemination. Cancer metastasis is based on aberrant cell migration facilitated by increased cell motility, allowing tumors to invade and colonize surrounding as well as distant tissues (Coutts, Weston et al. 2009).

JMY is a protein that integrates cell adhesion and motility with the p53 response. It negatively regulates levels of expression of E and N Cadherins, which inhibits cell motility. "In vitro" experiments have shown that following DNA damage, more protein is translocated into the nucleus, where it accumulates (Coutts, Weston et al. 2009). Furthermore "scratch wound assays" have shown that in DNA damaged cells cytoplasmic JMY was not able to augment cell motility compared to non-DNA damaged conditions (Coutts, Weston et al. 2009) implying that JMY's ability to facilitate motility is diminished in the setting of DNA damage.

Given its association with cellular motility in actin filament formation and tumor suppressor activity as a p53 regulator, an understanding of JMY expression in normal and neoplastic human tissues would shed light on its role in cancer. However no JMY antibodies were available to investigate JMY expression on formalin fixed paraffin embedded tissue samples.

In this study I describe the making and characterization of a monoclonal antibody against JMY and the main patterns of expression of this protein in normal and neoplastic human tissues. This antibody specifically recognizes JMY protein and is suitable for both immunohistochemistry on paraffin embedded material and Western blotting.

4.2 Results

4.2.1 Specificity of Anti-JMY Antibodies

4.2.1.1 Western Blotting

The procedure for JMY antibody production is described in the materials and methods chapter. Western blots of MCF7 and HeLa cell lines demonstrated the expected band at approximately 130 kD. The JMY band was seen in MCF7 and HeLa cell lines transfected with non-target control (NTC) siRNA but was absent after transfection with specific JMY siRNA. In U2OS cell lines, only a faint JMY band was detected in negative control doxycycline non-induced cells but a clear JMY band was observed in doxycycline induced JMY over expression.

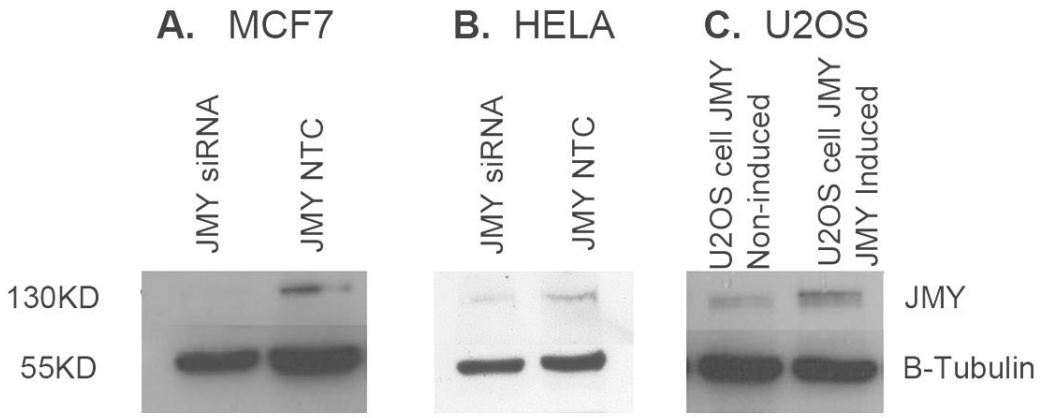

Figure 4.1.Western blot characterization of the anti-JMY antibody. (A) MCF7 cell line treated with JMY siRNA demonstrates decreased JMY protein expression and MCF7 cell line treated with JMY non-target control (NTC) RNA demonstrated JMY protein expression . (B) HELA cell line treated with JMY siRNA demonstrated decreased JMY protein expression and HELA cell line treated with JMY non-target control (NTC) RNA demonstrates JMY protein (C) U2OS cell line with non-induced JMY expression demonstrates endogenous JMY protein

expression and U2OS cell line treated with doxycycline inducing JMY expression (JMY over expression) demonstrates both endogenous and exogenous induced JMY protein expression.

4.2.1.2 Immunohistochemistry

Corresponding cell pellets of the above cell lines were formalin fixed, paraffin embedded and histological slides were prepared from them and stained by IHC. Consistent with western blot results, MCF7 and HeLa cells pellets treated with NTC RNA were positive while pellets of JMY siRNA treated cells were negative (Figure 4.1). Cell pellets of non-induced U2OS cells expressed the endogenous JMY, and the over expression induced U2OS cells expressed both endogeous and exogenously induced JMY protein expression.

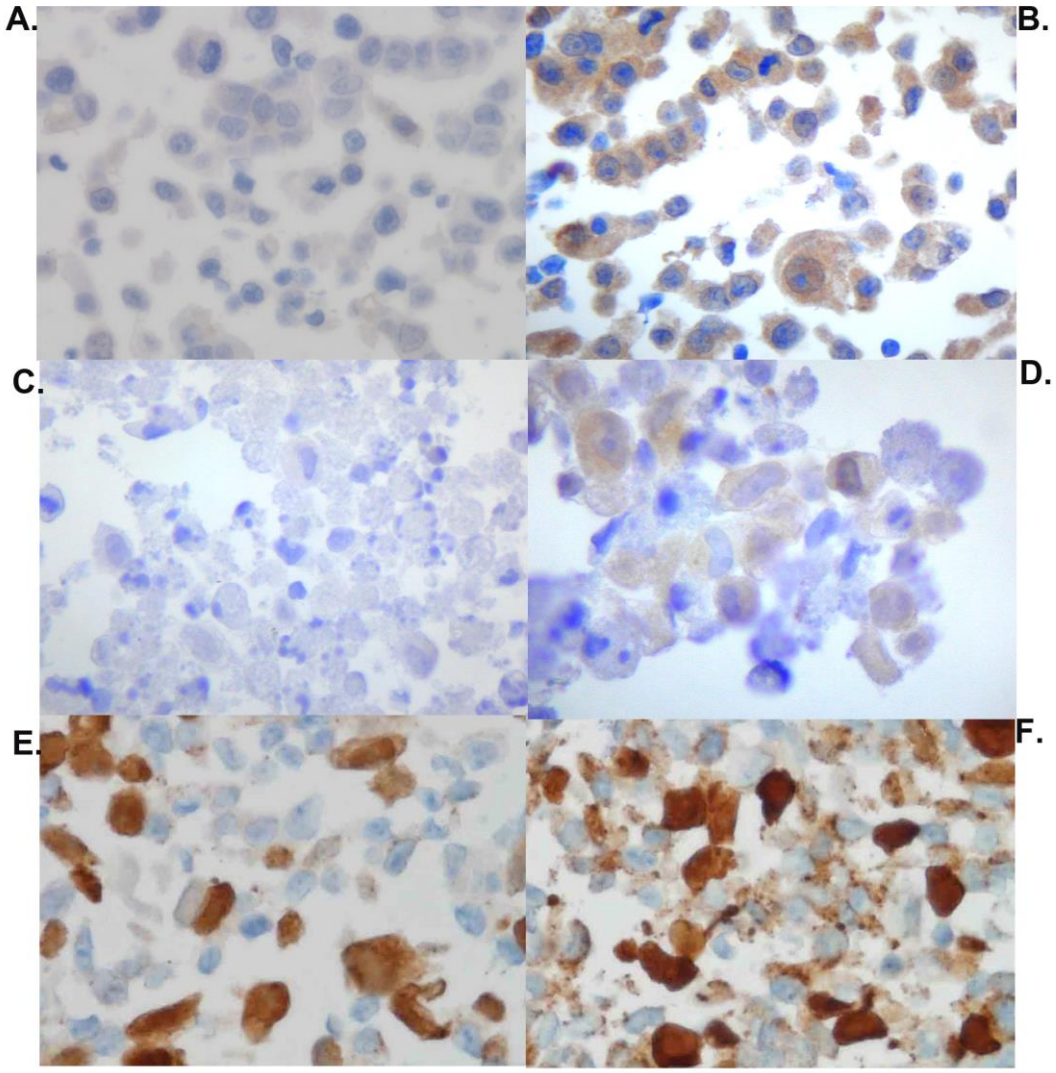

Figure 4.2.Cell pellet immunostain characterization of anti-JMY antibody. MCF7 cell pellet: (A) treated with JMY siRNA demonstrates decreased JMY protein expression due to JMY siRNA effect; (B) treated with JMY non-target control (NTC) RNA demonstrates undiminished expression of endogeous JMY protein. HeLa cell pellet: (C) treated with JMY siRNA shows diminished JMY protein expression as a result of JMY siRNA effect; (D) treated with JMY non-target control (NTC) RNA shows positive endogenous JMY protein expression. U2OS cell pellet: (E) with non induced JMY expression shows JMY protein expression with fewer cells expressing JMY compared to "F"; (F) with doxycycline induced JMY protein expression showing a prominent JMY expression with more cells expressing the JMY protein .

4.2.2 JMY expression in normal tissues.

JMY is widely expressed in many types of tissue: the main patterns of staining are summarized in Table 1 and some are presented in Figure 3. In all the tissues co-expression of cytoplasmic and nuclear JMY was observed with the exception of the spinous layer of the oesophagus where only nuclear JMY expression is present. The intensity of the cytoplasmic and nuclear staining was variable across the different tissues and sometimes even within the same tissue. Alongside JMY, p53 expression, using the DO7 antibody (Monoclonal mouse anti human p53 antibody, Dako A/S, Glostrup, Denmark) - was also recorded. While cytoplasmic staining for JMY was observed only in adrenal cortex, a striking correlation was present between JMY staining (cytoplasmic and nuclear) and nuclear p53 expression (Table 4.1). E-Cadherin also is widely expressed in normal tissues but there was no E-Cadherin expression correlation to either JMY or p53 (Table 4.1).

		JMY		P53		E Cadherin	
Organ		**Cytoplasm**	**Nucleus**	**Cytoplasm**	**Nucleus**	**Cytoplasm**	**Membrane**
Lymph node	germinal centres	+++	+	-	++	-	-
	mantle	+	+	-	+/-	-	-
	paracortex	+++	+	-	++/+	-	-
Tonsil	germinal centres	+++	+	-	++	-	-
	mantle	+	+	-	+/-	-	-
	paracortex	+++	+	-	++/+	-	-
	epithelium	+	++	-	+	+	+
Spleen	white pulp	+++	++	-	+		
	splenic cords	+/-	+/-	-	-		
Thymus	cortex	+/-	+/-	-	+/-		
	medulla	+++	++	-	+		
Lung	Bronchioli, basal	++	+/-	-	+/-		
	Bronchioli, columnar	++	+/-	-	++		
	Alveoli	-	-	-	-	-	-
Salivary glands		++	++	-	+	-	-
Oesophagous	epithelium, basal layer	+	++	-	+++	+/-	+++
	epithelium, spinous layer	-	++	-	++	-	+++
Stomach	cryptae	+++	-	-	+	++	+
	glands	+	-	-	+/-	++	++
Gall bladder	glands,	-	-	-	-	-	+/-
	cryptae	+	++	-	+/-	-	-
Pancreas	Exocrine	++	++	-	+	-	+++
Liver	hepatocytes	+	+	-	-	++	+++
Colon	Glands, upper half	+++	+++	-	++	-	+
	Glands, crypts	+	+	-	++	-	+/-
Kidney	tubules	+	+	-	++	+	+/-
	glomeruli	-	+/-	-	+/-	-	-
Breast	lobules, epithelial	++	++	-	+	+	+++
Uterus	Endometrium,	++	++	-	+/-	+/-	+/-
	myometrium	+	+	-	-	-	-
Placenta		-	-	-	+/-	+	-
Prostate		+/-	+/-	=	+	++	+/-
Testis	seminiferous tubules	+++	++	-	+++/++	-	-
Para thyroid	Chief cells	++	+	-	+/-	+/-	-
	Oxyphilic cells	++	+	-	+/-	+/-	-
Adrenal	cortex	+++	+++	+/-	++	-	-
Fat Tissue		-	-	-	-	-	-

* C Cytoplasmic, N Nuclear Me membranous . Intensity: + weak, ++ intermediate and +++ strong

Table 4.1 JMY, P53 and E-Cadherin expression in normal tissues by immunohistochemistry.

Table shows vast JMY expression through the tissues with co-expression in both the nucleus and cytoplasm. There is also a correlation in JMY and p53 co-expression such that when there is strong/intermediate JMY cytoplasmic and nucleus expression, there is a correlative strong/intermediate cytoplasmic and nucleus p53 expression. There is however no associative expression of E-cadherin to JMY or p53.

4.2.3 JMY expression in primary tumors.

JMY was found to be expressed in all the types of tumors stained although the number of negative cases, the proportion of positive cells (Table 4.2) and the combined Intensity/Percentage Staining (the IPS score, Table 4.3) were very variable. However in all the positive tumors, a close correlation between cytoplasmic and nuclear IPS score was found (Table 4.3).

In breast, the normal epithelium is JMY positive. In all but one “in situ” carcinoma JMY was also positive, while only a proportion of invasive carcinomas expressed JMY (Table 2). It is important to note that the IPS score is also higher in “in situ” than in invasive carcinomas (Table 4.3).

Diagnosis	Compartment	0%	1-25%	26-50%	51-75%	76-100%
Follicular (NHL)	Cyto	2	0	2	0	49
	Nuc	2	0	3	0	48
Diffuse B (NHL)	Cyto	1	2	3	7	84
	Nuc	1	2	3	7	84
Lung(Small cell)	Cyto	3	0	0	0	21
	Nuc	3	0	1	0	20
Lung (NSCLC)	Cyto	12	13	10	16	53
	Nuc	5	15	25	17	42
Bladder (TCC)	Cyto	8	4	2	0	19
	Nuc	9	1	2	1	20
Head & neck carcinoma	Cyto	12	5	13	7	27
	Nuc	11	1	2	18	32
Head & neck (node mets.)	Cyto	10	3	13	7	46
	Nuc	1	2	5	16	55
Breast (DCIS)	Cyto	1	0	0	2	14
	Nuc	1	0	3	4	9
Breast (Invasive)	Cyto	133	8	16	6	121
	Nuc	94	11	33	20	126
Colon (ADC)	Cyto	33	2	5	2	51
	Nuc	46	4	10	10	23
Colon (node mets.)	Cyto	1	1	1	0	19
	Nuc	0	0	1	1	20
Colon (liver mets.)	Cyto	23	0	1	0	25
	Nuc	17	1	3	2	26
Renal Ca	Cyto	73	4	4	0	27
	Nuc	65	4	8	4	27
Prostate (ADC)	Cyto	72	5	7	2	24
	Nuc	26	13	19	4	48

Table 4.2. Number of tumor cases distributed according to the percentage of cells positive for JMY (% score) in each case.

Table reflects the close correlation of JMY expression in cytoplasm and nucleus, where cells of tissues with high cytoplasm JMY expression had a relatively equally high nucleus JMY expression and cells with low cytoplasmic JMY expression had a co relational low nucleus JMY expression.

Diagnosis	No. Cases	Cytoplasmic			Nuclear			Cyto v Nuc	
		Median	Mean	SD	Median	Mean	SD	Spearman	P-value (2 tail)
Follicular (NHL)	53	200	189.6	67.5	200	185.8	66.8	0.95	<0.0001
Diffuse B (NHL)	97	200	195	84.3	200	185.3	81.8	0.95	<0.0001
Lung (Small cell)	24	200	165.5	81.4	200	163.8	81.1	0.97	<0.0001
Lung (NSCLC)	104	100	122.8	98.9	100	122.3	81.7	0.81	<0.0001
Bladder (TCC)	33	100	106.1	87.5	100	111.5	85.26	0.96	<0.0001
Head & neck carcinoma	64	70	83.9	79.2	100	116.7	81	0.82	<0.0001
Head & neck (node mets.)	79	100	116.2	87.2	180	163.4	72.9	0.7	<0.0001
Breast (DCIS)	17	300	249.4	76.4	200	201.1	82	0.75	0.004
Breast (Invasive)	284	30	68.4	82	80	78.9	76.1	0.76	<0.0001
Colon (ADC)	93	100	87.7	86.1	10	48.9	68	0.51	<0.0001
Colon (node mets.)	22	200	176.3	79.1	200	198.4	67.6	0.4	0.0614
Colon (liver mets.)	49	80	65.5	71.4	100	83.4	77	0.88	<0.0001
Renal carcinoma	108	0	31.9	54.4	0	34.6	50.7	0.59	<0.0001
Prostate (ADC)	110	0	27.3	43.3	50	56	47.9	0.54	<0.0001

Table 4.3. JMY expression in tumors (IPS score)

Data showing JMY protein expression with significant correlation between cytoplasmic and nucleus expression in various tissue tumors. With a Spearman correlation which when the closer the number is to 1 the higher the correlation between cytoplasmic and nucleus JMY expression.

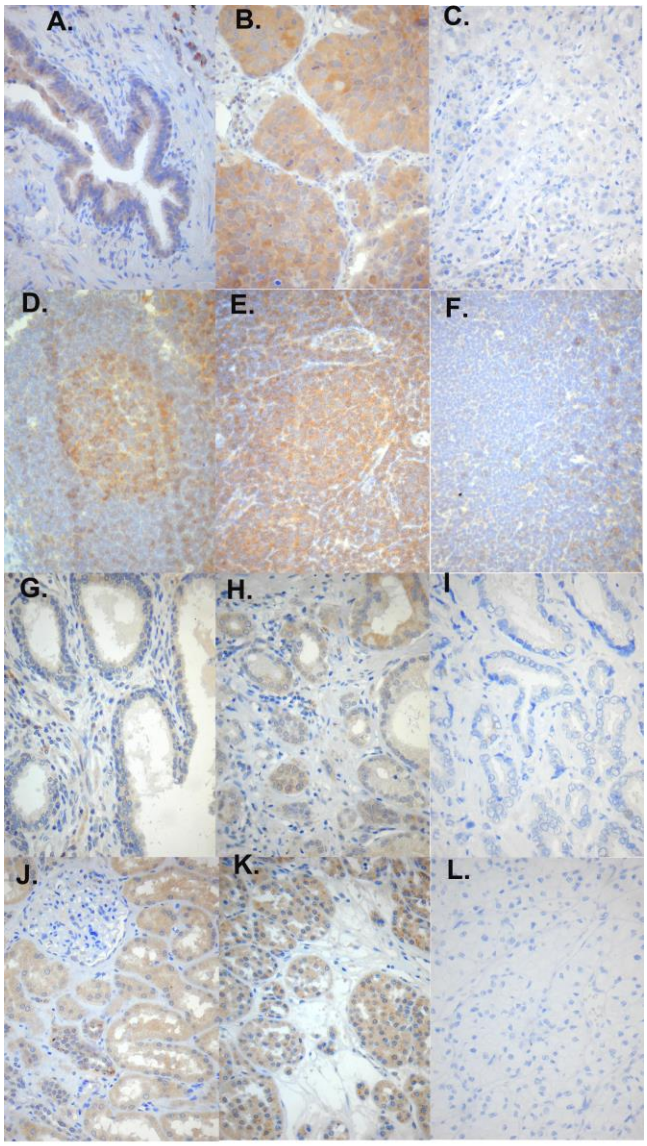

Figure 4.3.JMY's variable expression pattern in tissues and tumors.

(A) Positive JMY expression in normal lung, bronchial mucosa. (B) Positive JMY expression in non-small cell lung cancer. (C) Negative JMY expression in non-small cell lung cancer. (D) Positive JMY expression in germinal centers of reactive lymph node. (E) Positive JMY expression of Follicular Lymphoma. (F) Negative JMY expression of Follicular Lymphoma. (G) Weakly JMY positivity of normal prostate epithelium. (H) Positive JMY expression of prostate adenocarcinoma. (I)Negative JMY expression of prostate adenocarcinoma. (J) Positive JMY expression in tubular epithelium of normal kidney and Negative JMY expression glomeruli epithelium of normal kidney. (K) Positive JMY expression of Renal clear cell carcinoma. (L) Negative JMY expression of Renal clear cell carcinoma.

4.2.4 JMY Expression in primary versus metastatic tumours.

Expression (defined as average IPS scoring) in primary tumors and synchronous node metastases was compared in a series of head and neck and colorectal carcinomas (Figure 4.3). In the latter, JMY expression was also compared to that of tumors relapsing as liver metastases. There was a significant increase of JMY expression, both cytoplasmic and nuclear, in node metastases compared to primary carcinomas in both head/neck and colorectal carcinoma (Table 4). Additionally a higher nuclear but not cytoplasmic expression was also observed in colorectal carcinoma metastatic to the liver (Table 4.4).

Diagnosis	JMY Expression	Primary N Cases/IPS	Node Mets. N Cases/IPS	Liver Mets. N Cases/IPS	P-value (2 tail)
Head & neck carcinoma	Nuclear	64 / 116.7	79 / 163.4		0.0003
	Cytoplasmic	64 / 83.9	79 / 116.2		0.02
Colon (ADC)	Nuclear	93 / 48.9	49 / 198.4		<0.0001
		93 / 48.9		22 / 83.4	0.006
	Cytoplasmic	93 / 87.7	49 / 176.3		<0.0001
		93 / 87.7		22 / 65.5	0.14

Table 4.4. JMY expression in primary versus metastatic lesions (IPS score)

Table reflecting statistically significant increase in JMY expression in both nucleus and cytoplasm (p= 0.0003 and 0.02 respectively) in head and neck carcinoma node metastasis, as well as in colon node and liver metastasis in the nucleus (p<0.0001 and 0.006). There is also increased cytoplasmic JMY expression in colon metastsis to the node (p<0.0001) but a decrease of cytoplasmic JMY expression in colon metastsis to the liver.

4.2.5 Correlation between JMY and p53 expression

Correlation between JMY and p53 expression (defined as IPS scoring) was investigated in 241 invasive breast carcinomas and 87 non-small cell lung carcinomas (NSCLC). In both types of

tumors: nuclear p53 expression correlated directly with both cytoplasmic and nuclear JMY expression (Table 4.5) with p values of 0.01 and 0.03 respectively in invasive breast carcinoma; p values of 0.006 and 0.001 respectively in NSCLC.

Diagnosis	JMY	P53	p-val	r	n
Breast (invasive)	Cyto	Cyto	0.09	0.12	241
	Cyto	Nuc	0.01	0.17	
	Nuc	Cyto	0.3	0.06	
	Nuc	Nuc	0.03	0.8	
Lung (NSCLC)* (*Cyto p53 absent)	Cyto	Nuc	0.006	0.29	87
	Nuc	Nuc	0.001	0.35	

Cyto= Cytoplasm, Nuc= Nucleus, NSCLC= Non small cell lung carcinoma

Table 4.5. Relationship of JMY expression to p53 in invasive breast cancer and non-small cell lung carcinoma.

Shows a significant correlation between nucleus JMY and p53 expression in invasive breast cancer and Non small cell lung cancer (p=0.03 and 0.001 respectively).

4.2.6 Correlation between JMY and E-Cadherin expression

Correlation between JMY and E-Cadherin expression (defined as IPS scoring) was investigated in 235 invasive breast carcinomas and 17 In situ breast carcinomas. In invasive breast carcinoma, an inverse correlation (r=-0.140, p value of 0.032) was found only between cytoplasmic JMY and membranous E-Cadherin but no correlation was seen among the other patterns of JMY and E-Cadherin expression (Table 4.6). In in-situ carcinoma, there was no observable correlation in the JMY and E-Cadherin expression patterns (Table 4.6).

Diagnosis	JMY	E cadherin	p-val	r	n
Breast (invasive)	Cyto	Cyto	0.285	-0.070	235
	Cyto	Mem	0.032	-0.140	
	Nuc	Cyto	0.122	-0.101	
	Nuc	Mem	0.054	-0.126	
Breast (in situ)	Cyto	Cyto	0.81	0.09	9
	Cyto	Mem	1	0	
	Nuc	Cyto	0.91	0.05	
	Nuc	Mem	0.46	0.28	

Cyto= Cytoplasm, Nuc= Nucleus

Table 4.6 Relationship of JMY to E Cadherin expression in invasive 235 breastcarcinomas and 17 "in situ" lesions.

Showing a significant inverse correlation between cytoplasmic JMY expression and membranous E-cadherin expression (p=0.032).

Clinical features	Number
Total number of patients	284
Age – median (range), years	58 (32 – 90)
<50	83
=>50	201
Not recorded	0
Lymph node status	
Negative / Positive	178 / 100
Not recorded	6
Tumor size – median (range), cm	2.1 (0.2 – 9)
<2	112
=>2	171
Not recorded	1
Histology	
Ductal	229
Lobular	28
Mixed	18
Other	9
Not recorded	0
Grade	
I	35
II	126
III	88
Not recorded	35
Estrogen receptor status	
Negative / Positive	62 / 202
Not recorded	20
Survival follow-up – median (range), days	3724 (65 – 5941)
Deaths, recurrences	125, 115
Not recorded	0

Table 4.7. Clinical and pathological features of patients with breast cancers.

4.2.7 JMY, p53 and E-Cadherin expression and correlations with clinical outcome

I have investigated the relationship between JMY expression and survival in 284 consecutive breast cancers with associated clinical data (Table 8) for which tissue was represented in the breast carcinoma tissue micro arrays (TMAs). A significant observation made was that cytoplasmic expression of JMY was associated with shorter relapse free survival (RFS) with 60% survival observed in cytoplasmic JMY positive patients and 80% survival in cytoplasmic JMY negative patients after 16 years (=6000days), p value =0.046. There was no observable associated overall survival (OS) with this analysis (Table 8 and Figure 4). Additionally, nuclear JMY co-expression with p53 was associated with an even shorter RFS. The survival curve of JMY and p53 co-nuclear expression showed a 40% relapse free survival in patients with JMY and p53 co-nuclear expression but an 80% relapse free survival in patients with absence of JMY and p53 co-nuclear expression after 16 years, p value=0.001 (Table 4.8 and Figure 4.4).

The relationship between JMY cytoplasmic or nuclear expression and E-Cadherin membrane positivity in 235 patients with breast cancer was investigated. There was no RFS association observed (Table 8).There was an observable association between the status of membranous E-Cadherin expression and nuclear but not cytoplasmic JMY expression. The study showed that there was only a 25% overall survival (OS) in patients with high membranous E-Cadherin and nuclear JMY expression but a 70% OS in patients with low membranous E-Cadherin and nuclear JMY expression over the course of 16years (Table 4.8 and Figure 4.4).

Clinical outcome according to JMY, p53 and E Cadherin expression.

JMY Expression	Survival	Hazard ratio	C.I. 95%	P-value
Cytoplasmic (positive v negative)	RFS	1.43	0.99 – 2.07	0.056
	OS	1.13	0.79 – 1.6	0.505
Nuclear (positive v negative)	RFS	1.74	1.19 – 2.55	0.005
	OS	1.44	0.99 – 2.07	0.05

Table 4.8a Survival in 283 breast cancers over 6000 days according to expression of JMY.

Shows nuclear JMY expression is associated with decreased Relapse Free Survival (RFS) (hazard ratio=1.74, p= 0.005) and Overall Survival (OS) (hazard ratio 1.44, p=0.05) compared to general population that could be as low as 1.19 and as high as 2.55 for RFS and as low as 0.99 and as high as 2.07 for the OS.

JMY and E Cadherin Expression	Survival	Hazard ratio	C.I. 95%	P-value
JMY nuc pos/P53 nuc pos vs JMY nuc pos/P53 nuc neg vs JMY nuc neg/P53 nuc pos vs JMY nuc neg /P53 nuc neg	RFS	n.a.	n.a.	0.0040
	OS	n.a.	n.a.	0.3005

Positive = any positive tumor cell expression, Negative = no positive tumor cell expression
Nuc= nuclear, n.a= not-applicable

Table 4.8b Survival in 283 breast cancers over 6000 days according to expression of JMY and P53.

Shows that increased nucleus JMY and p53 expression is associated with decreased Relapse Free Survival p= 0.004 in these breast cancer cases.

JMY and p53 Expression	Survival	Hazard ratio	C.I. 95%	P-value
JMY nuc pos / p53 nuc pos vs. JMY nuc neg / p53 nuc neg	RFS	2.42	1.47 – 3.98	0.0005
	OS	1.3	0.79 – 2.14	0.31
P53 nuc pos vs. P53 nuc neg	RFS	1.83	1.23 – 2.73	0.003
	OS	0.97	0.66 – 1.42	0.88

Positive =any positive tumor cell expression, Negative = no positive tumor cell expression
Nuc= nuclear, n.a= not-applicable

Table 4.8c Survival in 283 breast cancers over 6000 days according to expression of JMY and P53.

Shows increased nucleus JMY and p53 co-expression is associated with decreased Relapse Free Survival (p=0.0005). While also general increase in nucleus p53 expression is associated with decreased Relapse Free Survival (p=0.003).

JMY and E Cadherin Expression	Survival	Hazard ratio	C.I. 95%	P-value
E Cadherin mem pos/Jmy cyt pos vs E Cadherin mem pos/Jmy cyt neg vs E Cadherin mem neg/Jmy cyt pos vs E Cadherin mem neg/Jmy cyt neg	RFS	n.a.	n.a.	0.2615
	OS	n.a.	n.a.	0.0502
E Cadherin mem pos/Jmy nuc pos vs E Cadherin mem pos/Jmy nucneg vs E Cadherin mem neg/Jmy nuc pos vs E Cadherin mem neg/Jmy nuc neg	RFS	n.a.	n.a.	0.1497
	OS	n.a.	n.a.	0.0051

Positive= any positive tumor cell expression, Negative= no positive tumor cell expression
Mem= membranous, Nuc= nuclear, n.a= not-applicable

Table 4.8d Survival in 235 breast cancers over 6000 days according to expression of JMY and E Cadherin.

Shows that increased nucleus JMY and membranous E-cadherin co-expression is associated with decreased Overall Survival.

A.

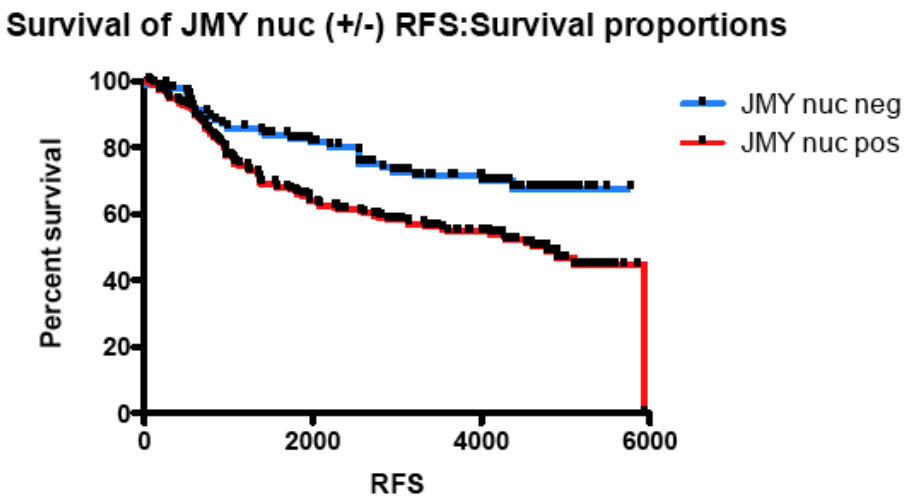

p= 0.046

B.

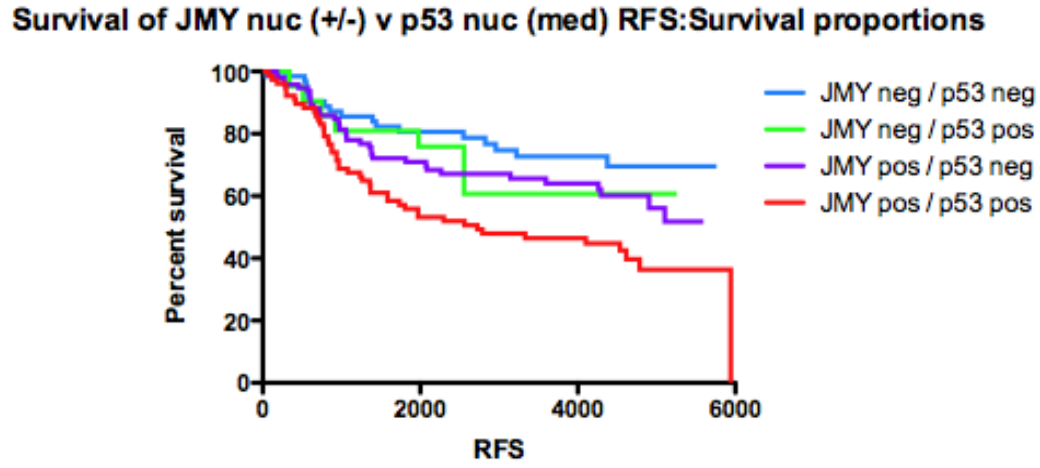

p= 0.001

Figure 4.4 continued

C.

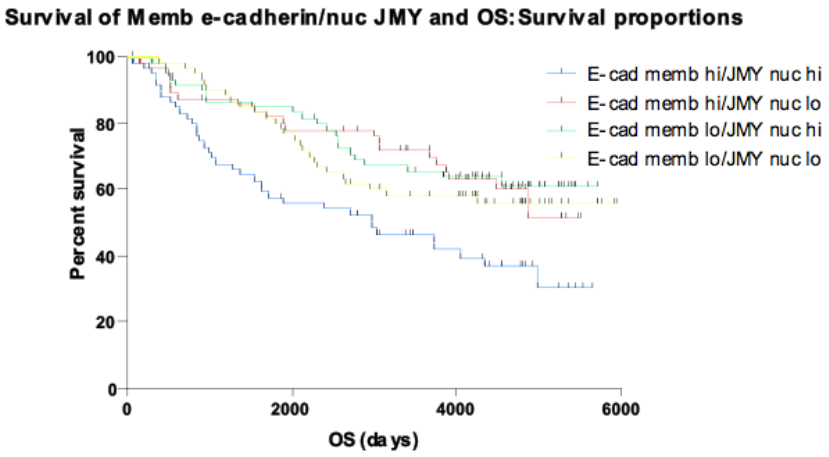

p= 0.0051

Figure 4.4. Relapse free and Overall survival curves in breast cancer patients

(A) In 283 breast cancer patients, cytoplasmic expression of JMY is associated with shorter relapse free survival (RFS) with 60% survival in cytoplasmic JMY positive patients and 80% survival in cytoplasmic JMY negative patients after 16 years (=6000days) p value =0.046. (B) In 283 breast cancer patients, the survival curve of JMY and p53 co-nuclear expression showed only 40% relapse free survival in patients with JMY and p53 co-nuclear expression but 80% relapse free survival in patient with absence of JMY and p53 co-nuclear expression after 16 years, p value=0.001. (C) In 235 breast cancer patients, the survival curve of E-cadherin membranous expression in association with JMY nuclear expression showed that high co-expression of membranous E-cadherin and nuclear JMY is associated with only 25-30% overall survival (OS) after 16 years, while low co-expression of membranous E-cadherin and nuclear JMY is associated with 70% overall survival (OS) after 16 years.

4.3 Discussion

JMY is a protein at the centre of a complex pathway connecting cell motility and invasion with the p53 response to DNA damage(Coutts, Pires et al. 2011). As a protein promoting cell invasion it could be a relevant therapeutic target to blocking tumor progression (Coutts, Pires et al. 2011). However there is a dichotomy in the roles that JMY plays, since JMY also has tumor suppressive activity by being a p53 enhancer in the event of DNA damage (Shikama, Lee et al. 1999). Hence in this respect, targeting of JMY could prove to be detrimental, as this would in essence counteract its anti-oncogenic role.

The question that then continues to loom over this novel protein is how to reconcile JMY's apparent dual roles of transcriptional activation and actin dynamic regulation and its involvement in tumorigenesis (Roadcap et al., 2009).

JMY is a relatively recently discovered protein and no study to date has explored its expression in human normal and neoplastic tissue samples (Wang 2010) as no antibodies were available for immunohistochemical (IHC) studies. In this study, I have now set the precedence of raising and characterizing a monoclonal antibody that detects JMY in both Western blotting and immunohistochemistry in formalin-fixed paraffin embedded (FFPE) tissue.

Using the anti JMY monoclonal antibody in a first immunhistochemical study I found that in normal tissues JMY is widely expressed both in a cytoplasmic and nuclear localization although the intensity of staining in these two localizations are variable from tissue to tissue (Table 4.1). As expected from its described role in p53 regulation, most of the tissues found to be positive for JMY in the cytoplasm and nucleus also expressed wild type P53.This seems to implicate the associative affiliation of JMY to the augmentation of wild type p53 activation

(Shikama, Lee et al. 1999) such that in a normal healthy cell, a functional JMY protein is capable of facilitating wild type p53 activation in the event of DNA damage.

In primary tumors, JMY displayed variable expression (Table 4.2). Interestingly in breast, colon, head and neck carcinomas and lymphomas, JMY expression is highly variable while in their comparable normal tissues, there is a significant degree of JMY expression. In breast, JMY is prominently expressed in the normal epithelium and in the "in situ" lesions. However there is a very variable pattern of expression in the invasive carcinomas. In the germinal centers of reactive lymph nodes and the indolent Follicular lymphoma, there is a strongly positive JMY expression. However a loss of JMY expression is seen in the aggressive Large B Cell Lymphomas.

A possible explanation for loss of JMY expression in some carcinomas could also be tied to its role in promoting p53 activation: tumors with lack of JMY but with wild type p53 could fail to trigger a full p53 activation and therefore a subsequent loss, at least in part, of its anti oncogenic effect. In the normal breast and in situ breast carcinoma that is yet to take on an aggressive phenotype there is evidently some JMY protein present to help effect the tumor suppressor activity in the case of the normal breast or help attenuate aggressiveness in the case of the in situ breast carcinomas. But potentially as carcinoma becomes more advanced as in invasive breast carcinoma, the eventual loss of JMY and its anti-oncogenic effect possibly allows for the propagation of the aggressiveness of this carcinoma phenotype. These findings further support the possible anti-oncogenic role for JMY, as predicted by its function in promoting wild type p53 activity in normal tissue (Coutts and La Thangue 2005, Coutts, Boulahbel et al. 2007, Coutts, Weston et al. 2009).

Further evidence of JMY's main role in cancer being possibly impingent on its function in the p53 functional pathway is strongly underlined in the outcome of my pilot studies in a series of breast carcinomas showing that nuclear co-expression of JMY and p53 was associated with shorter overall survival (Table 4.8 and Figure 4.4). The underlying molecular basis of the co-expression of these two proteins is not fully known yet, but suggests that the recurrent theme of a defect in JMY/p53 tumor suppressor activity possibly contributing to nuclear accumulation of non-functional JMY and p53 in these tumors is the most likely factor contributing to a higher mortality rate in breast cancer patients with nucleic JMY/p53 co-expression.

These data then suggest that the next steps in the study of the role of JMY in cancer should be on clinical samples in order to thoroughly compare JMY with p53 expression and p53 genetic alterations (both mutations and deletions). Also in "In vitro" experiments exploring the effect of p53 genetic damage to the presence of JMY in the cell.

As previously mentioned, JMY also plays a role in actin dynamics and regulation having the capacity to nucleate actin, co-localize with actin in the cell periphery and promote increased cell motility. In localization studies by Zuchero et al they showed that JMY was mostly nuclear in undifferentiated myeloid HL60 cells but when differentiated into highly motile neutrophil-like cells JMY was exclusively localized in the cytoplasm (Zuchero, Coutts et al. 2009). However from my immunohistochemistry (IHC) studies thus far, JMY's cytoplasmic expression pattern is widely distributed. This wide distribution of cytoplasmic JMY expression is also present in many non-motile cells contrary to what Zuchero et al have demonstrated in their localization studies (Zuchero, Coutts et al. 2009). Hence it is possible that the JMY's cytoplasmic expression pattern in IHC is probably not representative of JMY's actin nucleation

activity. Immunofluorescence studies of undifferentiated and differentiated HL60 cells using our anti JMY antibody would be required to confirm Zuchero et al's studies.

Furthermore immunohistochemistry of head and neck and colorectal tumors for which there were corresponding lymph node metastases, as well as the colorectal adenocarcinoma [ADC] liver metastases, showed that JMY cytoplasmic expression was high in nodal metastases of colorectal ADC, but not in the liver metastases, nor in the nodal metastases of primary Head and Neck cases. A larger case study of these tumors is also required to truly establish whether cytoplasmic JMY expression is involved in the tumor metastatic process. For now, I hypothesize that IHC cytoplasmic expression of JMY by itself is not representative of actin activation.

I also examined the relationship between JMY and E Cadherin expression. Coutts et al (Coutts, Weston et al. 2009) described up-regulation of E-Cadherin in JMY depleted MCF7 cells and vice versa and concluded that one of the ways JMY influences motility is through regulation of E-Cadherin. However my data suggest the relationship between JMY and E-Cadherin both in normal and neoplastic tissue is more complex. The observed co–expression of these two proteins is widespread. Of particular interest is the breast cancer model: while there is co-expression of both proteins in all the "in situ" carcinomas, there is evidence of an inverse expression relationship between these two proteins in invasive breast carcinomas. Furthermore correlation with clinical outcome shows that there is no correlation between JMY and E-Cadherin and relapse free survival. However, intriguingly patients whose tumors expressed high membranous E-Cadherin and high nuclear JMY had the shortest overall survival. This data suggests that there might be a possible association between E-Cadherin and JMY

associated with cancer progression in vivo. However that relationship is more complex than the previously assumed inverse relationship.

4.4 Conclusion

In conclusion this first clinical study of JMY confirms that this gene could have either a suppressor or an oncogenic effect, as predicted from “in vitro” studies. It also shows further evidence that it could play a major role in most human cancers with JMY being a major p53 co-activator. Larger studies and correlations with the occurrence of genetic damage will be necessary for more insight into understanding the specific role played by JMY in tumors.

CHAPTER 5
THE ASSOCIATION BETWEEN TRAP1 AND JMY

5.1 Introduction

From gene array work done in our laboratory TRAP1 mRNA transcription was observed to be directly associated with genes involved in cellular proliferation and promoting cell-cell/cell matrix adhesion, tight junctions and cadherins but inversely linked to an increase in transcription of genes associated with metastatic activity and cell motility (Tan, Pezzella et al. 2007, Liu, Hu et al. 2010). Amongst these genes associated with metastatic activity we found JMY.

JMY is a putative metastatic marker, primarily localized in the nucleus (Coutts, Weston et al. 2009, Roadcap and Bear 2009) but able to shuttle between the nucleus and cytoplasm (Coutts, Weston et al. 2009, Roadcap and Bear 2009). In the nucleus it acts as a transcriptional cofactor to augment the p53 response in the event of DNA damage (Coutts and La Thangue 2005, Coutts, Boulahbel et al. 2007). In the cytoplasm JMY acts to enhance cell motility via its ability to promote actin nucleation and elongation in the cytoplasm (Coutts, Weston et al. 2009) and this is the attribute of JMY that renders it a potential metastatic inducing protein. JMY hence could have a dual role as a tumor suppressor in the nucleus and a potential oncogene in the cytoplasm.

Our gene array data suggested an inverse correlation between TRAP1 and JMY with JMY transcription increasing after TRAP1 inhibition. I have therefore investigated the in vitro

relationship between TRAP1 and JMY expression both in normoxia and hypoxia and via immunohistochemistry to verify the hypothesis that TRAP1 is a negative regulator of JMY.

5.2 Results

5.2.1 Cell line screening for high endogenous JMY production

I screened several cell lines for endogenous JMY production. Cell lines were screened by immunostaining their cell pellets with an anti -JMY antibody (NDCLS, Oxford, antibody production discussed in chapters 2 and 4) using an optimized protocol as described in the materials and methods chapter. JMY was found to be highly expressed in the MCF7, SUDHL-1 and Hela cell lines.

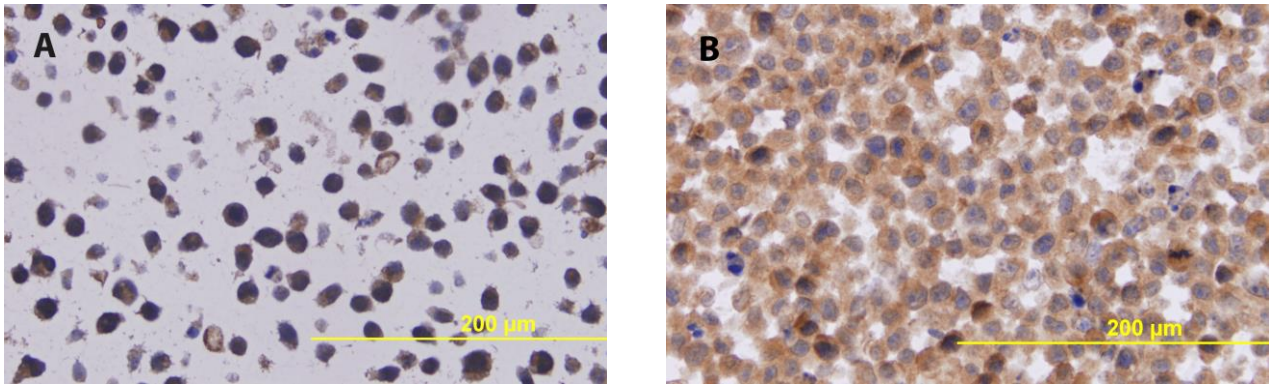

Figure 5.1 JMY immunostaining screening for high endogenous JMY production in cell lines. (A). SUDHL-1 cell pellet with positive nuclear and cytoplasmic JMY staining. (B). Hela cell pellet with positive nuclear and cytoplasmic JMY staining.

5.2.3 Western Blot quantification of TRAP1 and JMY protein in cell lines

5.2.3.1 JMY Knockdown has no effect on TRAP1 protein expression

To ascertain the effect of JMY knockdown on TRAP1 protein expression, SUDHL and Hela cell lines were transfected with siRNA against JMY and non target control siRNAs respectively. Cells were cultured in normoxia for 72 hours. Whole cell lysates were extracted from cells and resolved on 10% SDS-PAGE then immunoblotted with the anti-JMY antibody (NDCLS, Oxford), an anti-TRAP1 antibody (Santa Cruz, US), and an anti-Tubulin antibody (Ab-cam). JMY was observed to be adequately silenced in all the cell lines. There was no significant observable effect of JMY silencing on TRAP1 protein levels.

A. B

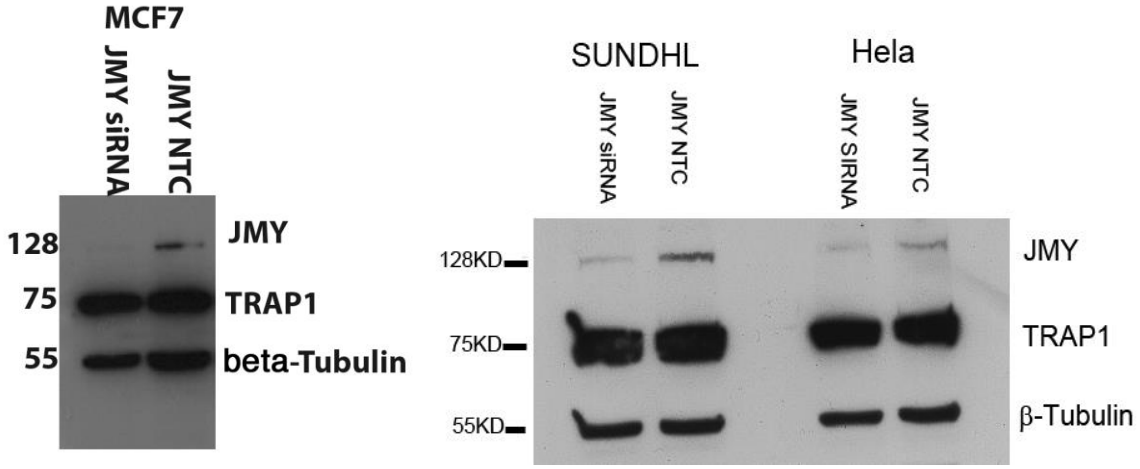

Figure 5.2 Effect of JMY silencing on TRAP1

(A) MCF7, (B) SUDHL-1 and Hela cell lines transfected with NTC siRNA for control or siRNA against JMY. JMY silencing does not significantly affect TRAP1 protein expression.

5.2.3.2 TRAP1 knockdown reduces JMY protein expression.

To evaluate the effect of TRAP1 silencing on JMY, MCF7 cell lines were transfected with siRNA against TRAP1 and non-target control siRNA and cultured in normoxia for 72 hours. Whole cell lysates were extracted and resolved on 10% SDS-PAGE gel transferred to nitrocellulose membrane and immunoblotted for TRAP1 to confirm TRAP1 knockdown. The membrane was subsequently immunoblotted for JMY protein and its expression was observed to be reduced with TRAP1 silencing (Figure 6).

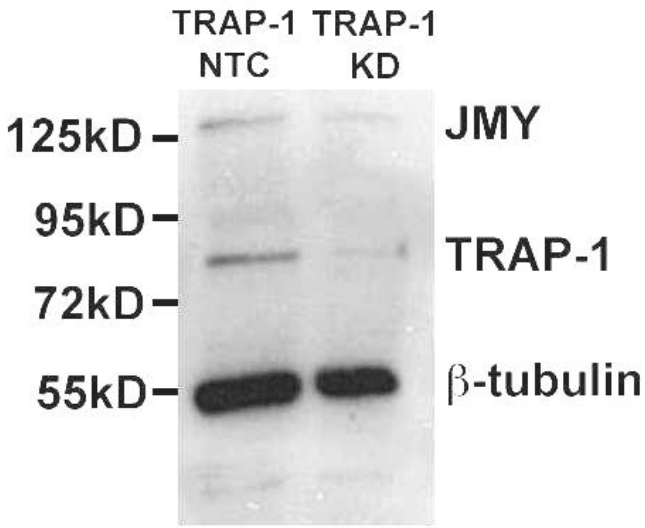

Figure 5.3 TRAP1 and JMY expression in an MCF7 cell line transfected with TRAP1. Non-targeted control siRNA (TRAP1 NTC) and TRAP1 siRNA (TRAP1 KD) respectively. β-tubulin is a loading control. TRAP1 silencing decreases JMY protein expression.

5.2.4 RT-PCR quantifying JMY expression in TRAP1 negative and positive cells

5.2.4.1 JMY mRNA transcription increases in TRAP1 transfected MDA231 and diminishes in TRAP1 silenced A549

As confirmed in chapter 3, MDA-MB-231 produces minimal endogenous TRAP1 protein and hence is an appropriate cell line to use for studies evaluating the effect of TRAP1 restoration/overexpression on JMY. Conversely A549 cell lines produce significant endogenous TRAP1 and is a cell line that I have used to verify the effect of knocking down TRAP1, as described in chapter 3. This is therefore also a suitable cell line to use to further investigate the JMY/TRAP1 relationship. JMY mRNA expression level was quantified in MDA-MB-231 cells with restored TRAP1 or mock transfection as controls and A549 cells transfected with TRAP1 siRNA or non-targeted control siRNA. Cells were cultured in normoxia for 72 hours. Whole cell lysates and fractional lysate for mRNA were extracted using the PARIS kit (Ambion). cDNA was obtained using a retro script kit (Ambion) as described in Chapter 2. Samples were normalized against levels of β-actin and quantified by qRT-PCR. Results of the expression are a composite of triplicate experiments.

RT-PCR data indicated that in normoxia restoration of TRAP1 into MDA-MB-231 cells ("MTn" equivalent MDA-MB-231 TRAP1 positive cells in normoxia) was associated with an increase in JMY mRNA that is about 4.5 fold higher than JMY mRNA transcription in the mock transfected MDA-MB-231 ("MEn" equivalent to MDA-MB-231 the TRAP1 negative cells in normoxia). Additionally in normoxia a knockdown of TRAP1 in A549 cell ("Atn" equivalent to A549 TRAP1 negative cells in normoxia) was associated with about a 40% decrease in JMY mRNA transcription as compared to the scrambled/non targeted control

siRNA transfected A549 cell ("Asn" equivalent to the A549 TRAP1 positive cells in normoxia).

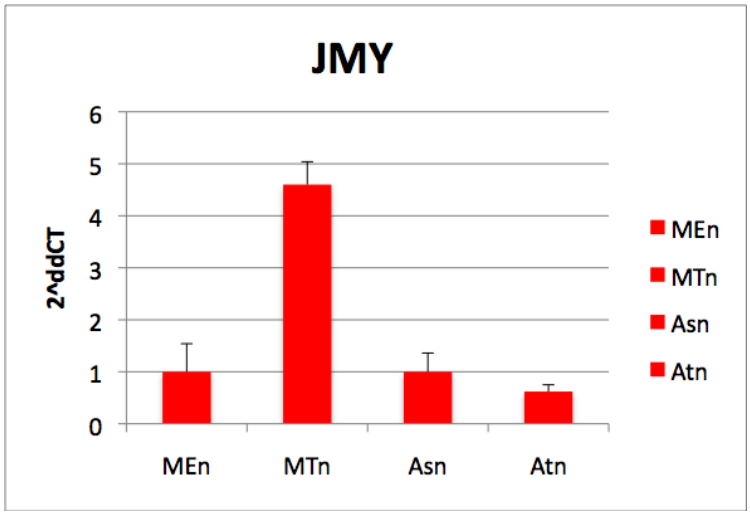

Figure 5.4 RT-PCR quantification of JMY expression in TRAP1 negative and positive cells.

MTn (MDA-MB-231 in normoxia with TRAP1 restored via viral transfection equivalent to MDA-MB-231 TRAP1 positive cells in normoxia) is associated with a correspondingly increased JMY mRNA transcription as compared to the TRAP1 depleted MDA-MB-231 MEn (MDA-MB-231 in normoxia with empty vector transfection equivalent to MDA-MB-231 TRAP1 negative cells in normoxia) and a TRAP1 knockdown in A549 Atn (A549 in normoxia transfected with TRAP1 siRNA equivalent to A549 TRAP1 negative cells in normoxia) is also associated with a decrease in JMY mRNA transcription as compared to the TRAP1 positive A549 cell transfected with non-targeted control siRNA Asn (A549 TRAP1 positive cells in normoxia). Error bars are representative of standard deviations. Beta-actin is the control gene used.

5.2.5 JMY and TRAP1 protein interaction

5.2.5.1 JMY and TRAP1 protein interact directly

Having observed a direct correlation between TRAP1 and JMY mRNA transcription and protein expression, I decided to ascertain if TRAP1 and JMY directly interact with each other using an immunoprecipitation assay. Hela cell lines were cultured for 72 hours in normoxia. Whole cell lysates were then prepared and immunoprecipitated respectively with an anti-JMY antibody, anti-TRAP1 antibody and anti-IGG antibody as a control. Immunoprecipitated lysates were then resolved by 10% SDS-PAGE electrophoresis and immunoblotted with anti-TRAP1 and anti-JMY antibodies respectively.

TRAP1 protein was clearly detected in the whole cell lysate immunoprecipitated with anti-JMY antibody. Also, JMY was detected in the whole cell lysate immunoprecipitated with the anti-TRAP1 antibody (Figure 5.8).

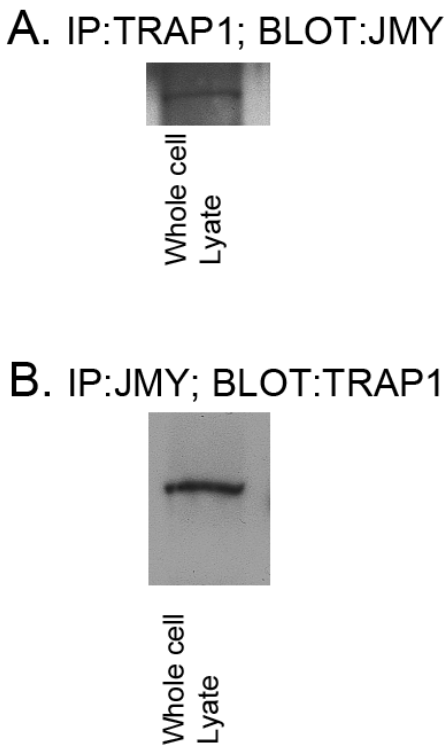

Figure 5.5 Immunoprecipitation using Hela cell lines.
This suggests a TRAP1 / JMY protein interaction as anti-JMY antibody detects JMY in TRAP1 immunoprecipitated lysate and anti TRAP1 antibody detects TRAP1in JMY immunoprecipitated lysate.

5.2.5.2 Cytoplasmic Subcellular localization of TRAP1 and JMY interactions

The above immunoprecipitation protocol was repeated using the Hela cell line. I chose to use the Hela cell line for this particular study because of all the cell lines I used for this study, the Hela cells gave the highest yield of endogenous protein after the protein extraction process. This is important since immunoprecipitation assays require an ample protein presence in order to get a clear detection of protein/protein interactions, especially if such protein/protein interactions were very transient or subtle. Hela cells were cultured for 72 hours in normoxia, then lysate extraction was done separating the cytoplasmic pool from the nucleic pool using the Paris kit (Ambicon).

The nuclear and cytoplasmic lysate pools were resolved in 10% SDS-PAGE gel and immunoblotted for TRAP1 and JMY respectively as described in Chapter 2. Immunoblotting for TRAP1 on the JMY immunoprecipitate detected TRAP1 in the cytoplasmic pool but not in the nuclear pool. Likewise immunoblotting for JMY on TRAP1 immunoprecipitates detected TRAP1 only in the cytoplasmic pool but not in the nuclear pool. A repeat immunoprecipitation assay will be done for validation of this result.

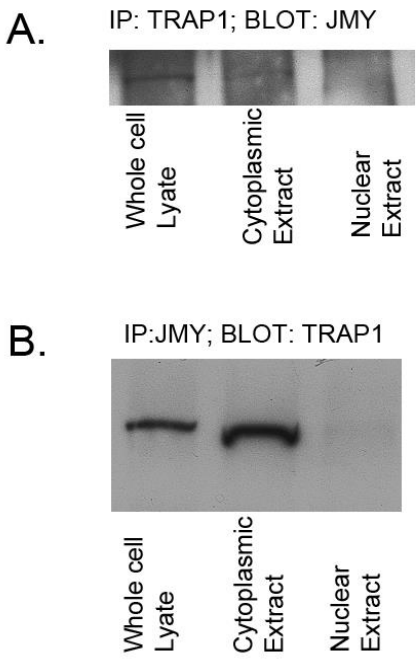

Figure 5.6 Immunoprecipitation showing cytoplasmic subcellular localization for JMY and TRAP1 interaction.

(A)Hela whole cell, cytoplasmic pool and nuclear pool lysates immunoprecipitated with anti-TRAP1 antibody and immunoblotted with anti-JMY antibody and blot shows JMY detection in the whole cell and cytoplasmic pool lystate but no JMY detection in the nuclear pool lysate.(B) Hela whole cell, cytoplasmic pool and nuclear pool lysates immunoprecipitated with anti-JMY antibody and immunoblotted with anti-TRAP1 antibody shows TRAP1 detection in the whole cell and cytoplasmic pool lystate but no TRAP1 detection in the nuclear pool lysate.

5.2.6 Immunohistochemistry of TRAP1 and JMY in Breast cancer cases

5.2.6.1 TRAP1 protein expression directly correlates with JMY protein expression in breast cancer cases

Breast cancer cases used are made up of a total of 304 infiltrating ductal carcinoma with 235 estrogen receptor positive, 69 estrogen receptor negative and average age of patients is 57.3years.Only 283 cases were available in the tissue microarray, either because the missing cores had been used up , damaged or fallen out. These cases were respectively immunostained with anti-TRAP1 and anti-JMY antibodies as described in chapter 2 then manually scored generating an IPS for the staining of both proteins. Statistical analysis of the IPS showed a direct correlation between JMY and TRAP1 localization. Cases as reflected in Figure 5.10 with a high cytoplasmic TRAP1 (Figure 5.10-"TRAP cyto high") had an equivalent high cytoplasmic JMY level and cases with low cytoplasmic TRAP1 (Figure 5.10 "TRAP cyto low") had an equivalent low cytoplasmic JMY level p value <0.0001 . Additionally, cases with high nuclear TRAP1 (Figure 5.10 "TRAP nuc high") also had an equivalent high nuclear JMY and cases with low nuclear TRAP1 (Figure 5.10 "TRAP nuc low") also had low nuclear JMY p value = 0.0112.

A. Cytoplasmic JMY and cytoplasmic TRAP1

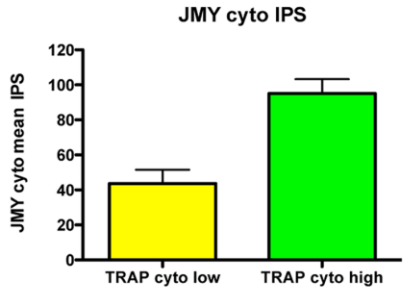

Mann Whitney test	
P value	< 0.0001
Exact or approximate P value?	Gaussian Approximation
P value summary	****
Are medians signif. different? (P < 0.05)	Yes
One- or two-tailed P value?	Two-tailed
Sum of ranks in column A,B	4869 , 10531
Mann-Whitney U	2313

	TRAP cyto low	TRAP cyto high
Number of values	71	104

B. Nuclear JMY and nuclear TRAP1

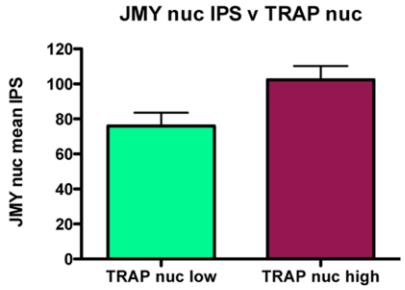

Mann Whitney test	
P value	0.0112
Exact or approximate P value?	Gaussian Approximation
P value summary	*
Are medians signif. different? (P < 0.05)	Yes
One- or two-tailed P value?	Two-tailed
Sum of ranks in column A,B	7350 , 8050
Mann-Whitney U	2979

	TRAP nuc low	TRAP nuc high
Number of values	93	82

Figure 5.7 Graphical depiction of the IPS score for immunostaining 283 breast cancer cases.

IPS score for immunostaining 283 breast cancer cases and statistical analysis of IPS showing a direct correlation between the TRAP1 and JMY proteins. A. Cytoplasmic presence of TRAP1 and JMY protein correlate such that cases with high cytoplasmic TRAP1 protein also had high cytoplasmic JMY protein and cases with low cytoplasmic TRAP1 protein also had low cytoplasmic JMY protein. B. Nuclear presence of TRAP1 and JMY proteins correlated, as cases with high nuclear TRAP1 protein also had high nuclear JMY protein and cases with low nuclear TRAP1 protein also had low nuclear JMY protein.

5.2.7 Significant prognosis factor for TRAP1 and JMY cytoplasmic interaction

In an effort to find any possible prognostic association to TRAP1 and JMY expression correlation, I examined the prognostic value of the immunohistochemistry IPS of TRAP1 and JMY co-expression in the cytoplasm in the series of 283 breast cancer cases. The analysis showed a significant shorter Overall Survival after 5 years for patients with high JMY and TRAP1 cytoplasmic co-expression, having a overall survival (OS) of 57% compared to 77% overall survival of cases with low TRAP1 and JMY cytoplasmic co-expression, and a significant p value of 0.025.

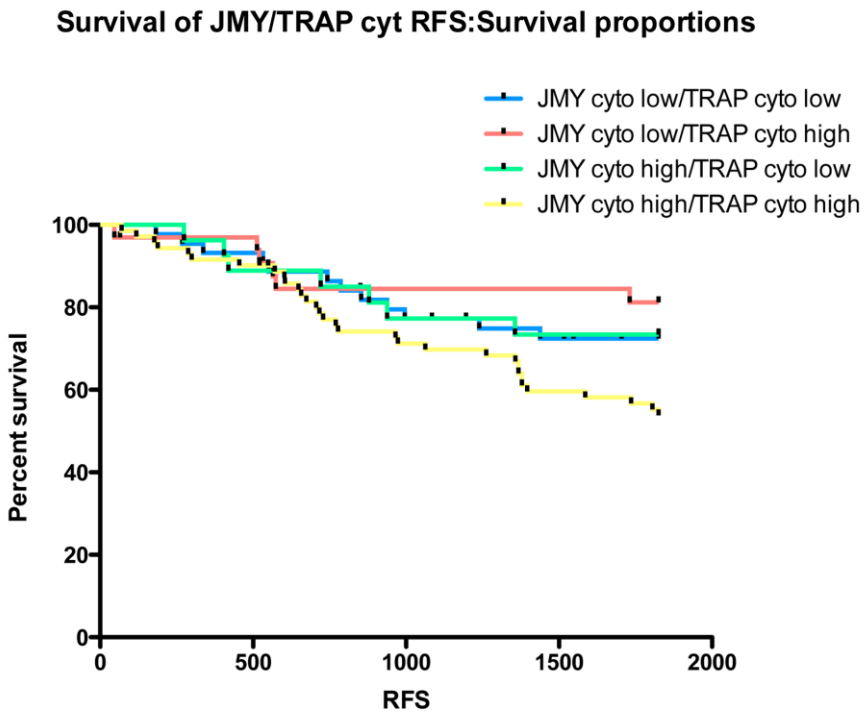

Log-rank (Mantel-Cox) Test	
Chi square	7.925
df	3
P value	0.0476
P value summary	*
Are the survival curves sig different?	Yes
Logrank test for trend	
Chi square	5.005
df	1
P value	0.0253
P value summary	*
Sig. trend?	Yes

Figure 5.8 Analysis indicating a potential poor prognostic association with high JMY and high TRAP1.

Analysis indicating a potential poor prognostic association with high JMY and high TRAP1 cytoplasmic co-expression with a 57% overall survival rate after 5 years compared to a 77% overall survival rate of low JMY/low TRAP1 cytoplasmic co-expression.

5.3 Discussion

As Liu et al (Liu, Hu et al. 2010) suggested a possible inverse relationship between expression of TRAP1 and JMY mRNA in their microarray study, the aim of this chapter was to investigate whether this is the case. Micro array is a powerful tool for data mining. However despite the enormous potential of this technology, it does face numerous pitfalls such as the variation in the statistical rigor to which data can be subjected (Hofman 2005). Hence the validation of relative expressions obtained from genome wide microarray is critical.

My results do demonstrate that a relational association does indeed exist between TRAP1 and JMY but this is more of a direct converse to Liu et al's (Liu, Hu et al. 2010) speculation of an inverse association between these two proteins.

The direct relationship between the two proteins is reflected in Western blots of MCF7 TRAP1 knockdowns (Figure 5.3) showing TRAP1 silencing resulting in a corresponding JMY protein decrease. Also at the mRNA level (Figure 5.4) an increase in TRAP1 as seen in the restoration of TRAP1 into MDA-MB-231, was associated with a corresponding rise in JMY mRNA of about 4.5 fold. Also, a decrease in TRAP1 mRNA as in TRAP1 knockdowns in A549 cells was followed by a decrease in JMY mRNA. These results all indicate a strong direct relationship that has a bearing on a dependence of one protein on the other where the absence of one of the proteins such as knocking-down TRAP1 directly impairs the transcription and protein expression of JMY.

This also implies a possible direct regulatory relationship between TRAP1 and JMY, where TRAP1 is most likely the upstream/regulatory protein. Results shown in Figure 5.2 confirm that JMY is the down stream protein, as JMY knockdown in the Hela, MCF7 and SUDHL cells do not effect any observable change in TRAP1 levels. However as seen in Figure 5.3, TRAP1 knockdown exerts a corresponding effect of a decreased JMY protein and JMY mRNA. TRAP1 restoration induces a corresponding increase in JMY mRNA transcription.

This is somewhat counter intuitive to the implications regarding metastasis as studies (Liu, Hu et al. 2010) have shown that transfecting TRAP1 into the MDA231cell line causes a decreased expression of MMP9 genes which diminishes cell mobility and metastatic capability. Hence, it was also expected that these cells with TRAP1 restoration would also down-regulate and diminish production of a putative metastatic protein like JMY. As this was not the case, it raised an interesting question as to how TRAP1 is associated with the JMY protein.

It is possible that TRAP1 is dependent on JMY for its function via the TNF pathway as is evident in the result of Figures 5.2 and 5.3. As the upstream protein, in terms of regulation, it is possible that TRAP1 either triggers a transcription factor that can turn on JMY transcription and the subsequent up regulation of JMY protein that then facilitates or promotes TRAP1's activity.

Immunoprecipitation assays were helpful in giving more insight into the relationship between these two proteins. Data obtained from this assay suggests that there is not just a direct relationship but also a possible direct/crucial physical interaction between TRAP1 and JMY proteins that occurs primarily in the cytoplasm. This is reflected in Figures 5.5 and 5.6 where JMY was detected in the TRAP1 whole cell lysate and cytoplasmic pool immunoprecipitate,

but not in the TRAP1 nuclear pool immunoprecipitate. Also TRAP1 was detected in JMY's whole cell lysate and cytoplasmic pool immunoprecipitate, but not in the nuclear pool immunoprecipitate.

TRAP1's presence in the cytoplasm primarily influences cell proliferation via its involvement with the TNF pathway (Liu, Hu et al. 2010) while JMY in the cytoplasm is involved with nucleation of actin filaments enhancing cell motility and invasion (Coutts, Weston et al. 2009, Roadcap and Bear 2009, Zuchero, Coutts et al. 2009). The fact that TRAP1 and JMY can interact in the cytoplasm suggests that JMY's effort to enhance tumor invasiveness via actin nucleation in the cytoplasm could be facilitated by TRAP1 as their interaction possibly triggers a synergistic dynamic where TRAP1 promotes cell proliferation via the TNF pathway which in turn produces more tumor cells needed to seed the new territory being acquired by the JMY induced tumor invasion. This premise further renders high TRAP1 and JMY expression in cancer as factors that predispose the tumor to acquiring increased aggressive characteristics such as metastasis.

Furthermore, the immunohistochemistry study verifying the localization of TRAP1 and JMY in a series of breast cancer cases confirmed this direct relationship between TRAP1 and JMY. In these cases when TRAP1 protein was high in the cytoplasm or nucleus, there was an equivalent increased JMY presence in the cytoplasm or nucleus. Also, when TRAP1 was low in either the cytoplasm or nucleus, JMY was also low indicating a tight direct association between these two proteins.

An additional intriguing result obtained from these breast cancer cases was the statistical analysis showing that the overall survival rate after 5 years was lower (57%) in patients who

had high cytoplasmic co-expression of JMY and TRAP1 as compared to the 77% survival rate in patients with low cytoplasmic co-expression of JMY (Figure 5.8). This result further strengthens the premise that then presence of TRAP1 and JMY, particularly in the cytoplasm, confers aggressive characteristics to tumors, most likely heightening metastasis.

5.4 Conclusion

In this chapter, I have demonstrated that in contrast to the inverse association of TRAP1 and JMY in MDA231 and A549 cells found with micro RNA experiments, there is actually a direct association between these proteins. Even more intriguingly, there is a direct physical interaction between them, possibly implying a synergistic contribution of these proteins towards increased tumor aggressiveness. With regards to the fact that high cytoplasmic co-expression of these two proteins is associated with potential cancer aggressiveness, further evaluation of the interaction between these 2 proteins is in order. Deciphering the exact pathway activated by their cytoplasmic interaction would be beneficial to a better understanding of the biology behind their impact in tumors. In general, this chapter provides strong evidence for identifying TRAP1 and JMY as directly interacting proteins with their interaction potentially conferring aggressive behavior on tumors, hence deeming these proteins as potential cancer therapeutic targets.

CHAPTER 6
IMMUNOPHENOTYPE OF ANGIOGENIC AND NON-ANGIOGENIC LUNG CANCER

6.1 Introduction

While many tumors entirely destroy the tissue in which they grow when re-establishing blood supply through neo angiogenesis, tumors arising in originally well-vascularized tissue environments may infiltrate between structures surrounding blood vessels a process known as "vascular co-optation". These vessels can then supply these tumor infiltrates, allowing them to grow without altering the original vascular architecture (Pezzella, Pastorino et al. 1997, Passalidou, Trivella et al. 2002).

The role of angiogenesis in neoplastic growth is controversial. Initially, it was thought that the formation of new capillaries (neovascularization), usually mediated by angiogenic molecules released by tumor cells and activated macrophages, was essential for all tumor growth (Perez-Atayde, Sallan et al. 1997, Folkman 2002). However there is growing evidence that in certain situations tumors can obtain sufficient blood supplies from pre-existing vascular beds to grow without angiogenesis. This form of neoplastic growth has been termed non-angiogenesis (Pezzella, Pastorino et al. 1997, Holash, Maisonpierre et al. 1999, Pezzella, Harris et al. 2001, Passalidou, Trivella et al. 2002).

Patterns of non-angiogenic growth have also been described by Wesseling et al (Wesseling, van der Laak et al. 1994) in glioblastoma multiforme, lymphoma(Passalidou, Stewart et al. 2003) and by our group in a large series of non-small cell lung carcinomas (Pezzella, Pastorino et al.

1997). In the latter non-angiogenesis was described as neoplastic cells filling the alveolar spaces (Pezzella, Pastorino et al. 1997) with no evidence of vascularization but growing by co-opting pre-existing pulmonary blood vessels. These non angiogenic cases made up about 16% of the series and were more aggressive clinically than the predominant angiogenic tumors (Pezzella, Di Bacco et al. 1996, Pezzella, Pastorino et al. 1997, 2000, Pezzella, Harris et al. 2001, Passalidou, Trivella et al. 2002, Adighibe, Micklem et al. 2006) (Donnem et al., 2012 manuscript submitted).

Studies done in the past suggesting the presence of non-angiogenic growth were based on observations made on standard histological slides. Hence to better demonstrate the presence of vascular co-optation I have investigated tumor growth and its spatial relation to vessels, in either angiogenic or nonangiogenic tumors, in 3 dimensions. To achieve this, I performed a study using computer aided three dimensional (3D) reconstructions to demonstrate the distinct differences in vascular architecture between the non-angiogenic and angiogenic lung tumors (Adighibe, Micklem et al. 2006).

In order to carry out this study and as described in a previous paper (Adighibe, Micklem et al. 2006), I chose to use the fluorescence staining technique because it has the advantage over regular optical microscopy, of allowing the possibility to observe a variety of colors of different structures in tandem. In this study, I had opportunity to superimposed, observe and analyze the structures of the nuclei (blue), vasculature (red) and cytokeratin (green) of the cells of tissues being studied. Three samples of tissue were chosen for this study: one sample of normal lung, another of an angiogenic and that of a non–angiogenic tumor. I created a topographic 3 dimensional (3D) rendering of these samples by first cutting 200 of 5μm thick serial sections of paraffin-embedded tissue for each of the chosen tissue samples. Then on each section double

immunostaining was performed for CD34 (in red) and cytokeratin (in green) with nuclei being counterstained with Diamidino-2-phenylindole dye (DAPI) (in blue). A 3D reconstruction for each of the three samples was created from the images of pictures taken of the individual slides of each sample using an Imaris Software (Adighibe, Micklem et al. 2006).

Results of the 3 D reconstruction showed architectural similarities between the vascular networks (CD34 (red)),of the normal lung (Figure 2) and the non-angiogenic lung tumor (Figure 3); implying that the integrity of the lung vascular is preserved in the non-angiogenic tumor. The difference between the normal lung and non-angiogenic lung tumor can only be seen when their cytokeratin (green) staining for the cytoskeleton are superimposed onto their respective CD34 stainings. It then becomes evident that the sponge-like morphology of the normal lung (Figure 2) becomes filled by neoplastic cells in the non-angiogenic tumor (Figure 3).

In contrast, the 3 D reconstruction of the angiogenic tumor (Figure 4) showed a non defined/ non-intact vascular architectural pattern. The angiogenic tumor's vascular network was chaotically distributed with some of it's blood vessels almost twice the size of adjoining vasculature. Additionally, the original lung architectural pattern is not preserved in the angiogenic tumor.

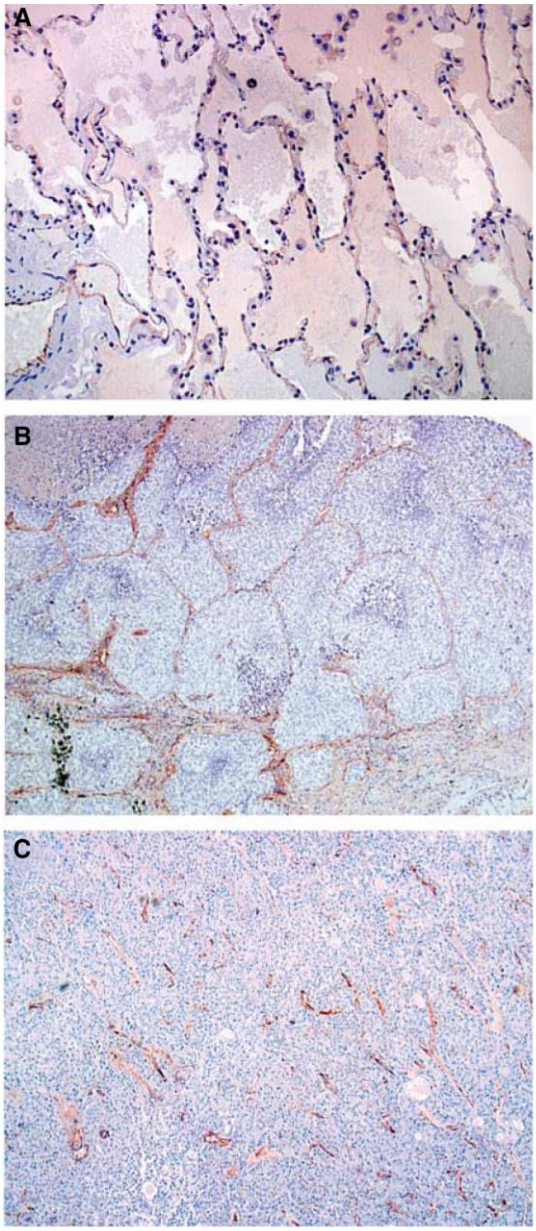

Figure 6.1 CD34 immunostaining.

From (Adighibe, Micklem et al. 2006), CD34 immunostaining (red) with hematoxylin counter stain of (A) normal lung with alveolar spaces and interalveolar septa containing alveolar capillaries. (B) Non-angiogenic lung tumor showing the filling of alveoli by neoplastic cells, a lack of parenchymal destruction, as well as an absence of neovascularization and tumor associated stroma. The only blood vessels present are those of the alveolar septa. (C) An angiogenic lung tumor with the hallmark destruction of normal lung architecture with the production of tumor-associated stroma and of new blood vessels erratically scattered within a sea of neoplastic cells.

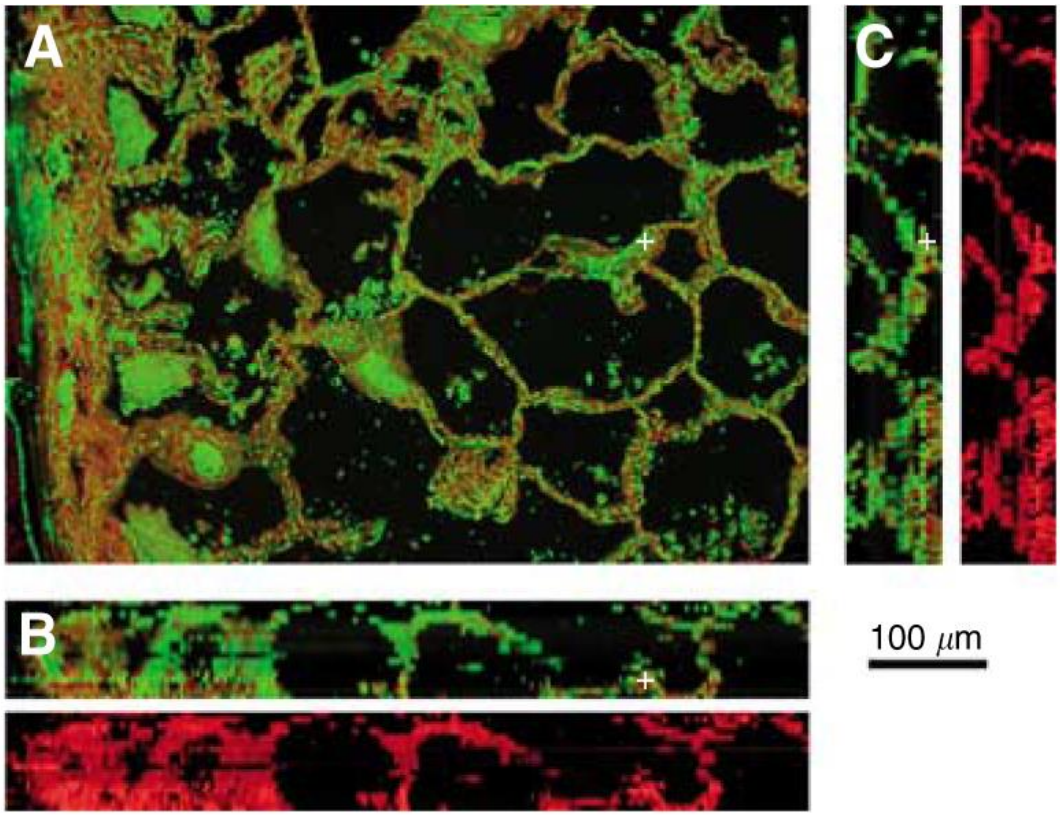

Figure 6.2 Immunofluorescence staining normal lung

Immunofluorescence staining, red is CD34 staining of blood vessels and green is the cytokeratin staining of the cytoskeleton (A) 2 Dimensional rendering of a normal lung. (B and C) Orthogonal views of the normal lung with the vascular network (red) followed by the superimposition of cytoskeleton (green). Picture from Adighibe et al (Adighibe, Micklem et al. 2006).

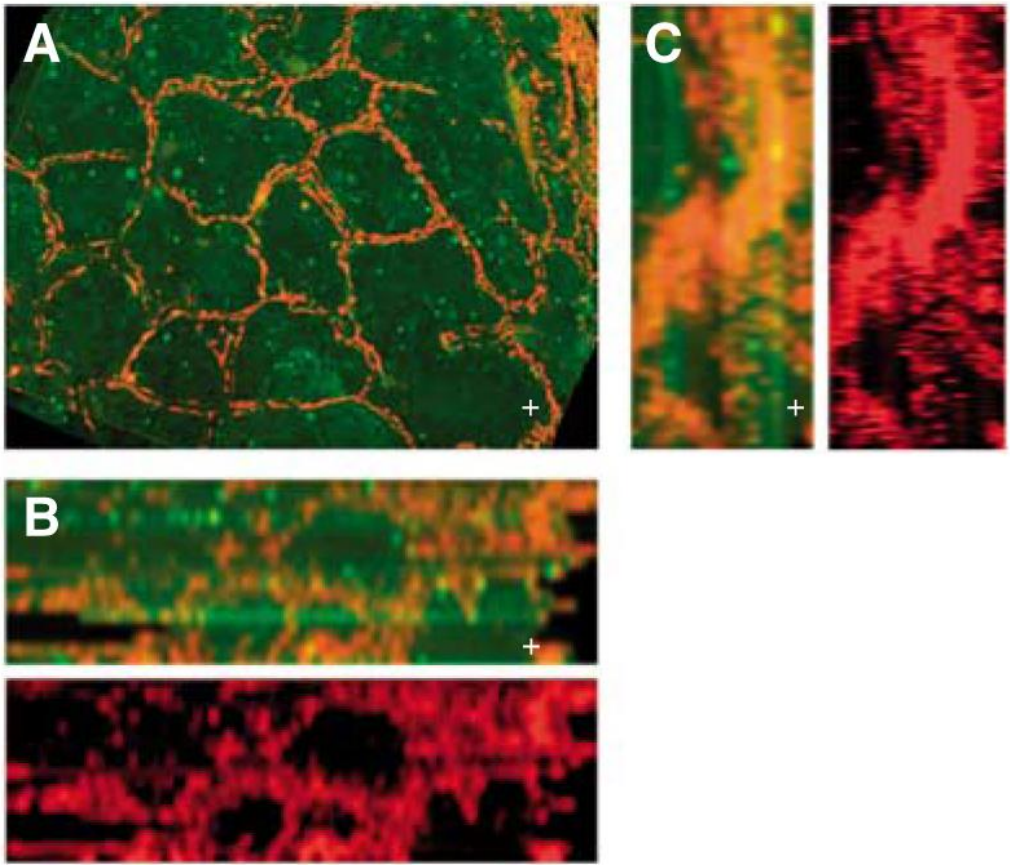

Figure 6.3 Immunofluorescence staining non-angiogenic lung tumor.

Immunofluorescence staining for CD34 and cytokeratin (A) 2 Dimensional view of non-angiogenic cancerous lung with blood vessels (red) still intact and similar to that of the normal lung except that in the former the alveoli are filled with tumor cells (green). (B) 2 Dimensional orthogonal view showing that the blood vessel staining of the non-angiogenic lung looks like a replica of a normal lung with no destruction to the vascular network (red) followed by the superimposition of the cytokeratin (green) staining showing neoplastic cell filled alveoli. (C) 2 Dimensional orthogonal view from a non-angiogenic tumor of a large long blood vessel that remains intact and snakes through from the surface deep into the tissue with no evidence of vascular eruption. From Adighibe et al.,(Adighibe, Micklem et al. 2006).

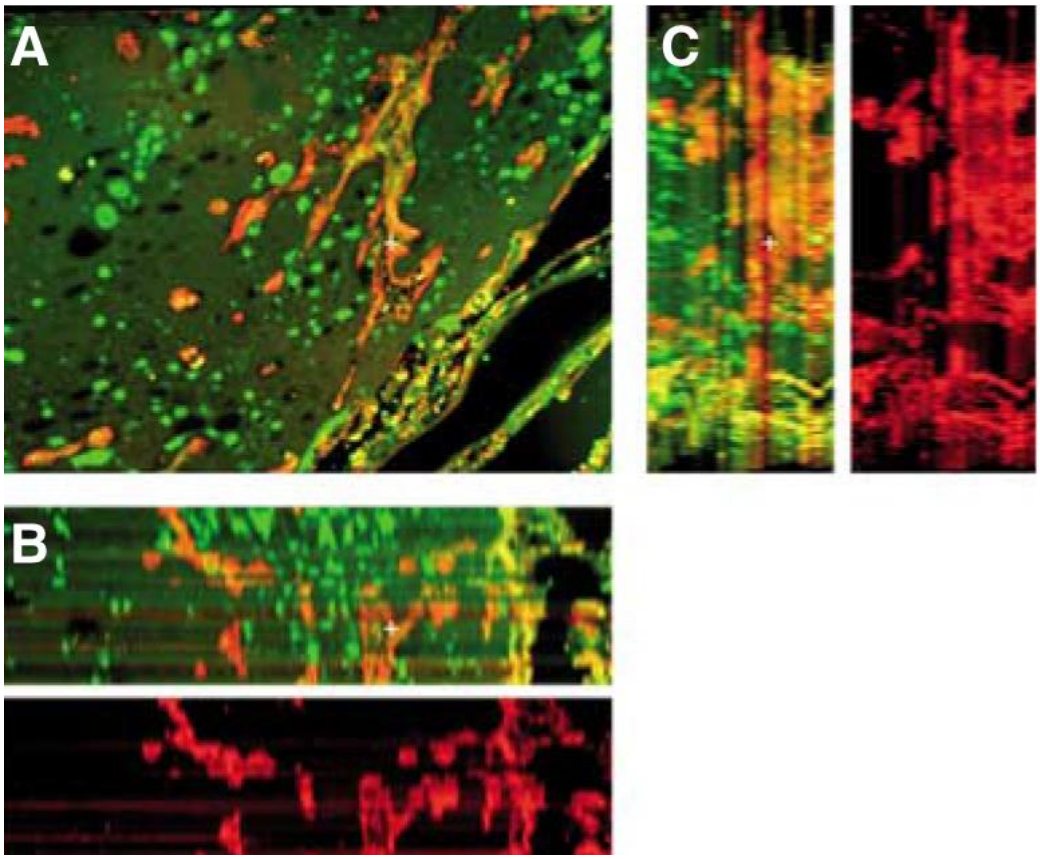

Figure 6.4 Immunofluorescence staining angiogenic lung tumor.
Immunofluorescence staining for CD34 and cytokeratin and 2D rendering of an angiogenic lung tumor showing tortuous blood vessels (red) of heterogeneous sizes. There evidently is no retention of the original architecture of the normal lung's cytoskeleton (green) and blood vessels in the angiogenic tumor as in the non-angiogenic tumors. Picture from Adighibe et al.,(Adighibe, Micklem et al. 2006).

Research related to angiogenesis has been intense and numerous anti-angiogenic drugs have been developed and approved for clinical treatment. Anti-angiogenic drugs such as the anti-VEGF antibody, Bevacizumab in combination with chemotherapy have been shown to help slow metastatic disease progression but it is not necessarily associated with increased overall survival (Ebos and Kerbel 2011). Some studies on liver metastases have shown that in patients with colorectal secondaries, the great majority of the metastases has an angiogenic phenotype

while in breast cancer patients most of the metastatic lesions had a co-opted vascular pattern (Stessels, Van den Eynden et al. 2004). Though only speculative, this may be one of several potential explanations why Bevacizumab so far is proven more effective in metastatic colorectal cancer compared to advanced breast cancer.

Since co-opted vessels are important in the early stage of tumor development (Donnem et al., 2012 manuscript submitted) it would be of interest to know whether vessel co-option is one of the reasons that anti-angiogenic treatments have not succeeded in an adjuvant setting. The fact that tumors may grow to a clinically detectable size without angiogenesis makes them less likely, during that phase, to respond to drugs designed to target the abnormal vasculature produced by angiogenesis. Even if only the invading edge of the tumor remains able to progress without angiogenesis one may speculate that anti-angiogenic drugs are likely to be ineffective in this setting. Therefore a better understanding of the biology of angiogenic and non-angiogenic tumors is likely to be crucial to improve treatment.

Micro array studies in our laboratory have determined that the angiogenic and non-angiogenic tumors have different gene signature patterns (Hu, Bianchi et al. 2005). Surprisingly, among the genes that differentiated these two tumor phenotypes the most prominent were genes involved in glucose metabolism and not genes involved in the classical hypoxic or angiogenesis pathways.

Micro array results are however data not always representative of true protein expression pattern. To investigate how the classic hypoxia and angiogenesis associated proteins are differentially expressed in these tumor phenotypes, an immunohistochemical study was undertaken to ascertain the distribution pattern of proteins involved in the hypoxia pathway

[such as HIF1α and the PHDs] and the angiogenic pathway [such as VEGF, KDR and P53] in these angiogenic and non-angiogenic tumors.

The angiogenic and non-angiogenic tumor phenotypes were discovered in our lab from results of TRAP1's genomic analysis in non-small cell cancer hence it was important to evaluate the TRAP1 expression pattern in these tumor phenotypes. Also taking into consideration the relational association between TRAP1 and JMY, an analysis of JMY's expression signature in these tumor phenotypes was as well evaluated.

Finally, as results from analyzing these markers demonstrated a salient differential expression pattern of p53 in these tumor phenotypes, I further conducted a pilot sequencing study looking at p53 gene mutations in the angiogenic and non-angiogenic lung tumors.

6.2 Results

6.2.1 Marker profile analysis

The details of the antibodies used, the immunostaining techniques, scoring methodology and statistical analysis are reported in detail in Chapter 2 (Material and methods). The immunostaining was a collaborative effort between me and a colleague Dr Mary Ferguson (Ferguson, Angiogenesis in human lung tumors, 2008), markers stained by Dr Ferguson are indicated by asterisk.

Briefly immunostainings were scored for cytoplasmic and nuclear localization and, for some proteins, membrane staining. Tumors were evaluated for percentage of positive cells (on a scale from 0 to 4) and intensity of staining (from 0 to 3); these two values were then multiplied to provide a score called the "Intensity Percentage Grade" (IPG), the maximum score being 12. The TSP marker is the only marker scored in percentage as its analysis was only based on percentage of stroma stained. Mann Whitney testing was done for the statistical analysis using the GraphPadPRISM program (GraphPad software Inc., San Diego CA). The results for the cytoplasmic and membranous stainings are reported in Table 1 while the results for nuclear stainings are in Table 2.

In the angiogenic tumor I observed a higher expression of TSP in the stromal cells; PHD2, CFOS and STAT3 in the cytoplasm of its neoplastic cells. While HIF1α, BNIP3 and PI3 had a higher level of expression in the nucleus of its neoplastic cell (Figures 5-11).

In the non- angiogenic neoplastic cells, I found higher levels of cytoplasmic CA9 and p53 expression (Figures 12-13). Additionally, there were higher levels of TRAP1 and JMY expression in both the cytoplasm and nucleus of the non-angiogenic neoplastic cells (Figures 14-15).

Protein	Positive mean IPG angio	S.E	Positive mean IPG non-angio	S.E	P value	Highest expression in:
*HIF1α	6.22	0.33	6.00	0.48	0.87 ns	
*CA9 cyto	2.38	0.16	3.5	0.23	<0.001 s	Non-angio
*CA9 membr	4.00	0.40	3.30	0.88	0.6201 ns	
*VEGF	8.83	0.35	7.38	0.78	0.07 ns	
*KDRp34	10.40	0.30	10.55	0.62	0.71 ns	
*FIH	9.10	0.32	10.00	0.47	0.22 ns	
*PHD1	3.74	0.27	4.2	0.48	0.47 ns	
*PHD2	3.5	0.30	2.46	0.53	0.02 s	Angio
*TSP stroma	16.98	2.75	2.00	1.74	0.0004 s	Angio
*SOD1	4.36	0.45	9.39	4.22	0.27 ns	
Bcl2	1.05	0.25	0.68	0.35	0.54 ns	
C-FOS	8.05	0.37	5.31	0.55	0.0005 s	Angio
FGF	9.20	0.42	9.72	0.71	0.74 ns	
NIP3	6.08	0.36	5.92	0.82	0.88 ns	
P53	0.28	0.12	2.28	0.56	0.0001 s	Non-angio
PI3	4.62	0.36	4.92	0.61	0.51 ns	
SP1	3.70	0.37	3.38	0.55	0.86 ns	
STAT3	8.78	0.39	7.11	0.79	0.03 s	Angio
JMY	1.84	0.18	2.42	0.31	0.05 s	Non-Angio
TRAP1	4.22	0.28	5.48	0.32	0.001 s	Non-Angio

Table 6.1.Cytoplasmic staining of Angiogenic versus Non-angiogenic tumors.

ns = not significant; s = significant; Angio = Angiogenic tumor; Non-angio = Non-angiogenic tumor; membr=membrane. S.E= Standard error; *= Staining performed by Dr Ferguson. There higher significant expression of *PHD2, C-FOS, STAT3 in the cytoplasm and *TSP stroma of cells of the Angiogenic tumor than in the Non-angiogenic tumors. While there is higher significant expression of *CA9, P53, JMY and TRAP1 in the cytoplasm of cells of the Non-angiogenic tumor than the Angiogenic tumor.

Protein	Positive mean IPG angio	S.E.	Positive mean IPG non-angio	S.E.	P value	Highest expression in:
*HIF1α	5.49	0.31	3.79	0.39	0.01 s	Angio
*VEGF	6.09	0.52	5.62	0.32	0.74 ns	
*KDRp34	11.69	0.16	11.45	0.39	0.77 ns	
*FIH	7.50	0.35	8.15	0.72	0.50 ns	
*PHD1	3.10	0.34	2.50	0.35	0.99 ns	
*PHD2	2.56	0.27	1.41	0.35	0.02 s	Angio
*SOD1	4.21	0.45	5.00	0.91	0.44 ns	
C-FOS	7.50	0.52	5.53	0.75	0.049 s	Angio
FGF	7.51	0.38	8.68	0.76	0.11 ns	
Nip3	3.96	0.40	0	0	<0.0001	Angio
P53	2.66	0.36	2.32	0.53	0.91 ns	
PI3	0.53	0.13	0	0	<0.02 s	Angio
SP1	5.31	0.46	4.04	0.60	0.24 ns	
STAT3	7.80	0.39	6.31	0.81	0.09 ns	
JMY	2.01	0.17	2.60	0.27	0.07 ns	
TRAP1	1.57	0.18	4.58	0.32	<0.0001s	Non-Angio

Table 6.2 Angiogenic versus Non-angiogenic tumors - nuclear staining.

ns = not significant; s = significant; Angio = Angiogenic tumor; Non-angio = Non-angiogenic tumor. S.E= Standard error; *=Staining performed by Dr Ferguson. There is higher expression of *HIF1α, *PHD2, C-FOS, Nip3 and PI3 in the nucleus of cells of the Angiogenic tumor than in the Non-angiogenic tumor. While there is higher expression of TRAP1 in the nucleus of the Non-Angiogenic tumor than in the Angiogenic tumor.

6.2.1.1 Protein expression in the angiogenic versus the non-angiogenic tumor.

Graphical Depiction of higher protein expressivity in the angiogenic tumor.

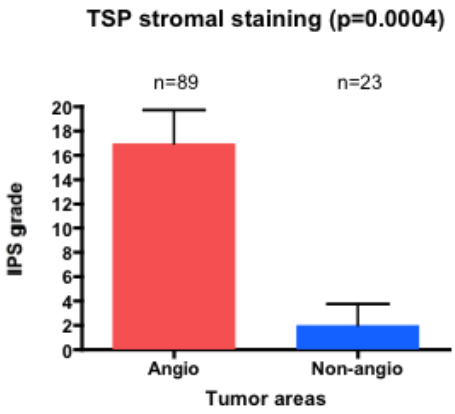

Figure 6.5 Analysis of TSP in stroma of angiogenic and non-angiogenic tumors
Showing a higher expression of TSP in the stroma of the angiogenic tumor with a significant p value of 0.0004. The TSP marker is the only marker scored in percentage as its analysis was only base on percentage of stroma stained.

A. **B.**

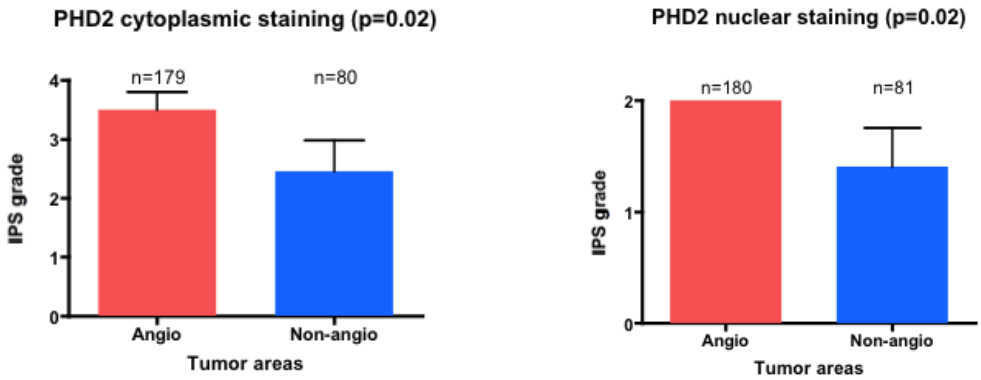

Figure 6.6 Marker analysis of PHD2 in angiogenic and non-angiogenic tumors
Showing high PHD2 protein expression in the angiogenic tumor. **A.** PHD2 analysis of cytoplasmic staining, showing higher PHD2 protein in the cytoplasm of angiogenic tumor with a significant p value of 0.02. **B.** PHD2 analysis of nuclear staining , showing higher PHD2 in the nucleus of angiogenic tumor with a significant p value of 0.02.

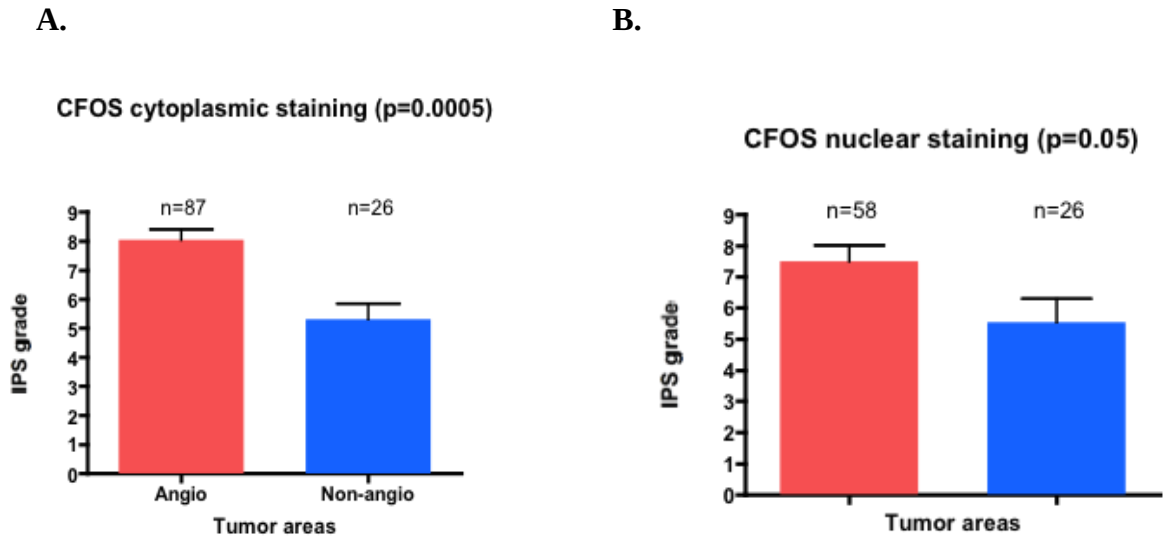

Figure 6.7 Marker analysis of CFOS in angiogenic and non-angiogenic tumors
Showing higher CFOS protein expression in the angiogenic tumor. **A.** CFOS analysis of cytoplasmic staining , showing higher CFOS protein in the cytoplasm of angiogenic tumor with a significant p value of 0.0005. **B.** CFOS analysis of nuclear staining , showing higher CFOS in the nucleus of angiogenic tumor with a significant p value of 0.05.

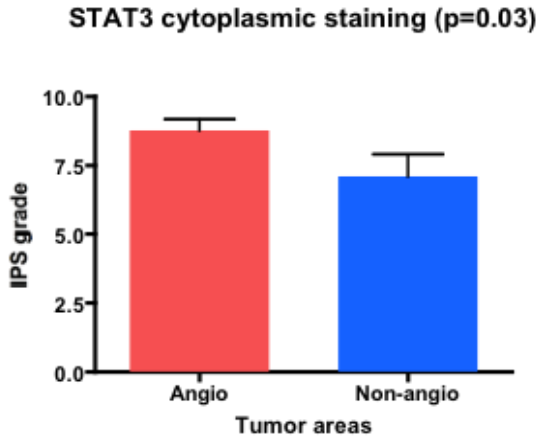

Figure 6.8 Analysis of STAT3 in cytoplasm of angiogenic and non-angiogenic tumors
Showing a higher expression of STAT3 in the cytoplasm of the angiogenic tumor with a significant p value of 0.03.

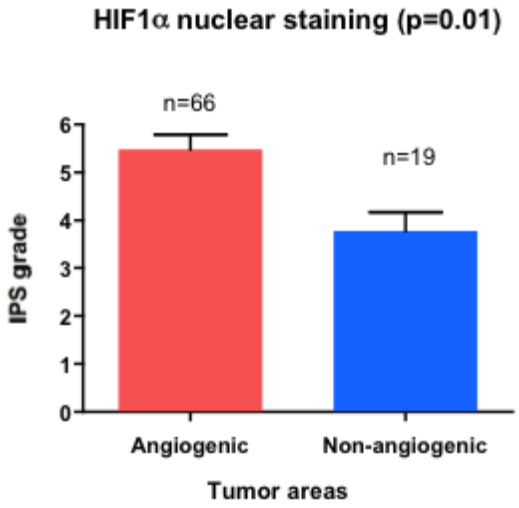

Figure 6.9 Analysis of HIF-1α in nucleus of angiogenic and non-angiogenic tumors

Showing a higher expression of HIF-1α in the nucleus of the angiogenic tumor with a significant p value of 0.01.

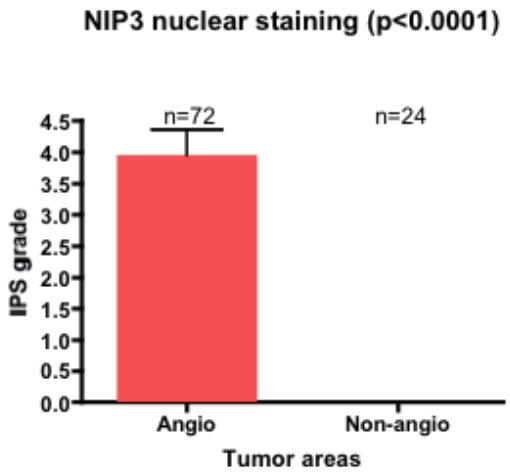

Figure 6.10 Analysis of BNIP3 in nucleus of angiogenic and non-angiogenic tumors

Showing a higher expression of BNIP3 in the nucleus of the angiogenic tumor and an absence of BNIP3 in the nucleus of the non-angiogenic tumor with a significant p value of 0.0001.

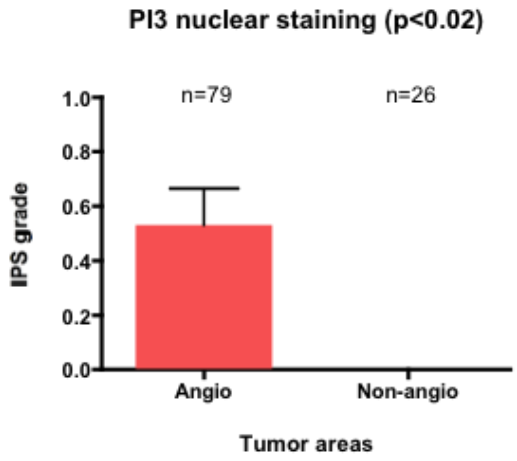

Figure 6.11 Analysis of PI3 in nucleus of angiogenic and non-angiogenic tumors
Showing a higher expression of PI3 in the nucleus of the angiogenic tumor and an absence of PI3 in the nucleus of the non-angiogenic tumor with a significant p value of <0.02.

Graphical Depiction of higher protein expressivity in the non-angiogenic tumor.

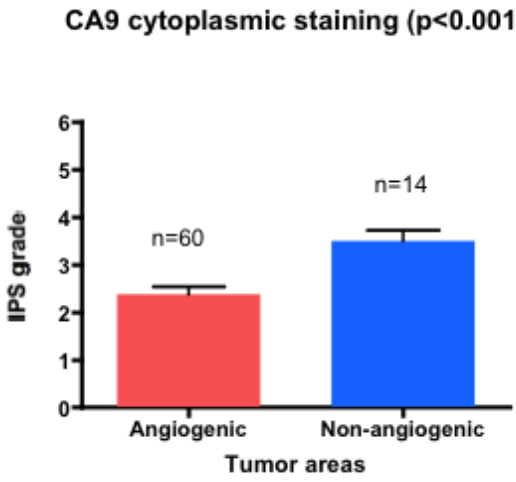

Figure 6.12 Analysis of CA9 in the cytoplasm of angiogenic and non-angiogenic tumors
Showing a higher expression of CA9 in the cytoplasm of the non-angiogenic tumors with a significant p value < 0.001.

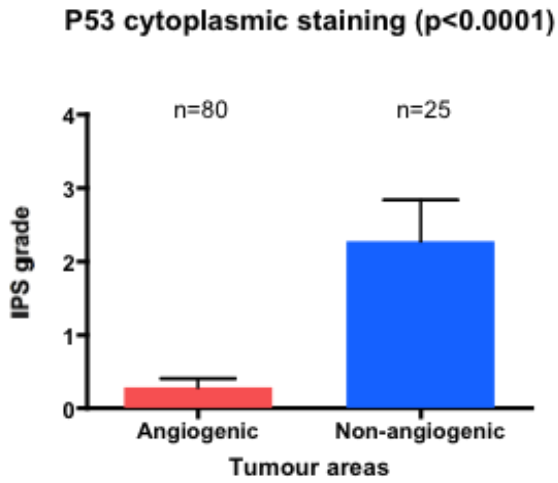

Figure 6.13 Analysis of p53 in the cytoplasm of angiogenic and non-angiogenic tumors
Showing a high expression of p53 in the cytoplasm of the non-angiogenic tumors and an almost absence of p53 protein expression in the cytoplasm of the angiogenic tumours; significant p value < 0.0001.

A. **B.**

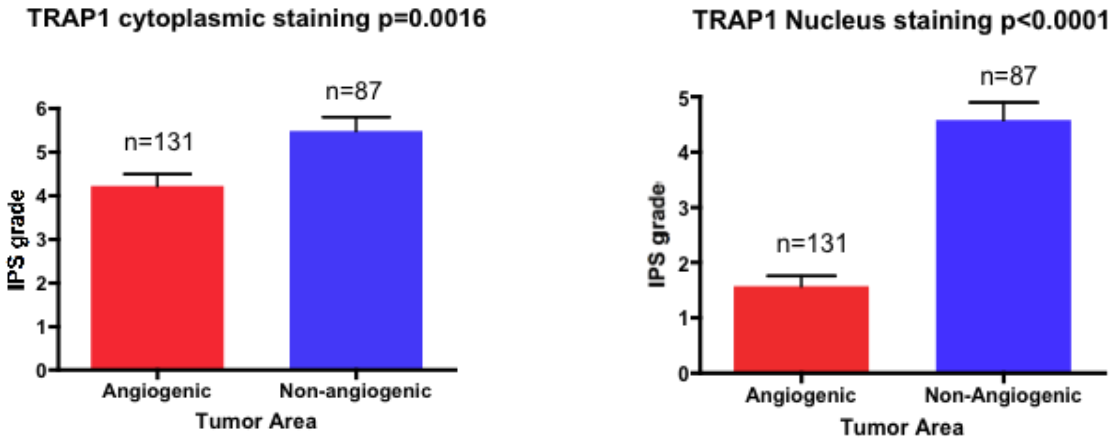

Figure 6.14 Marker analysis of TRAP1 in angiogenic and non-angiogenic tumors
Showing high TRAP1 protein expression in the non-angiogenic tumor. **A.** TRAP1 analysis, cytoplasmic staining , showing higher TRAP1 protein in the cytoplasm, non-angiogenic tumor with a significant p value of 0.001. **B.** TRAP1 analysis, nuclear staining , showing higher TRAP1 in the nucleus of non-angiogenic tumor, statistically significant p<0.0001.

A. **B.**

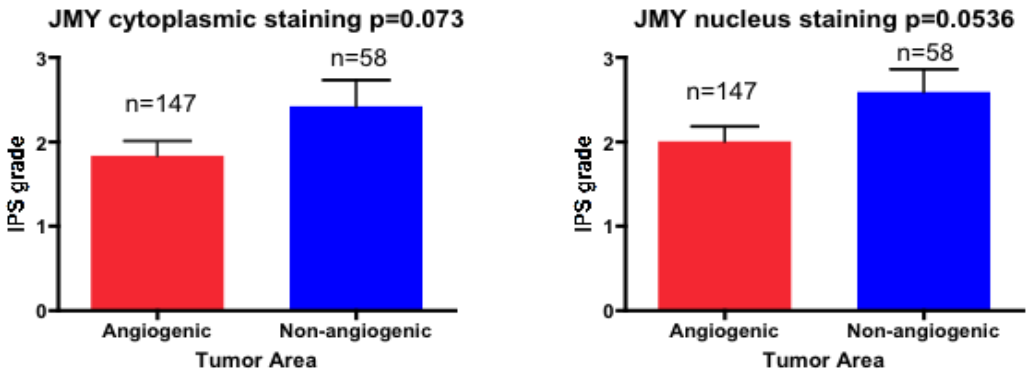

Figure 6.15 Marker analysis of JMY in angiogenic and non-angiogenic tumors
Though not statistically significant shows a higher JMY expression both in. **A.** JMY cytoplasmic staining and **B.** JMY nuclear staining.

6.2.2 Sequencing of the P53 gene in Angiogenic and Non-angiogenic tumors

The high cytoplasmic p53 expression in the non-angiogenic tumors as compared to the angiogenic tumors got me curious about characterizing the type of p53 proteins being expressed in both these tumor phenotypes. Were they the wild type p53 or mutated P53?

To address this question I performed a pilot study sequencing the p53 of both angiogenic and non-angiogenic tumors. The initial sequencing study and analysis was done by me with assistance from Ms. Marta Fernandez-Mercado (Leukemia Lymphoma Research Molecular Haematology Unit, Nuffield Department of Clinical Laboratory Sciences, University of Oxford) and the duplicate study and analysis was done by Marta Fernandez-Mercado.

P 53 mutations were observed in 8 out of 25 Angiogenic cases (32%) and in 5 out of 7 Non-angiogenic cases (71.4%) (Table 6.3 and 6.4). Additionally, the location of the mutations was

randomly distributed across the sequenced region. No specific pattern of mutation location seems to be related to tumor subtype (angiogenic or non angiogenic) (Figure 6.14).

Non Angiogenic	5/7	(71.4%)
Angiogenic	8/25	(32.0%)
Two-tailed Fisher´s exact test		p=0.0906

Table 6.3 Number and percentage of p53 mutations in non-angiogenic versus Angiogenic cases.

All detected mutations were heterozygous and almost all of them corresponded to hot spots previously reported in different tumor types. Software used to predict the functional effect of the detected sequence changes is- PolyPhen_2(Adzhubei, Schmidt et al. 2010).

Sample ID	Sample type	Mutation location	Mutation type	Domain	Predicted effect in protein activity
249	Non Angiogenic	c.314G>GA; p.G105D	Missense	DNA binding	Damaging
121	Non Angiogenic	c.488A>AG; p.Y163C	Missense	DNA binding	Damaging
152	Non Angiogenic	c.634T>TG; p.F212V	Missense	DNA binding	Benign
105	Non Angiogenic	c.734G>GA; p.G245D	Missense	HCD IV	Damaging
104	Non Angiogenic	c.761T>TA; p.I254S	Missense	HCD IV	Damaging
138	Angiogenic	c.824G>GA; p.C275Y	Missense	HCD IV	Damaging
139	Angiogenic	c.het_del216C; p.V73Wfs48X	Frameshift	Proline Rich	Truncated protein
141	Angiogenic	c.407A>AC; p.Q136P	Missense	HCD II	Damaging
274	Angiogenic	c.471_472TC>GA; p.V157G	Missense	DNA binding	Damaging
133	Angiogenic	c.511G>GT; p.E171X	Nonsense	HCD III	Truncated protein
147	Angiogenic	c.524G>GA; p.R175H	Missense	HCD III	Potentialy damaging
98	Angiogenic	c.524G>GA; p.R175H	Missense		

Table 6.4 Summary of P53 mutations detected in non-angiogenic and angiogenic cases.

Affected domains are listed. The number of mutations for each particular codon reported in the TP53 database is shown as comments. Software to predict the functional effect of the detected sequence changes is- PolyPhen_2(Adzhubei, Schmidt et al. 2010). Activity of the mutant p53 using a waf1 reporter gene is shown as a percentage where relevant information was available. For translation of codon site used - http://en.wikipedia.org/wiki/Genetic_code.

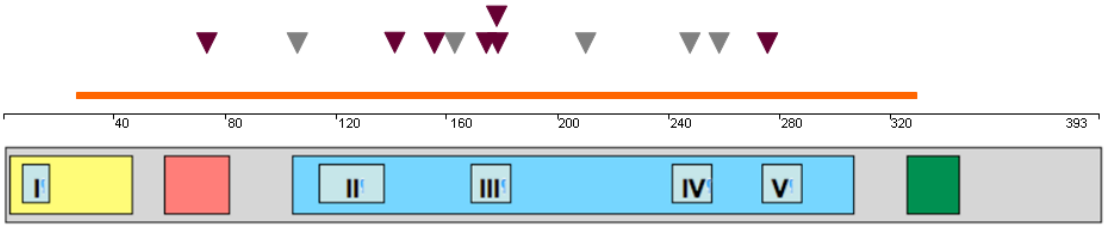

Figure 6.16 p53 sequence.

The sequenced region is indicated with a orange line in the figure above. Mutation locations are indicated with arrowheads (brown: mutations found in angiogenic samples; grey: mutations found in non angiogenic samples). Human p53 protein (Hp53) can be divided into five domains, each corresponding to specific functions: Yellow is the Highly conversed domain I (HCD I) /transactivation domain; Red is the second transactivation domain which is proline rich; Blue is the DNA binding domain essential for p53-DNA interactions that also contains HCD II-V and is the target of 90% of the p53 mutations found in human cancers; Green is the nuclear export signal (NES) localized in the oligomerization domain of p53.

6.3 Discussion

The existence of a putative non-angiogenic tumor phenotype raises the question of what biological relevance this would have to cancer in regards to detection, prognosis and most importantly adjuvant treatment with anti-angiogenic drugs. Studies in mice have shown that not all experimental metastases respond to anti-angiogenic agents (Donnem et al., 2012 manuscript submitted) Also clinical trials results suggest the possibility that some of these unresponsive tumors are of a distinct phenotype from the responsive angiogenic tumors (Gasparini, Longo et al. 2005, Gasparini, Longo et al. 2005).

In tumors, hypoxia is considered an important cause of radiotherapy and chemotherapy failure and also a major cause of aggressive behavior with increased invasion and metastatic potential

(Giatromanolaki, Koukourakis et al. 2004). Hypoxia influences the expression of genes involved in cell death and energy homeostasis mainly by stabilization and activation of the hypoxia inducible factor (HIF) family of transcription factors, influencing angiogenesis (VEGF), glycolysis (GLUT1), pH regulation (CA9), apoptosis (TP53, BNIP3) and autophagy (BNIP3) (Bacon and Harris 2004, Keith and Simon 2007).

Based on results obtained from this study, I have categorized the protein expression pattern for markers that I have evaluated in angiogenic and non-angiogenic tumors into 2 groups; "the primary effectors" and "adaptive responding" proteins.

I describe the primary effectors as proteins of genes that actively induce angiogenesis such as Hif 1α and Vegf, while the "adaptive responders" are proteins of genes activated in response to angiogenesis. From my observation, the "responder" such as Tsp generally seem to be activated by the cells in an attempt to attenuate angiogenesis.

Two of the first markers I analyzed were the Prolyl hydroxylases (PHDs): PHD1 and PHD2. PHDs are important cellular molecules regulating the HIF pathway by hydroxylating and targeting HIF1α for degradation (Teodoro, Evans et al. 2007, Semenza 2010, Semenza 2012). They are the cellular antennae that sense molecular oxygen status, hence their activity is oxygen dependent (Teodoro, Evans et al. 2007), and as a result, are highly expressed in oxygenated environment and downregulated in hypoxic environments (Teodoro, Evans et al. 2007). Previous work done in our laboratory has shown that the non-angiogenic tumors upregulate more genes coding for proteins localized in the mitochondria than the angiogenic tumors does (Hu, Bianchi et al. 2005). This led to Hu et al's proposals that increased hypoxia

induces an increase in mitochondrial function in non-angiogenic tumor and in this way compensating for diminished oxygenation and allowing this tumor to grow without triggering angiogenesis (Hu, Bianchi et al. 2005). It also further implies that the non-angiogenic cells are very effective and thrive better in hypoxia than in a highly oxygenated environment. This could then explain why there is decreased PHD (Figure 6.6), an oxygen dependent protein, in the hypoxia loving non-angiogenic tumors. This is further supported by the fact that the hypoxia marker, CA9, is very highly expressed in the Non-angiogenic tumor (Figure 6.12). CA9 will be further discussed in paragraphs below.

Thrombospondin (TSP) is one of the proteins designated as the product of an "adaptive response gene" to angiogenesis: It is a p53 target gene and one of the endogenous factors found to inhibit angiogenesis (Good, Polverini et al. 1990, Tolsma, Volpert et al. 1993, Dameron, Volpert et al. 1994). The Tsp gene is downregulated in response to expression of oncogenes such as Ras and Myc, highlighting the opposing effects that oncogenes and tumor suppressors have on angiogenesis (Teodoro, Evans et al. 2007). Antiangiogenic factors such as TSP upregulated by p53 are in most cases secreted into the extracellular matrix(Teodoro, Evans et al. 2007). TSP has also been shown to inhibit angiogenesis through several mechanism and a noted mechanism is its negative regulation of growth and migration of endothelial cells in vitro and in vivo (Jimenez, Volpert et al. 2000, Nor, Mitra et al. 2000). TSP was found in my marker analysis to be more highly expressed in the stroma of the angiogenic than the non-angiogenic tumors (Figure 6.5). This correlates with the fact that since more angiogenesis is occurring in the angiogenic tumors than in the non-angiogenic tumors, it is then reasonable to expect that TSP playing the role of an "adaptive responder", rising to curtail angiogenesis, should be more highly expressed in the stroma of the angiogenic tumor than in the non-angiogenic tumor.

Hence my marker analysis corroborates the already know fact of TSP being antiangiogenic factor (Jimenez, Volpert et al. 2000, Teodoro, Evans et al. 2007).

The central regulating component responding to hypoxia is HIF (Pugh and Ratcliffe 2003). HIF is also a crucial primary instigator of angiogenesis. HIF-1α is stabilized and is upregulated in response to oxygen deprivation, and it is commonly highly expressed in most tumors (Harris 2002). HIF-1α subsequently, together with the constitutively expressed HIF1 β, binds to its cognate DNA binding sites of genes such as Vegf, whch has a hypoxic response elements (HRE) and is a potent tumor angiogenesis promoter (Forsythe, Jiang et al. 1996, Carmeliet, Dor et al. 1998). As such, it is also not surprising that the HIF-1α protein was found in my marker analysis to be more highly expressed in the angiogenic tumor where it will be promoting angiogenesis than in the non-angiogenic tumors that are striving to avert angiogenesis (Figure6. 9).

My marker analysis also yielded a higher expression in the angiogenic tumors of factors STAT3, PI3 and CFOS. Interestingly the expression of these three proteins is associated with growth, cell proliferation and invasion (Datta, Brunet et al. 1999, Regis, Pensa et al. 2008, Schiavone, Avalle et al. 2011). As previously described, angiogenic tumors upregulate genes that code for neoangiogenesis, remodeling and inflammation related pathways (Hu, Bianchi et al. 2005). PI3, a protein involved in HIF activation (Harris 2002, Hu, Bianchi et al. 2005) was observed to be more highly expressed in the angiogenic tumors in the marker analysis (Figure6. 11). PI3 is also involved in the PI3K signaling cascade which is frequently overactivated in human cancer (Vivanco and Sawyers 2002, Carnero 2010) and plays critical roles both in the initiation and progression of NSCLC (Datta, Brunet et al. 1999, Hanada, Feng et al. 2004). The

PI3K pathway regulates cellular functions such as proliferation, survival, motility and angiogenesis that are critical to the growth and maintenance of tumors (Memmott and Dennis 2010, Xu, Jin et al. 2010)..

Additionally, PI3 breakdown products function as cytoplasmic second messengers to activate transcription of c-fos (Rollins and Stiles 1988). CFOS is an immediate-early gene that is induced by a plethora of physiological signals: growth factors, cytokines and hormones, and environmental stimuli. Upon activation c-fos heterodimerizes with C/jun to form AP1 transcription factor and transduce its effect of regulating a wide range of cellular processes, including cell proliferation, death, survival, and differentiation (Shaulian and Karin 2002, Wagner and Eferl 2005). My marker analysis showing a higher expression of CFOS (Figure 6.7) in the angiogenic tumor than the non-angiogenic is also in line as evidence of its participation in the PI3K pathway promoting angiogenesis.

Furthermore, the transcription factor STAT3 is an oncogene constitutively active in a high number of primary tumors of various origins, where it promotes proliferation, survival and tissue invasion. It also mediates the downstream signaling of cytokines and growth factor receptors (Schiavone, Avalle et al. 2011) such as c-fos. My marker analysis as well showed STAT3 (Figure 6.8) as rightfully falling in place within this common pathway of being more highly expressed in the angiogenic tumor than in the non-angiogenic tumor.

Bnip3 is one of the HIF1α activated genes in response to hypoxia and is capable of inducing autophagy (Zhang and Ney 2009) and cell death, although this mechanism remains unclear (Mellor and Harris 2007). However, BNIP3 expression in cancer does not always result in cell death suggesting that additional factors have the potential of suppressing the effect of BNIP3 or

cooperate with it to induce death (Mellor and Harris 2007, Zhang and Ney 2009). BNIP3 expression is generally upregulated in many tumor types when compared to normal tissues (Giatromanolaki, Koukourakis et al. 2004). In my marker analysis, BNIP3 was observed to be equally expressed in the cytoplasm of both angiogenic and non-angiogenic tumors (Table 6.1 and 6.2). However, the angiogenic tumors had an extensive nuclear BNIP3 expression not observed in the non-angiogenic tumors (Figure 6.10).

A possible explanation for the lack of nuclear BNIP3 expression in the non-angiogenic tumor is that it could be due to an inherent BNIP3 mutation that resulted in improper folding (Borgese, Driessen et al. 2009), or a modification of the BNIP3 protein in non-angiogenic tumor which caused an inhibition of translocation into nucleus and a subsequent BNIP3 cytoplasmic sequestration in the non-angiogenic tumor phenotype. Such inhibition of protein translocation into the nucleus has been seen in prostate receptor cofactor mutation which contributes to tumorigenesis(Gu, Zhou et al. 2011). However, a sequence analysis of BNIP3 in the angiogenic and non-angiogenic tumors is required to ascertain if the nonangiogenic tumor could possibly have a specific BNIP3 associated mutation not found in the angiogenic tumor that would cause this protein's cytoplasmic arrest in the non-angiogenic tumor but not in the angiogenic tumor.

The non-angiogenic tumors had a higher expression of CA9 and p53 in the cytoplasm of their neoplastic cells than in the angiogenic tumors (Figures 6.12-6.13). CA9 serves as a marker for metabolic adaptation during hypoxia (Cleven, Wouters et al. 2008). Higher CA9 expression in the non-angiogenic tumors could imply that a higher degree of hypoxia is occurring in the non-angiogenic tumors as has been previously mentioned (Hu, Bianchi et al. 2005) and also a possible sign of a more aggressive behavior as has been observed in non- angiogenic lung cancers (Pastorino, Andreola et al. 1997, Giatromanolaki, Koukourakis et al. 2004).

The salient finding with of my marker analysis which also substantiates a characteristic difference between the non-angiogenic and the angiogenic tumors is the p53 expression pattern (Figure 6.13) in these tumors. The non-angiogenic phenotype has an abundance of cytoplasmic p53 compared to the angiogenic tumor's expression of minimal to almost complete absence of cytoplasmic p53. There are two plausible explanations for this observation.

The first explanation for cytoplasmic p53 sequestration in the non-angiogenic tumors could be associated with the roles that p53 plays in angiogenesis. Wild Type P53 is a potent inhibitor of angiogenesis (Teodoro, Evans et al. 2007) and its mechanism of regulating angiogenesis is threefold: 1) inhibition of the hypoxia-sensing system, 2) downregulation of proangiogenic genes and 3) upregulation of antiangiogenic pathways (Teodoro, Parker et al. 2006). The non-angiogenic tumors most likely capitalize on the first mechanism by impeding hypoxia induced angiogenesis via downregulating HIF-1α a central responder to hypoxia and a major promoter for neovascularization and angiogenesis (Teodoro, Evans et al. 2007, Semenza 2010). p53 is able to directly bind HIF1α in the cytoplasm and target it for protein degradation as seen in Figure 6.17. (Ravi, Mookerjee et al. 2000, Teodoro, Evans et al. 2007). Hence, it is possible that the high cytoplasmic p53 expression in non-angiogenic tumors could be an anti-angiogenic mechanism whereby it targets HIF-1α for degradation. This in effect would mean that less HIF-1α translocates into the nucleus which will in turn halting VEGF's activation of neovascularization and angiogenesis. This way, the non-angiogenic tumor ultimately progresses without making new blood vessels but thrives via co-opting already existing blood vessels (2000, Pezzella, Harris et al. 2001, Adighibe, Micklem et al. 2006). This premise also fits well with work by Rubenstien et al who have shown that blocking VEGF signaling with an

antibody increases blood vessel co-option and growth of satellite tumors (Rubenstein, Kim et al. 2000).

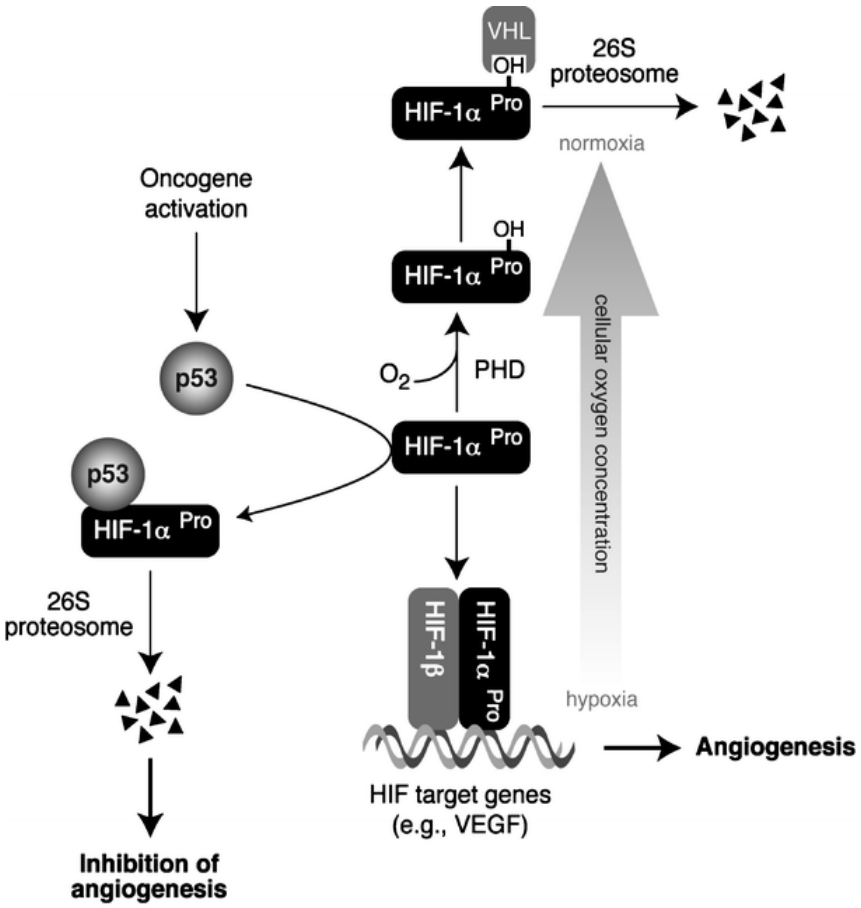

Figure 6.17 The p53 tumor suppressor protein limiting angiogenesis by inhibiting the central regulator of hypoxia, HIF.

Diagram from Teodoro et al., 2007 Inhibition of tumor angiogenesis by p53: a new role for the guardian of the genome (Teodoro, Evans et al. 2007).

The second explanation for cytoplasmic p53 sequestration in the non-angiogenic tumors could be that this happens due to an "inherent p53 mutation" in these non-angiogenic tumors. To validate this "inherent p53 mutation" hypothesis I conducted a pilot study of p53 sequencing in the angiogenic and non-angiogenic tumor phenotypes. Interestingly my pilot study appears to give this "inherent p53 mutation" premise some credence. The sequence study showed that

74% of the non-angiogenic tumor cases had p53 mutations compared to only 32% of the angiogenic tumor cases having p53 mutation. Though the p value from this study was not significant, as this was a pilot study with a small sample size, a 74% mutation rate in the non-angiogenic tumors is quite impressive. A much larger case study is now needed to further strengthen this "inherent p53 mutation" hypothesis. Additionally, it is worth mentioning that all the non-angiogenic tumor p53 mutations observed were purely missense mutations (Table 6.4), while the mutations in angiogenic tumors were a combination of frameshifts and nonsense mutations (Table6.4). This possibly also implies that the non-angiogenic tumor has exclusively selected for a "missense mutation" to be efficient in inactivating p53, rendering it incapable of translocating into the nucleus and by so doing curtailing and escaping p53 induced cell death. Support for this premise comes from some studies that have shown tumors being able to select for cells with defective cell death regulators, such as p53 mutation, and in the non-selected cells activate p53-mediated G0/G1 arrest or apoptosis eliminating these non-selected cells (Graeber, Osmanian et al. 1996). However future work of sequencing a larger non-angiogenic sample pool is required to confirm if indeed the cytoplasmic p53 accumulation in the non-angiogenic tumor is truly as a result of its p53 mutation.

Finally, evaluation of TRAP1 and JMY expression in the angiogenic and non-angiogenic tumors has helped to further elucidate the distinct characteristics between these 2 tumor phenotypes. TRAP1 is more highly expressed in both the cytoplasm and nucleus of the non-angiogenic than the angiogenic tumor. This high TRAP1 expressivity in the non-angiogenic tumor is more pronounced in the nucleus, with a powerful significant value of $p < 0.0001$. This could imply that the role which TRAP1 plays in the nucleus, i.e. its tumor suppressive role, is most likely one of the pathways in the non-angiogenic tumor which contributes to either effect or is affected in the non-angiogenic evolutionary divergence away from angiogenesis.

Additionally, JMY is also more highly expressed in the non-angiogenic tumor than the angiogenic tumor (although statistically not significant with p values of 0.073 and 0.0536 respectively for the cytoplasm and nuclear JMY expression). This result correlates with the noted direct association between JMY and TRAP1. However, again a larger study will be needed to establish a statistically significant clarity of there being a higher JMY expression in the non-angiogenic tumor than in the angiogenic tumor.

6.4 Conclusion

Why the non-angiogenic tumors fail to trigger angiogenesis and only thrive from already existing blood vessels remains intriguing. Having provided evidence for the existence of a putative non-angiogenic tumor phenotype I would like to propose a possible explanation for this phenomenon. It is possible that the mechanism involved here could be the result of the evolution of tumor cells with a specific genetic profile that leads to an alternative response to hypoxia not involving angiogenesis but rather a metabolic re-programming leading to the ability to co-opt pre-existing vessels.

Owing to hypoxic events that frequently occur during cancer cell progression, genes such as those governing efficient regulation of oxygen homeostasis could be properties clonally selected for by evolving cancer cells (Pugh and Ratcliffe 2003). This suggestion is supported by findings in our lab that non-angiogenic tumors have higher levels of genes coding for proteins involved in mitochondrial metabolism (Hu, Bianchi et al. 2005). It is also known that clonal chromosomal changes found in malignant tumors have a strong correlation with tumor morphology (Gisselsson, Bjork et al. 2001, Gisselsson, Jonson et al. 2001, Gisselsson 2002). Hence, I suggest that by means of natural selection either through interactions between the

microenvironment and the variability inherent in cell populations (Kozlov 1996) like p53 mutation (Hammond and Giaccia 2006), tumors cells have evolved to this non-angiogenic form in an effort to establish a survival advantage such as being able to highly regulate their mitochondria and co-opting pre-existing vessels.

The clinical implications of this are that cancer treatment will need to take into account the potential of angiogenic cancers to escape into a non-angiogenic phenotype, or even randomly switching between both phenotypes in effort to evade eradication. Regulators of signaling pathways for each stage are potential targets for cancer prevention (Boutwell 1989). Having deciphered some characteristics of the non-angiogenic cancer in this study is a good start towards understanding the regulators of this phenotype. This provides one explanation for the problems encountered with pure anti-angiogenic cancer treatments and makes a strong case for incorporating additional adjuvant therapeutic coverage into anti-cancer treatments.

CHAPTER 7
CONCLUSION

The main objective of this thesis was to evaluate the effects of the loss of chaperone protein HSP75 (TRAP1) in human cancer; its relationship with a newly identified protein, the Junctional Mediating and Regulatory protein (JMY) and the characterization of the angiogenic and non-angiogenic cancer phenotypes.

HSPs are frequently up regulated in cancer (Chant, Rose et al. 1995) this primarily points to the high demand for protein refolding in the tumorgenic environment consistent with acidosis, nutritional and O2 deprivation, severe hypoxia and oncogenic mutation. However in micro array studies done in our lab, we made a surprising observation of a down regulation of HSP75 (TRAP1) in some non-small cell lung cancers cases that were being compared to normal lung. Initial work on TRAP1 suggested a tumor suppressor role for TRAP1, since TRAP1 is a chaperone to Rb where in the event of heat shock, TRAP1 which is primarily located in the cytoplasm, translocates to the nucleus to refold heat shock denatured Rb back to its active conformation (Chen, Chen et al. 1996).

In further data from our laboratory, TRAP1 was observed to be directly associated with cell proliferation suggesting an oncogenic role for TRAP1. Work by Liu et al (Liu, Hu et al. 2010) shows that TRAP1 regulates cell proliferation both in normoxia and hypoxia via TNF activated pathways.

In this thesis, my result primarily shows strong evidence of an oncogenic role for TRAP1 in human cancer. Previous studies on TRAP1 in association with cell proliferation were done in

the 2 dimensional milieu of a Petri dish, so I began this thesis work investigating TRAP1 in a 3 dimensional spheroid model. As tissue growth is in 3 dimensions and is influenced by 3 dimensional cell-cell interactions, this model mirrors the state of a tissue better than a monolayer cell culture.

7.1 Spheroid model

In chapter 3 of this thesis, using the spheroid model, I have demonstrated that TRAP1 promotes rapid cell proliferation, which is reflected by TRAP1 positive spheroids steadily out growing TRAP1 negative spheroids. Since the spheroid model also emulates the characteristic tumor necrotic core development, I was also able to show that due to a rapid proliferation in TRAP1 positive spheroid, their onset of hypoxia and necrosis was more dramatic and sooner than in the setting of TRAP1 absence. Extrapolating the implication of this result to real life in vivo tumors, I raised the hypothesis that tumors with up regulated TRAP1 could be more prone to rapid hypoxia development which equates to poor prognosis for patients. As hypoxia is a catalyst for metastasis (Mellor and Harris 2007, Semenza 2010), such tumors are very likely to trigger rapid metastasis.

Future work would include replicating TRAP1 knockdown and spheroid growth in other cell lines. In this present work using CA9 staining of the spheroid, I demonstrated the pattern of progressive decreased oxygen penetration of the spheroid's core, but future work to show solid evidence of hypoxic core in these spheroids will involve preparing spheroids with pimonidazole, a hypoxia marker. Having optimized the spheroid growth in vitro, it would be imperative to take the next step of translating in vitro spheroid growth of TRAP1 positive and negative cells to xenograft studies in mice. However there are still technical problems to be

solved before this can be done. One of the technicalities includes my observation that even with the lentiviral knock down of TRAP1 which is supposed to be a long term "knockdown", there still was a slight TRAP1 up-regulation in the TRAP1 knocked down cell after 14 days. Additionally, previous work by colleagues on TRAP1 knockdown in xenographs has already been attempted but showed a TRAP1 up regulation within 7 days. This TRAP1 up-regulation in knocked down cells makes it difficult to study effective long-term TRAP1 depletion in cancer. It as well emphasizes how dependent tumors could be on this TRAP1 protein for continual survival. Since TRAP1 is a potential therapeutic target we will continue pursuing effective mechanisms for long term TRAP1 knockdown. It would be beneficial to my work to consult with chemists to produce either a TRAP1 antagonist or a decoy TRAP1 receptor that will arrest TRAP1 at the protein level and attenuate its effect. This would then allow for potential longer term TRAP1 knock down.

7.2 Characterization of the JMY protein

In Chapter 4, I delved into characterization of the JMY protein as previous work from our lab also showed TRAP1 to be inversely linked to metastatic genes up-regulation and one of these genes coded for the JMY protein. JMY as well plays dichotomous roles in cancer being a putative metastatic protein with its capacity to promote cell motility (Paunola, Mattila et al. 2002, Coutts, Weston et al. 2009) and possessing a tumor suppressive activity by being a p53 enhancer in the event of DNA damage(Shikama, Lee et al. 1999).

At the time of my research work, there was no commercially available anti-JMY antibody for immunohistochemistry study, so I developed and characterized a monoclonal anti-JMY antibody which was then used to study JMY's expression in normal and neoplastic tissues.

In normal tissues JMY was widely expressed, having both cytoplasmic and nuclear co-expressions. The intensity of the JMY cytoplasmic and nucleic stains were variable across the different tissues and sometimes even within the same tissue.

In neoplastic tissues, comparing primary versus node metastatic cancer in head and neck and colorectal carcinoma, JMY was found to have significantly higher expression both in the cytoplasm and nucleus of the node metastasis than in the primary tumors. This higher JMY expression in the metastatic than in the primary neoplasm is probably related to JMY's capacity to activate actin and promote metastasis.

However in reality the expression, function and regulation of JMY just like many other oncogenic proteins are much more complex than are theoretically hypothesized. If the logic of high JMY expression correlating with rapid metastasis were followed, it would then be expected that JMY should be more highly expressed in aggressive tumors. However that was not necessarily the observation made with breast cases. In breast, JMY was moderately expressed in the normal tissue, very highly expressed in the in situ breast cancer, but had variable expression in the invasive breast cancer ranging from strong expression in well differentiated to weak expression in less properly differentiated invasive breast cancer.

Furthermore, in regards to JMY's tumor suppressive role, I also demonstrated a note worthy relationship between JMY and p53 in tumor samples. A pilot study I conducted in 283 breast cancer patients showed that patients with nuclear co-expression of JMY and P53 had a considerably shorter overall survival than patients who do not co-express nuclear JMY and p53. The underlying molecular basis of the co-expression for these two proteins could further

support the suggestion that JMY's involvement in oncogenesis is also strongly associated with p53, a potent tumor suppressor (Pinhasi-Kimhi, Michalovitz et al. 1986, Dameron, Volpert et al. 1994, Coutts and La Thangue 2005, Soussi 2005). This also possibly reflects/suggests a relationship between p53 and JMY where in normal tissue, wild-type p53 is functional and is able to be activated by JMY in event of DNA damage; however in tumors, there could be a possible deregulation of p53 pathway which affects or is effected by JMY and this consequently promotes tumorigenesis. To further strengthen this pilot study a mutli-variate statistical analysis of the data will be performed to ensure that p53/JMY staining is an independent risk factor for breast cancer.

These results thus far suggest that the next steps in the study of the role of JMY in cancer should be on clinical samples, where a thorough comparison of JMY with p53 expression should be investigated. Additionally p53 genetic alterations (both mutations and deletions) and the fate of JMY as a result of this should also be queried in these samples.

7.3 TRAP1 and JMY

Chapter 5 addressed the relational association between TRAP1 and JMY, since we took notice of an inverse relationship between JMY and TRAP1 in micro array work previously done in our lab (Liu, Hu et al. 2010). Micro array is a powerful tool on data mining that promises to be invaluable to study the expression of genes in cancer (Tan, Pezzella et al. 2007). Despite the enormous potential of this technology, it does face numerous pitfalls such as variation of statistical rigor to which data can be subjected to, or the variation in threshold for quantitative evaluation (Hofman 2005). Hence the validation of relative expression obtained from genome wide microarray is critical. This was my impetus to characterize the relationship between

TRAP1 and JMY. Validation of relational expression between these 2 proteins with western blotting and immunohistochemistry actually indicated a direct association, as supposed to the inverse relationship observed in micro array work. Additionally immunoprecipitation assay further suggest a direct interaction between TRAP1 and JMY, which could imply a functionally direct dependence of both proteins on each other. However, a repeat immunoprecipitation assay showing control lanes will be done to validate the reproducibility of this result. Knock-down studies also corroborate a direct relationship between TRAP1 and JMY as it was observed that knocking-down TRAP1 directly impairs the transcriptional protein expression of JMY. This result also suggests a possible direct regulatory relationship between TRAP1 and JMY, where TRAP1 is most likely the upstream/regulatory protein.

I also demonstrated that the relationship between TRAP1 and JMY possibly implies a synergistic contribution of these proteins towards increased tumor aggressiveness. The basis of this speculation is from the 5 year survival study, which showed that JMY and TRAP1 cytoplasmic co-expression/interaction was associated with shorter relapse free survival rates. All taken together, this then makes a case for TRAP1 and JMY proteins being potential targets for cancer therapeutics.

Further direction with the JMY and TRAP1 relationship would be deciphering the exact form and cue for interaction between the two proteins. Crystallography would be a valuable tool to manipulate in this case as it will allow a better visualization of the cytoplasmic TRAP1 and JMY interaction and how this could tangibly reinforce cancer aggressiveness.

7.4 Angiogenic and non-angiogenic phenotypes

Finally in chapter 6, I demonstrated the evidence of distinct characteristic differences between the classical angiogenic tumor phenotype and a putative non-angiogenic tumor phenotype. The most salient difference between these two tumor phenotypes and perhaps the major divergent point between them is the cytoplasmic p53 sequestration seen in the non-angiogenic phenotype that is absent in the angiogenic phenotype. A pilot study appears to validate this sequestration as being due to a possible p53 mutation in the non-angiogenic tumor, which might facilitate p53 cytoplasmic accumulation and degradation. This in effect prevents VEGF activation and ultimately non-angiogenic tumor's evasion of angiogenesis.

Non-angiogenic tumors also appear to be efficient in utilization their mitochondria in the setting of hypoxia (Hu, Bianchi et al. 2005) and can thus thrive by co-opting already existing blood vessels (Pezzella, Harris et al. 2001, Adighibe, Micklem et al. 2006). Hence I suggest that via means of natural selection and alterations such as p53 mutation, the non-angiogenic tumor has evolved, claiming the survival advantage of being able to highly regulate its mitochondria despite hypoxia and this is a possible resistance mechanism to cancer therapeutic. Additionally, there was higher nuclear TRAP1 expressivity in the non-angiogenic than the angiogenic tumor with a powerful significant p value of <0.0001. This could imply that the role TRAP1 plays in the nucleus, i.e. its tumor suppressive role, is one of the pathways in the non-angiogenic tumor which is either affected or effects the non-angiogenic evolutionary divergence away from angiogenesis.

The implications of this would then be that cancer treatments will need to take into account the pitfalls of traditional chemotherapy and the potential of cancer escaping into the non-angiogenic phenotype in an effort to evade eradication. This makes a case for anti-cancer therapy to incorporate additional adjuvant coverage that would account for such potential cancer phenotypic escape.

APPENDIX A
Reagents

For immunohistochemistry:

10mM citrate pH 6.0	10mM tri-sodium citrate 1L distilled water adjusted to pH 6.0
Tris/EDTA pH 8.0	10mM Tris-Cl 1mM EDTA 1L distilled water adusted to pH 8.0
PBS	10 PBS tablets 1L distilled water

For handling DNA / RNA:

TE buffer	10mM Tris-Cl 1mM EDTA pH 8.0
LB medium	20.6g LB broth EZMix powder (containing enzymatic casein digest 10g/L, yeast extract 5g/L, NaCl 5g/L) 1L distilled water
1x TAE	40mM Tris-acetate 1mM EDTA

For protein analysis:

3x Laemmlli buffer	3ml 0.5M Tris-Cl / SDS, pH6.8 1.5ml β-mercapethanol 0.9g SDS 3ml glycerol 3mg bromophenol blue
6x Laemmlli buffer	70ml 0.5M Tris-Cl / SDS, pH6.8 3ml glycerol 1g SDS 0.93g DTT 12mg bromophenol blue

0.375M Tris-Cl pH 8.8 90.75g Tris-base
2g SDS
500ml distilled water
adjusted to pH 8.8

0.125M Tris-Cl pH 6.8 30.28g Tris-base
2g SDS
500ml distilled water
adjusted to pH 6.8

Stacking gel 1.3ml acrylamide
2.5ml 0.125M Tris-Cl pH 6.8
6.08ml distilled water
50µl 10% APS
10µl Temed

10x SDS running buffer 30.3g Tris-base
144.2g glycine
10g SDS
1L distilled water

Transfer buffer 50ml 10x SDS running buffer
100ml methanol
350ml distilled water

APPENDIX B
Publications

Publication

Adighibe O, Micklem K, Campo L, Ferguson M, Harris A, Pozos R, Gatter K, Pezzella F. Is non-angiogenesis a novel pathway for cancer progression? A study using 3 dimensional tumor reconstruction. Br J Cancer. 2006 Apr 24;94(8):1176-9.

Presentations

1. Cell Symposia: Angiogenesis, Metabolic Regulation, and Cancer Biology in association with VIB; Katholieke, Universiteit, Lueven, Belgium. July 6-8 2012.

   Role of TRAP1/Hsp75 chaperon protein in human cancer. Authors: Omanma Adighibe, Adrian Harris, Kevin Gatter, and Francesco Pezzella. Nuffield Department of Clinical Laboratory Sciences, University Of Oxford, UK. Presenting Author: O. Adighibe

2. 7th Annual Medical Sciences DPhil Day, July 12th 2011

   TRAP1 and JMY; Role and function in Human Cancer.

Courses Attended

1. Statistics Organized by IT learning programme , University of Oxford, UK.

REFERENCES

Adighibe, O., K. Micklem, L. Campo, M. Ferguson, A. Harris, R. Pozos, K. Gatter and F. Pezzella (2006). Is nonangiogenesis a novel pathway for cancer progression? A study using 3-dimensional tumour reconstructions. Br J Cancer **94**(8): 1176-1179.

Adzhubei, I. A., S. Schmidt, L. Peshkin, V. E. Ramensky, A. Gerasimova, P. Bork, A. S. Kondrashov and S. R. Sunyaev (2010). A method and server for predicting damaging missense mutations. Nat Methods **7**(4): 248-249.

Agoff, S. N., J. Hou, D. I. Linzer and B. Wu (1993). Regulation of the human hsp70 promoter by p53. Science **259**(5091): 84-87.

Aoki, K., T. Yoshida, N. Matsumoto, H. Ide, T. Sugimura and M. Terada (1997). Suppression of Ki-ras p21 levels leading to growth inhibition of pancreatic cancer cell lines with Ki-ras mutation but not those without Ki-ras mutation. Mol Carcinog **20**(2): 251-258.

Arnes, J. B., I. M. Stefansson, O. Straume, J. P. Baak, P. E. Lonning, W. D. Foulkes and L. A. Akslen (2011). Vascular proliferation is a prognostic factor in breast cancer. Breast Cancer Res Treat.

Arrigo, A. P. (2005). [Heat shock proteins as molecular chaperones]. Med Sci (Paris) **21**(6-7): 619-625.

Azam, F., S. Mehta and A. L. Harris (2010). Mechanisms of resistance to antiangiogenesis therapy. Eur J Cancer **46**(8): 1323-1332.

Bacon, A. L. and A. L. Harris (2004). Hypoxia-inducible factors and hypoxic cell death in tumour physiology. Ann Med **36**(7): 530-539.

Banerji, U., M. Walton, F. Raynaud, R. Grimshaw, L. Kelland, M. Valenti, I. Judson and P. Workman (2005). Pharmacokinetic-pharmacodynamic relationships for the heat shock protein 90 molecular chaperone inhibitor 17-allylamino, 17-demethoxygeldanamycin in human ovarian cancer xenograft models. Clin Cancer Res **11**(19 Pt 1): 7023-7032.

Bardwell, J. C. and E. A. Craig (1987). Eukaryotic Mr 83,000 heat shock protein has a homologue in Escherichia coli. Proc Natl Acad Sci U S A **84**(15): 5177-5181.

Basso, A. D., D. B. Solit, G. Chiosis, B. Giri, P. Tsichlis and N. Rosen (2002). Akt forms an intracellular complex with heat shock protein 90 (Hsp90) and Cdc37 and is destabilized by inhibitors of Hsp90 function. J Biol Chem **277**(42): 39858-39866.

Beere, H. M. (2001). Stressed to death: regulation of apoptotic signaling pathways by the heat shock proteins. Sci STKE **2001**(93): re1.

Beere, H. M. (2004). "The stress of dying": the role of heat shock proteins in the regulation of apoptosis. J Cell Sci **117**(Pt 13): 2641-2651.

Borgese, N., A. J. Driessen, D. Rapaport and C. Robinson (2009). The quest for a better resolution of protein-translocation processes. Conference on the Control, Co-ordination and Regulation of Protein Targeting and Translocation. EMBO Rep **10**(4): 337-342.

Boutwell, R. K. (1989). Model systems for defining initiation, promotion, and progression of skin neoplasms. Prog Clin Biol Res **298**: 3-15.

Bridges, E. M. and A. L. Harris (2011). The angiogenic process as a therapeutic target in cancer. Biochem Pharmacol **81**(10): 1183-1191.

Buchner, J. (1999). Hsp90 & Co. - a holding for folding. Trends Biochem Sci **24**(4): 136-141.

Calderwood, S. K., M. A. Khaleque, D. B. Sawyer and D. R. Ciocca (2006). Heat shock proteins in cancer: chaperones of tumorigenesis. Trends Biochem Sci **31**(3): 164-172.

Campellone, K. G. and M. D. Welch (2010). A nucleator arms race: cellular control of actin assembly. Nat Rev Mol Cell Biol **11**(4): 237-251.

Campisi, J. (2005). Senescent cells, tumor suppression, and organismal aging: good citizens, bad neighbors. Cell **120**(4): 513-522.

Carlsson, J., C. G. Stalnacke, H. Acker, M. Haji-Karim, S. Nilsson and B. Larsson (1979). The influence of oxygen on viability and proliferation in cellular spheroids. Int J Radiat Oncol Biol Phys **5**(11-12): 2011-2020.

Carmeliet, P., Y. Dor, J. M. Herbert, D. Fukumura, K. Brusselmans, M. Dewerchin, M. Neeman, F. Bono, R. Abramovitch, P. Maxwell, C. J. Koch, P. Ratcliffe, L. Moons, R. K. Jain, D. Collen and E. Keshert (1998). Role of HIF-1alpha in hypoxia-mediated apoptosis, cell proliferation and tumour angiogenesis. Nature **394**(6692): 485-490.

Carmeliet, P. and R. K. Jain (2011). Molecular mechanisms and clinical applications of angiogenesis. Nature **473**(7347): 298-307.

Carnero, A. (2010). The PKB/AKT pathway in cancer. Curr Pharm Des **16**(1): 34-44.

Chant, I. D., P. E. Rose and A. G. Morris (1995). Analysis of heat-shock protein expression in myeloid leukaemia cells by flow cytometry. Br J Haematol **90**(1): 163-168.

Chen, C. F., Y. Chen, K. Dai, P. L. Chen, D. J. Riley and W. H. Lee (1996). A new member of the hsp90 family of molecular chaperones interacts with the retinoblastoma protein during mitosis and after heat shock. Mol Cell Biol **16**(9): 4691-4699.

Chen, G., P. Cao and D. V. Goeddel (2002). TNF-induced recruitment and activation of the IKK complex require Cdc37 and Hsp90. Mol Cell **9**(2): 401-410.

Chen, S., W. P. Sullivan, D. O. Toft and D. F. Smith (1998). Differential interactions of p23 and the TPR-containing proteins Hop, Cyp40, FKBP52 and FKBP51 with Hsp90 mutants. Cell Stress Chaperones **3**(2): 118-129.

Ciocca, D. R. and S. K. Calderwood (2005). Heat shock proteins in cancer: diagnostic, prognostic, predictive, and treatment implications. Cell Stress Chaperones **10**(2): 86-103.

Cleven, A. H., B. G. Wouters, B. Schutte, A. J. Spiertz, M. van Engeland and A. P. de Bruine (2008). Poorer outcome in stromal HIF-2 alpha- and CA9-positive colorectal adenocarcinomas is associated with wild-type TP53 but not with BNIP3 promoter hypermethylation or apoptosis. Br J Cancer **99**(5): 727-733.

Colpaert, C. G., P. B. Vermeulen, P. Van Beest, A. Soubry, G. Goovaerts, L. Y. Dirix, A. L. Harris and E. A. Van Marck (2003). Cutaneous breast cancer deposits show distinct growth patterns with different degrees of angiogenesis, hypoxia and fibrin deposition. Histopathology **42**(6): 530-540.

Coman, D. R. and W. F. Sheldon (1946). The significance of hyperemia around tumor implants. Am J Pathol **22**: 821-831.

Coutts, A. S., H. Boulahbel, A. Graham and N. B. La Thangue (2007). Mdm2 targets the p53 transcription cofactor JMY for degradation. EMBO Rep **8**(1): 84-90.

Coutts, A. S. and N. B. La Thangue (2005). The p53 response: emerging levels of co-factor complexity. Biochem Biophys Res Commun **331**(3): 778-785.

Coutts, A. S., I. M. Pires, L. Weston, F. M. Buffa, M. Milani, J. L. Li, A. L. Harris, E. M. Hammond and N. B. La Thangue (2011). Hypoxia-driven cell motility reflects the interplay between JMY and HIF-1alpha. Oncogene **30**(48): 4835-4842.

Coutts, A. S., L. Weston and N. B. La Thangue (2009). A transcription co-factor integrates cell adhesion and motility with the p53 response. Proc Natl Acad Sci U S A **106**(47): 19872-19877.

D'Souza-Schorey, C. (2005). Disassembling adherens junctions: breaking up is hard to do. Trends Cell Biol **15**(1): 19-26.

Dameron, K. M., O. V. Volpert, M. A. Tainsky and N. Bouck (1994). Control of angiogenesis in fibroblasts by p53 regulation of thrombospondin-1. Science **265**(5178): 1582-1584.

Datta, S. R., A. Brunet and M. E. Greenberg (1999). Cellular survival: a play in three Akts. Genes Dev **13**(22): 2905-2927.

Denoyelle, C., G. Abou-Rjaily, V. Bezrookove, M. Verhaegen, T. M. Johnson, D. R. Fullen, J. N. Pointer, S. B. Gruber, L. D. Su, M. A. Nikiforov, R. J. Kaufman, B. C. Bastian and M. S. Soengas (2006). Anti-oncogenic role of the endoplasmic reticulum differentially activated by mutations in the MAPK pathway. Nat Cell Biol **8**(10): 1053-1063.

Druker, B. J. (2002). Inhibition of the Bcr-Abl tyrosine kinase as a therapeutic strategy for CML. Oncogene **21**(56): 8541-8546.

Dufau, I., C. Frongia, F. Sicard, L. Dedieu, P. Cordelier, F. Ausseil, B. Ducommun and A. Valette (2012). Multicellular tumor spheroid model to evaluate spatio-temporal dynamics effect of chemotherapeutics: application to the gemcitabine/CHK1 inhibitor combination in pancreatic cancer. BMC Cancer **12**: 15.

Ebos, J. M. and R. S. Kerbel (2011). Antiangiogenic therapy: impact on invasion, disease progression, and metastasis. Nat Rev Clin Oncol **8**(4): 210-221.

Felsher, D. W. and J. M. Bishop (1999). Reversible tumorigenesis by MYC in hematopoietic lineages. Mol Cell **4**(2): 199-207.

Felts, S. J., B. A. Owen, P. Nguyen, J. Trepel, D. B. Donner and D. O. Toft (2000). The hsp90-related protein TRAP1 is a mitochondrial protein with distinct functional properties. J Biol Chem **275**(5): 3305-3312.

Folkman, J. (1972). Anti-angiogenesis: new concept for therapy of solid tumors. Ann Surg **175**(3): 409-416.

Folkman, J. (1985). Toward an understanding of angiogenesis: search and discovery. Perspect Biol Med **29**(1): 10-36.

Folkman, J. (1995). Angiogenesis in cancer, vascular, rheumatoid and other disease. Nat Med **1**(1): 27-31.

Folkman, J. (2002). Role of angiogenesis in tumor growth and metastasis. Semin Oncol **29**(6 Suppl 16): 15-18.

Folkman, J., P. Cole and S. Zimmerman (1966). Tumor behavior in isolated perfused organs: in vitro growth and metastases of biopsy material in rabbit thyroid and canine intestinal segment. Ann Surg **164**(3): 491-502.

Forsythe, J. A., B. H. Jiang, N. V. Iyer, F. Agani, S. W. Leung, R. D. Koos and G. L. Semenza (1996). Activation of vascular endothelial growth factor gene transcription by hypoxia-inducible factor 1. Mol Cell Biol **16**(9): 4604-4613.

Funai, K., T. Yokose, G. Ishii, K. Araki, J. Yoshida, M. Nishimura, K. Nagai, Y. Nishiwaki and A. Ochiai (2003). Clinicopathologic characteristics of peripheral squamous cell carcinoma of the lung. Am J Surg Pathol **27**(7): 978-984.

Gasparini, G., R. Longo, M. Fanelli and B. A. Teicher (2005). Combination of antiangiogenic therapy with other anticancer therapies: results, challenges, and open questions. J Clin Oncol **23**(6): 1295-1311.

Gasparini, G., R. Longo, M. Toi and N. Ferrara (2005). Angiogenic inhibitors: a new therapeutic strategy in oncology. Nat Clin Pract Oncol **2**(11): 562-577.

Gatenby, R. A. and R. J. Gillies (2004). Why do cancers have high aerobic glycolysis? Nat Rev Cancer **4**(11): 891-899.

Georgopoulos, C. and W. J. Welch (1993). Role of the major heat shock proteins as molecular chaperones. Annu Rev Cell Biol **9**: 601-634.

Gerner, E. W. and M. J. Schneider (1975). Induced thermal resistance in HeLa cells. Nature **256**(5517): 500-502.

Ghioni, P., F. Bolognese, P. H. Duijf, H. Van Bokhoven, R. Mantovani and L. Guerrini (2002). Complex transcriptional effects of p63 isoforms: identification of novel activation and repression domains. Mol Cell Biol **22**(24): 8659-8668.

Giatromanolaki, A., M. I. Koukourakis, H. M. Sowter, E. Sivridis, S. Gibson, K. C. Gatter and A. L. Harris (2004). BNIP3 expression is linked with hypoxia-regulated protein expression and with poor prognosis in non-small cell lung cancer. Clin Cancer Res **10**(16): 5566-5571.

Gimbrone, M. A., Jr., R. S. Cotran, S. B. Leapman and J. Folkman (1974). Tumor growth and neovascularization: an experimental model using the rabbit cornea. J Natl Cancer Inst **52**(2): 413-427.

Gimbrone, M. A., Jr., S. B. Leapman, R. S. Cotran and J. Folkman (1972). Tumor dormancy in vivo by prevention of neovascularization. J Exp Med **136**(2): 261-276.

Gisselsson, D. (2002). Tumour morphology--interplay between chromosome aberrations and founder cell differentiation. Histol Histopathol **17**(4): 1207-1212.

Gisselsson, D., J. Bjork, M. Hoglund, F. Mertens, P. Dal Cin, M. Akerman and N. Mandahl (2001). Abnormal nuclear shape in solid tumors reflects mitotic instability. Am J Pathol **158**(1): 199-206.

Gisselsson, D., T. Jonson, A. Petersen, B. Strombeck, P. Dal Cin, M. Hoglund, F. Mitelman, F. Mertens and N. Mandahl (2001). Telomere dysfunction triggers extensive DNA fragmentation and evolution of complex chromosome abnormalities in human malignant tumors. Proc Natl Acad Sci U S A **98**(22): 12683-12688.

Goldmann, E. (1908). The Growth of Malignant Disease in Man and the Lower Animals, with special reference to the Vascular System. Proc R Soc Med **1**(Surg Sect): 1-13.

Good, D. J., P. J. Polverini, F. Rastinejad, M. M. Le Beau, R. S. Lemons, W. A. Frazier and N. P. Bouck (1990). A tumor suppressor-dependent inhibitor of angiogenesis is immunologically and functionally indistinguishable from a fragment of thrombospondin. Proc Natl Acad Sci U S A **87**(17): 6624-6628.

Graeber, T. G., C. Osmanian, T. Jacks, D. E. Housman, C. J. Koch, S. W. Lowe and A. J. Giaccia (1996). Hypoxia-mediated selection of cells with diminished apoptotic potential in solid tumours. Nature **379**(6560): 88-91.

Grenert, J. P., W. P. Sullivan, P. Fadden, T. A. Haystead, J. Clark, E. Mimnaugh, H. Krutzsch, H. J. Ochel, T. W. Schulte, E. Sausville, L. M. Neckers and D. O. Toft (1997). The amino-terminal domain of heat shock protein 90 (hsp90) that binds geldanamycin is an ATP/ADP switch domain that regulates hsp90 conformation. J Biol Chem **272**(38): 23843-23850.

Gu, Z., L. Zhou, S. Gao and Z. Wang (2011). Nuclear transport signals control cellular localization and function of androgen receptor cofactor p44/WDR77. PLoS One **6**(7): e22395.

Guedj, N., A. Couvelard, G. Arcangeli, S. Dubois, G. Thabut, G. Leseche, M. Fournier, C. Degott and O. Groussard (2004). Angiogenesis and extracellular matrix remodelling in bronchioloalveolar carcinomas: distinctive patterns in mucinous and non-mucinous tumours. Histopathology **44**(3): 251-256.

Hammond, E. M. and A. J. Giaccia (2006). Hypoxia-inducible factor-1 and p53: friends, acquaintances, or strangers? Clin Cancer Res **12**(17): 5007-5009.

Hanada, M., J. Feng and B. A. Hemmings (2004). Structure, regulation and function of PKB/AKT--a major therapeutic target. Biochim Biophys Acta **1697**(1-2): 3-16.

Hanahan, D. and R. A. Weinberg (2000). The hallmarks of cancer. Cell **100**(1): 57-70.

Hanahan, D. and R. A. Weinberg (2011). Hallmarks of cancer: the next generation. Cell **144**(5): 646-674.

Harris, A. L. (2002). Hypoxia--a key regulatory factor in tumour growth. Nat Rev Cancer **2**(1): 38-47.

Hershko, T., M. Chaussepied, M. Oren and D. Ginsberg (2005). Novel link between E2F and p53: proapoptotic cofactors of p53 are transcriptionally upregulated by E2F. Cell Death Differ **12**(4): 377-383.

Hirohashi, S. (2000). Molecular aspects of adhesion-epigenetic mechanisms for inactivation of the E-Cadherin-mediated cell adhesion system in cancers. Verh Dtsch Ges Pathol **84**: 28-32.

Hlatky, L., P. Hahnfeldt and J. Folkman (2002). Clinical application of antiangiogenic therapy: microvessel density, what it does and doesn't tell us. J Natl Cancer Inst **94**(12): 883-893.

Hofman, P. (2005). DNA microarrays. Nephron Physiol **99**(3): p85-89.

Holash, J., P. C. Maisonpierre, D. Compton, P. Boland, C. R. Alexander, D. Zagzag, G. D. Yancopoulos and S. J. Wiegand (1999). Vessel cooption, regression, and growth in tumors mediated by angiopoietins and VEGF. Science **284**(5422): 1994-1998.

Hsu, A. L., C. T. Murphy and C. Kenyon (2003). Regulation of aging and age-related disease by DAF-16 and heat-shock factor. Science **300**(5622): 1142-1145.

Hu, J., F. Bianchi, M. Ferguson, A. Cesario, S. Margaritora, P. Granone, P. Goldstraw, M. Tetlow, C. Ratcliffe, A. G. Nicholson, A. Harris, K. Gatter and F. Pezzella (2005). Gene expression signature for angiogenic and nonangiogenic non-small-cell lung cancer. Oncogene **24**(7): 1212-1219.

Jaattela, M. (2004). Multiple cell death pathways as regulators of tumour initiation and progression. Oncogene **23**(16): 2746-2756.

Jakob, U., H. Lilie, I. Meyer and J. Buchner (1995). Transient interaction of Hsp90 with early unfolding intermediates of citrate synthase. Implications for heat shock in vivo. J Biol Chem **270**(13): 7288-7294.

Jeanes, A., C. J. Gottardi and A. S. Yap (2008). Cadherins and cancer: how does cadherin dysfunction promote tumor progression? Oncogene **27**(55): 6920-6929.

Jimenez, B., O. V. Volpert, S. E. Crawford, M. Febbraio, R. L. Silverstein and N. Bouck (2000). Signals leading to apoptosis-dependent inhibition of neovascularization by thrombospondin-1. Nat Med **6**(1): 41-48.

Joab, I., C. Radanyi, M. Renoir, T. Buchou, M. G. Catelli, N. Binart, J. Mester and E. E. Baulieu (1984). Common non-hormone binding component in non-transformed chick oviduct receptors of four steroid hormones. Nature **308**(5962): 850-853.

Johnson, B. D., R. J. Schumacher, E. D. Ross and D. O. Toft (1998). Hop modulates Hsp70/Hsp90 interactions in protein folding. J Biol Chem **273**(6): 3679-3686.

Kamal, A., L. Thao, J. Sensintaffar, L. Zhang, M. F. Boehm, L. C. Fritz and F. J. Burrows (2003). A high-affinity conformation of Hsp90 confers tumour selectivity on Hsp90 inhibitors. Nature **425**(6956): 407-410.

Kang, B. H. (2012). TRAP1 regulation of mitochondrial life or death decision in cancer cells and mitochondria-targeted TRAP1 inhibitors. BMB Rep **45**(1): 1-6.

Kang, B. H. and D. C. Altieri (2009). Compartmentalized cancer drug discovery targeting mitochondrial Hsp90 chaperones. Oncogene **28**(42): 3681-3688.

Kang, B. H., J. Plescia, T. Dohi, J. Rosa, S. J. Doxsey and D. C. Altieri (2007). Regulation of tumor cell mitochondrial homeostasis by an organelle-specific Hsp90 chaperone network. Cell **131**(2): 257-270.

Keith, B. and M. C. Simon (2007). Hypoxia-inducible factors, stem cells, and cancer. Cell **129**(3): 465-472.

Kozlov, N. N. (1996). [Silent mutations in the region of overlapping genes]. Dokl Akad Nauk **350**(5): 699-703.

Kruhoffer, M., J. L. Jensen, P. Laiho, L. Dyrskjot, R. Salovaara, D. Arango, K. Birkenkamp-Demtroder, F. B. Sorensen, L. L. Christensen, L. Buhl, J. P. Mecklin, H. Jarvinen, T. Thykjaer, F. P. Wikman, F. Bech-Knudsen, M. Juhola, N. N. Nupponen, S. Laurberg, C. L. Andersen, L. A. Aaltonen and T. F. Orntoft (2005). Gene expression signatures for colorectal cancer microsatellite status and HNPCC. Br J Cancer **92**(12): 2240-2248.

Kusters, B., W. P. Leenders, P. Wesseling, D. Smits, K. Verrijp, D. J. Ruiter, J. P. Peters, A. J. van Der Kogel and R. M. de Waal (2002). Vascular endothelial growth factor-A(165) induces progression of melanoma brain metastases without induction of sprouting angiogenesis. Cancer Res **62**(2): 341-345.

Lane, D. P., C. Midgley and T. Hupp (1993). Tumour suppressor genes and molecular chaperones. Philos Trans R Soc Lond B Biol Sci **339**(1289): 369-372; discussion 372-363.

Lange, B. M., E. Rebollo, A. Herold and C. Gonzalez (2002). Cdc37 is essential for chromosome segregation and cytokinesis in higher eukaryotes. EMBO J **21**(20): 5364-5374.

Leav, I., J. Plescia, H. L. Goel, J. Li, Z. Jiang, R. J. Cohen, L. R. Languino and D. C. Altieri (2010). Cytoprotective mitochondrial chaperone TRAP-1 as a novel molecular target in localized and metastatic prostate cancer. Am J Pathol **176**(1): 393-401.

Lindquist, S. and E. A. Craig (1988). The heat-shock proteins. Annu Rev Genet **22**: 631-677.

Liu, D., J. Hu, J. Agorreta, A. Cesario, Y. Zhang, A. L. Harris, K. Gatter and F. Pezzella (2010). Tumor necrosis factor receptor-associated protein 1(TRAP1) regulates genes involved in cell cycle and metastases. Cancer Lett **296**(2): 194-205.

Ludlow, J. W., C. L. Glendening, D. M. Livingston and J. A. DeCarprio (1993). Specific enzymatic dephosphorylation of the retinoblastoma protein. Mol Cell Biol **13**(1): 367-372.

Luo, J., N. L. Solimini and S. J. Elledge (2009). Principles of cancer therapy: oncogene and non-oncogene addiction. Cell **136**(5): 823-837.

Madden, S. L., E. A. Galella, J. Zhu, A. H. Bertelsen and G. A. Beaudry (1997). SAGE transcript profiles for p53-dependent growth regulation. Oncogene **15**(9): 1079-1085.

Masuda, Y., G. Shima, T. Aiuchi, M. Horie, K. Hori, S. Nakajo, S. Kajimoto, T. Shibayama-Imazu and K. Nakaya (2004). Involvement of tumor necrosis factor receptor-associated protein 1 (TRAP1) in apoptosis induced by beta-hydroxyisovalerylshikonin. J Biol Chem **279**(41): 42503-42515.

Mattern, J., R. Koomagi and M. Volm (1999). Biological characterization of subgroups of squamous cell lung carcinomas. Clin Cancer Res **5**(6): 1459-1463.

Mayer, M. P. and B. Bukau (2005). Hsp70 chaperones: cellular functions and molecular mechanism. Cell Mol Life Sci **62**(6): 670-684.

Mellor, H. R., D. J. Ferguson and R. Callaghan (2005). A model of quiescent tumour microregions for evaluating multicellular resistance to chemotherapeutic drugs. Br J Cancer **93**(3): 302-309.

Mellor, H. R. and A. L. Harris (2007). The role of the hypoxia-inducible BH3-only proteins BNIP3 and BNIP3L in cancer. Cancer Metastasis Rev **26**(3-4): 553-566.

Memmott, R. M. and P. A. Dennis (2010). The role of the Akt/mTOR pathway in tobacco carcinogen-induced lung tumorigenesis. Clin Cancer Res **16**(1): 4-10.

Montesano Gesualdi, N., G. Chirico, G. Pirozzi, E. Costantino, M. Landriscina and F. Esposito (2007). Tumor necrosis factor-associated protein 1 (TRAP-1) protects cells from oxidative stress and apoptosis. Stress **10**(4): 342-350.

Nam, J. S., Y. Ino, Y. Kanai, M. Sakamoto and S. Hirohashi (2004). 5-aza-2'-deoxycytidine restores the E-cadherin system in E-cadherin-silenced cancer cells and reduces cancer metastasis. Clin Exp Metastasis **21**(1): 49-56.

Naresh, K. N., A. Y. Nerurkar and A. M. Borges (2001). Angiogenesis is redundant for tumour growth in lymph node metastases. Histopathology **38**(5): 466-470.

Nathan, D. F., M. H. Vos and S. Lindquist (1997). In vivo functions of the Saccharomyces cerevisiae Hsp90 chaperone. Proc Natl Acad Sci U S A **94**(24): 12949-12956.

Neckers, L. and S. P. Ivy (2003). Heat shock protein 90. Curr Opin Oncol **15**(6): 419-424.

Neckers, L., A. Kern and S. Tsutsumi (2007). Hsp90 inhibitors disrupt mitochondrial homeostasis in cancer cells. Chem Biol **14**(11): 1204-1206.

Neckers, L. and Y. S. Lee (2003). Cancer: the rules of attraction. Nature **425**(6956): 357-359.

Nelson, D. A. and E. White (2004). Exploiting different ways to die. Genes Dev **18**(11): 1223-1226.

Nimmanapalli, R., E. O'Bryan and K. Bhalla (2001). Geldanamycin and its analogue 17-allylamino-17-demethoxygeldanamycin lowers Bcr-Abl levels and induces apoptosis and differentiation of Bcr-Abl-positive human leukemic blasts. Cancer Res **61**(5): 1799-1804.

Nor, J. E., R. S. Mitra, M. M. Sutorik, D. J. Mooney, V. P. Castle and P. J. Polverini (2000). Thrombospondin-1 induces endothelial cell apoptosis and inhibits angiogenesis by activating the caspase death pathway. J Vasc Res **37**(3): 209-218.

Nylandsted, J., M. Gyrd-Hansen, A. Danielewicz, N. Fehrenbacher, U. Lademann, M. Hoyer-Hansen, E. Weber, G. Multhoff, M. Rohde and M. Jaattela (2004). Heat shock protein 70 promotes cell survival by inhibiting lysosomal membrane permeabilization. J Exp Med **200**(4): 425-435.

Obermann, W. M., H. Sondermann, A. A. Russo, N. P. Pavletich and F. U. Hartl (1998). In vivo function of Hsp90 is dependent on ATP binding and ATP hydrolysis. J Cell Biol **143**(4): 901-910.

Offersen, B. V., P. Pfeiffer, S. Hamilton-Dutoit and J. Overgaard (2001). Patterns of angiogenesis in nonsmall-cell lung carcinoma. Cancer **91**(8): 1500-1509.

Party, B. C. P. W. (2000). Evidence for novel non-angiogenic pathway in breast-cancer metastasis. Lancet **355**(9217): 1787-1788.

Passalidou, E., M. Stewart, M. Trivella, G. Steers, G. Pillai, A. Dogan, I. Leigh, C. Hatton, A. Harris, K. Gatter and F. Pezzella (2003). Vascular patterns in reactive lymphoid tissue and in non-Hodgkin's lymphoma. Br J Cancer **88**(4): 553-559.

Passalidou, E., M. Trivella, N. Singh, M. Ferguson, J. Hu, A. Cesario, P. Granone, A. G. Nicholson, P. Goldstraw, C. Ratcliffe, M. Tetlow, I. Leigh, A. L. Harris, K. C. Gatter and F. Pezzella (2002). Vascular phenotype in angiogenic and non-angiogenic lung non-small cell carcinomas. Br J Cancer **86**(2): 244-249.

Pastorino, U., S. Andreola, E. Tagliabue, F. Pezzella, M. Incarbone, G. Sozzi, M. Buyse, S. Menard, M. Pierotti and F. Rilke (1997). Immunocytochemical markers in stage I lung cancer: relevance to prognosis. J Clin Oncol **15**(8): 2858-2865.

Paunola, E., P. K. Mattila and P. Lappalainen (2002). WH2 domain: a small, versatile adapter for actin monomers. FEBS Lett **513**(1): 92-97.

Pelengaris, S., T. Littlewood, M. Khan, G. Elia and G. Evan (1999). Reversible activation of c-Myc in skin: induction of a complex neoplastic phenotype by a single oncogenic lesion. Mol Cell **3**(5): 565-577.

Perez-Atayde, A. R., S. E. Sallan, U. Tedrow, S. Connors, E. Allred and J. Folkman (1997). Spectrum of tumor angiogenesis in the bone marrow of children with acute lymphoblastic leukemia. Am J Pathol **150**(3): 815-821.

Pezzella, F., A. Di Bacco, S. Andreola, A. G. Nicholson, U. Pastorino and A. L. Harris (1996). Angiogenesis in primary lung cancer and lung secondaries. Eur J Cancer **32A**(14): 2494-2500.

Pezzella, F., A. L. Harris and K. C. Gatter (2001). Ways of escape: are all tumours angiogenic? Histopathology **39**(6): 551-553.

Pezzella, F., U. Pastorino, E. Tagliabue, S. Andreola, G. Sozzi, G. Gasparini, S. Menard, K. C. Gatter, A. L. Harris, S. Fox, M. Buyse, S. Pilotti, M. Pierotti and F. Rilke (1997). Non-small-cell lung carcinoma tumor growth without morphological evidence of neo-angiogenesis. Am J Pathol **151**(5): 1417-1423.

Pfaffl, M. W. (2001). A new mathematical model for relative quantification in real-time RT-PCR. Nucleic Acids Res **29**(9): e45.

Pfosser, A., M. Thalgott, K. Buttner, A. Brouet, O. Feron, P. Boekstegers and C. Kupatt (2005). Liposomal Hsp90 cDNA induces neovascularization via nitric oxide in chronic ischemia. Cardiovasc Res **65**(3): 728-736.

Pinhasi-Kimhi, O., D. Michalovitz, A. Ben-Zeev and M. Oren (1986). Specific interaction between the p53 cellular tumour antigen and major heat shock proteins. Nature **320**(6058): 182-184.

Potente, M., H. Gerhardt and P. Carmeliet (2011). Basic and therapeutic aspects of angiogenesis. Cell **146**(6): 873-887.

Pratt, W. B. and D. O. Toft (2003). Regulation of signaling protein function and trafficking by the hsp90/hsp70-based chaperone machinery. Exp Biol Med (Maywood) **228**(2): 111-133.

Prodromou, C., S. M. Roe, R. O'Brien, J. E. Ladbury, P. W. Piper and L. H. Pearl (1997). Identification and structural characterization of the ATP/ADP-binding site in the Hsp90 molecular chaperone. Cell **90**(1): 65-75.

Prodromou, C., G. Siligardi, R. O'Brien, D. N. Woolfson, L. Regan, B. Panaretou, J. E. Ladbury, P. W. Piper and L. H. Pearl (1999). Regulation of Hsp90 ATPase activity by tetratricopeptide repeat (TPR)-domain co-chaperones. EMBO J **18**(3): 754-762.

Proskuryakov, S. Y., A. G. Konoplyannikov and V. L. Gabai (2003). Necrosis: a specific form of programmed cell death? Exp Cell Res **283**(1): 1-16.

Pugh, C. W. and P. J. Ratcliffe (2003). Regulation of angiogenesis by hypoxia: role of the HIF system. Nat Med **9**(6): 677-684.

Raleigh, J. A., D. P. Calkins-Adams, L. H. Rinker, C. A. Ballenger, M. C. Weissler, W. C. Fowler, Jr., D. B. Novotny and M. A. Varia (1998). Hypoxia and vascular endothelial growth factor expression in human squamous cell carcinomas using pimonidazole as a hypoxia marker. Cancer Res **58**(17): 3765-3768.

Ramasamy, A., A. Mondry, C. C. Holmes and D. G. Altman (2008). Key issues in conducting a meta-analysis of gene expression microarray datasets. PLoS Med **5**(9): e184.

Ravi, R., B. Mookerjee, Z. M. Bhujwalla, C. H. Sutter, D. Artemov, Q. Zeng, L. E. Dillehay, A. Madan, G. L. Semenza and A. Bedi (2000). Regulation of tumor angiogenesis by p53-induced degradation of hypoxia-inducible factor 1alpha. Genes Dev **14**(1): 34-44.

Regis, G., S. Pensa, D. Boselli, F. Novelli and V. Poli (2008). Ups and downs: the STAT1:STAT3 seesaw of Interferon and gp130 receptor signalling. Semin Cell Dev Biol **19**(4): 351-359.

Roadcap, D. W. and J. E. Bear (2009). Double JMY: making actin fast. Nat Cell Biol **11**(4): 375-376.

Roberts, P. J. and C. J. Der (2007). Targeting the Raf-MEK-ERK mitogen-activated protein kinase cascade for the treatment of cancer. Oncogene **26**(22): 3291-3310.

Rohde, M., M. Daugaard, M. H. Jensen, K. Helin, J. Nylandsted and M. Jaattela (2005). Members of the heat-shock protein 70 family promote cancer cell growth by distinct mechanisms. Genes Dev **19**(5): 570-582.

Rollins, B. J. and C. D. Stiles (1988). Regulation of c-myc and c-fos proto-oncogene expression by animal cell growth factors. In Vitro Cell Dev Biol **24**(2): 81-84.

Rubenstein, J. L., J. Kim, T. Ozawa, M. Zhang, M. Westphal, D. F. Deen and M. A. Shuman (2000). Anti-VEGF antibody treatment of glioblastoma prolongs survival but results in increased vascular cooption. Neoplasia **2**(4): 306-314.

Sanchez, E. R., D. O. Toft, M. J. Schlesinger and W. B. Pratt (1985). Evidence that the 90-kDa phosphoprotein associated with the untransformed L-cell glucocorticoid receptor is a murine heat shock protein. J Biol Chem **260**(23): 12398-12401.

Sardari Nia, P., C. Colpaert, B. Blyweert, B. Kui, P. Vermeulen, M. Ferguson, J. Hendriks, J. Weyler, F. Pezzella, E. Van Marck and P. Van Schil (2004). Prognostic value of nonangiogenic and angiogenic growth patterns in non-small-cell lung cancer. Br J Cancer **91**(7): 1293-1300.

Sardari Nia, P., C. Colpaert, P. Vermeulen, J. Weyler, F. Pezzella, P. Van Schil and E. Van Marck (2008). Different growth patterns of non-small cell lung cancer represent distinct biologic subtypes. Ann Thorac Surg **85**(2): 395-405.

Schiavone, D., L. Avalle, S. Dewilde and V. Poli (2011). The immediate early genes Fos and Egr1 become STAT1 transcriptional targets in the absence of STAT3. FEBS Lett **585**(15): 2455-2460.

Schumacher, R. J., W. J. Hansen, B. C. Freeman, E. Alnemri, G. Litwack and D. O. Toft (1996). Cooperative action of Hsp70, Hsp90, and DnaJ proteins in protein renaturation. Biochemistry **35**(47): 14889-14898.

Semenza, G. L. (2010). Defining the role of hypoxia-inducible factor 1 in cancer biology and therapeutics. Oncogene **29**(5): 625-634.

Semenza, G. L. (2012). Hypoxia-inducible factors in physiology and medicine. Cell **148**(3): 399-408.

Sharma, S., S. C. Yang, L. Zhu, K. Reckamp, B. Gardner, F. Baratelli, M. Huang, R. K. Batra and S. M. Dubinett (2005). Tumor cyclooxygenase-2/prostaglandin E2-dependent promotion of FOXP3 expression and CD4+ CD25+ T regulatory cell activities in lung cancer. Cancer Res **65**(12): 5211-5220.

Shaulian, E. and M. Karin (2002). AP-1 as a regulator of cell life and death. Nat Cell Biol **4**(5): E131-136.

Shikama, N., C. W. Lee, S. France, L. Delavaine, J. Lyon, M. Krstic-Demonacos and N. B. La Thangue (1999). A novel cofactor for p300 that regulates the p53 response. Mol Cell **4**(3): 365-376.

Shing, Y., J. Folkman, R. Sullivan, C. Butterfield, J. Murray and M. Klagsbrun (1984). Heparin affinity: purification of a tumor-derived capillary endothelial cell growth factor. Science **223**(4642): 1296-1299.

Solimini, N. L., J. Luo and S. J. Elledge (2007). Non-oncogene addiction and the stress phenotype of cancer cells. Cell **130**(6): 986-988.

Song, H. Y., J. D. Dunbar, Y. X. Zhang, D. Guo and D. B. Donner (1995). Identification of a protein with homology to hsp90 that binds the type 1 tumor necrosis factor receptor. J Biol Chem **270**(8): 3574-3581.

Soussi, T. (2005). The p53 pathway and human cancer. Br J Surg **92**(11): 1331-1332.

Spiess, C., A. S. Meyer, S. Reissmann and J. Frydman (2004). Mechanism of the eukaryotic chaperonin: protein folding in the chamber of secrets. Trends Cell Biol **14**(11): 598-604.

Stessels, F., G. Van den Eynden, I. Van der Auwera, R. Salgado, E. Van den Heuvel, A. L. Harris, D. G. Jackson, C. G. Colpaert, E. A. van Marck, L. Y. Dirix and P. B. Vermeulen (2004). Breast adenocarcinoma liver metastases, in contrast to colorectal cancer liver metastases, display a non-angiogenic growth pattern that preserves the stroma and lacks hypoxia. Br J Cancer **90**(7): 1429-1436.

Sun, J. and J. K. Liao (2004). Induction of angiogenesis by heat shock protein 90 mediated by protein kinase Akt and endothelial nitric oxide synthase. Arterioscler Thromb Vasc Biol **24**(12): 2238-2244.

Syed, V., P. Mak, C. Du and K. C. Balaji (2008). Beta-catenin mediates alteration in cell proliferation, motility and invasion of prostate cancer cells by differential expression of E-cadherin and protein kinase D1. J Cell Biochem **104**(1): 82-95.

Taira, T., M. Sawai, M. Ikeda, K. Tamai, S. M. Iguchi-Ariga and H. Ariga (1999). Cell cycle-dependent switch of up-and down-regulation of human hsp70 gene expression by interaction between c-Myc and CBF/NF-Y. J Biol Chem **274**(34): 24270-24279.

Tan, E. Y., F. Pezzella and K. Gatter (2007). Loss of protein folding gene expression in human tumors D Phil, University of Oxford.

Tatar, M., A. A. Khazaeli and J. W. Curtsinger (1997). Chaperoning extended life. Nature **390**(6655): 30.

Teodoro, J. G., S. K. Evans and M. R. Green (2007). Inhibition of tumor angiogenesis by p53: a new role for the guardian of the genome. J Mol Med (Berl) **85**(11): 1175-1186.

Teodoro, J. G., A. E. Parker, X. Zhu and M. R. Green (2006). p53-mediated inhibition of angiogenesis through up-regulation of a collagen prolyl hydroxylase. Science **313**(5789): 968-971.

Tolsma, S. S., O. V. Volpert, D. J. Good, W. A. Frazier, P. J. Polverini and N. Bouck (1993). Peptides derived from two separate domains of the matrix protein thrombospondin-1 have anti-angiogenic activity. J Cell Biol **122**(2): 497-511.

Tsutsumi-Ishii, Y., K. Tadokoro, F. Hanaoka and N. Tsuchida (1995). Response of heat shock element within the human HSP70 promoter to mutated p53 genes. Cell Growth Differ **6**(1): 1-8.

Vandesompele, J., K. De Preter, F. Pattyn, B. Poppe, N. Van Roy, A. De Paepe and F. Speleman (2002). Accurate normalization of real-time quantitative RT-PCR data by geometric averaging of multiple internal control genes. Genome Biol **3**(7): RESEARCH0034.

Vargas-Roig, L. M., F. E. Gago, O. Tello, J. C. Aznar and D. R. Ciocca (1998). Heat shock protein expression and drug resistance in breast cancer patients treated with induction chemotherapy. Int J Cancer **79**(5): 468-475.

Vermeulen, P. B., C. Colpaert, R. Salgado, R. Royers, H. Hellemans, E. Van Den Heuvel, G. Goovaerts, L. Y. Dirix and E. Van Marck (2001). Liver metastases from colorectal adenocarcinomas grow in three patterns with different angiogenesis and desmoplasia. J Pathol **195**(3): 336-342.

Vermeulen, P. B., G. Gasparini, S. B. Fox, C. Colpaert, L. P. Marson, M. Gion, J. A. Belien, R. M. de Waal, E. Van Marck, E. Magnani, N. Weidner, A. L. Harris and L. Y. Dirix (2002). Second international consensus on the methodology and criteria of evaluation of angiogenesis quantification in solid human tumours. Eur J Cancer **38**(12): 1564-1579.

Viatour, P., M. P. Merville, V. Bours and A. Chariot (2005). Phosphorylation of NF-kappaB and IkappaB proteins: implications in cancer and inflammation. Trends Biochem Sci **30**(1): 43-52.

Vivanco, I. and C. L. Sawyers (2002). The phosphatidylinositol 3-Kinase AKT pathway in human cancer. Nat Rev Cancer **2**(7): 489-501.

Wadhwa, R., K. Taira and S. C. Kaul (2002). An Hsp70 family chaperone, mortalin/mthsp70/PBP74/Grp75: what, when, and where? Cell Stress Chaperones **7**(3): 309-316.

Wagner, E. F. and R. Eferl (2005). Fos/AP-1 proteins in bone and the immune system. Immunol Rev **208**: 126-140.

Wang, G. L., B. H. Jiang, E. A. Rue and G. L. Semenza (1995). Hypoxia-inducible factor 1 is a basic-helix-loop-helix-PAS heterodimer regulated by cellular O2 tension. Proc Natl Acad Sci U S A **92**(12): 5510-5514.

Wang, Y. (2010). JimMY on the stage: Linking DNA damage with cell adhesion and motility. Cell Adh Migr **4**(2): 166-168.

Webster, L., R. J. Hodgkiss and G. D. Wilson (1998). Cell cycle distribution of hypoxia and progression of hypoxic tumour cells in vivo. Br J Cancer **77**(2): 227-234.

Wegele, H., L. Muller and J. Buchner (2004). Hsp70 and Hsp90--a relay team for protein folding. Rev Physiol Biochem Pharmacol **151**: 1-44.

Weinstein, I. B. (2002). Cancer. Addiction to oncogenes--the Achilles heal of cancer. Science **297**(5578): 63-64.

Wesseling, P., J. A. van der Laak, H. de Leeuw, D. J. Ruiter and P. C. Burger (1994). Quantitative immunohistological analysis of the microvasculature in untreated human glioblastoma multiforme. Computer-assisted image analysis of whole-tumor sections. J Neurosurg **81**(6): 902-909.

Whitesell, L. and S. L. Lindquist (2005). HSP90 and the chaperoning of cancer. Nat Rev Cancer **5**(10): 761-772.

Workman, P. (2004). Altered states: selectively drugging the Hsp90 cancer chaperone. Trends Mol Med **10**(2): 47-51.

Wu, G., M. Osada, Z. Guo, A. Fomenkov, S. Begum, M. Zhao, S. Upadhyay, M. Xing, F. Wu, C. Moon, W. H. Westra, W. M. Koch, R. Mantovani, J. A. Califano, E. Ratovitski, D. Sidransky and B. Trink (2005). DeltaNp63alpha up-regulates the Hsp70 gene in human cancer. Cancer Res **65**(3): 758-766.

Xu, C. X., H. Jin, J. Y. Shin, J. E. Kim and M. H. Cho (2010). Roles of protein kinase B/Akt in lung cancer. Front Biosci (Elite Ed) **2**: 1472-1484.

Yokoyama, K., K. Fukumoto, T. Murakami, S. Harada, R. Hosono, R. Wadhwa, Y. Mitsui and S. Ohkuma (2002). Extended longevity of Caenorhabditis elegans by knocking in extra copies of hsp70F, a homolog of mot-2 (mortalin)/mthsp70/Grp75. FEBS Lett **516**(1-3): 53-57.

Young, J. C., V. R. Agashe, K. Siegers and F. U. Hartl (2004). Pathways of chaperone-mediated protein folding in the cytosol. Nat Rev Mol Cell Biol **5**(10): 781-791.

Zhang, J. and P. A. Ney (2009). Role of BNIP3 and NIX in cell death, autophagy, and mitophagy. Cell Death Differ **16**(7): 939-946.

Zhou, J., T. Schmid, R. Frank and B. Brune (2004). PI3K/Akt is required for heat shock proteins to protect hypoxia-inducible factor 1alpha from pVHL-independent degradation. J Biol Chem **279**(14): 13506-13513.

Zuchero, J. B., A. S. Coutts, M. E. Quinlan, N. B. Thangue and R. D. Mullins (2009). p53-cofactor JMY is a multifunctional actin nucleation factor. Nat Cell Biol **11**(4): 451-459.